Flow Analysis of a Four-strand Steelmaking Tundish Using Physical and Numerical Modelling

by

Jan Hendrik Cloete

Thesis presented in partial fulfilment

of the requirements for the Degree

of

MASTER IN ENGINEERING

(EXTRACTIVE METALLURGICAL ENGINEERING)

in the Faculty of Engineering

at Stellenbosch University

Supervisor

Professor Guven Akdogan

Co-Supervisor

Professor Steven M. Bradshaw

April 2014

Stellenbosch University http://scholar.sun.ac.za

Declaration

By submitting this thesis electronically, I declare that the entirety of the work contained therein is my own, original work, that I am the sole author thereof (save to the extent explicitly otherwise stated), that reproduction and publication thereof by Stellenbosch University will not infringe any third party rights and that I have not previously in its entirety or in part submitted it for obtaining any qualification.

Jan Hendrik Cloete **21 February 2014**

…… ……..

Signature Date

Copyright © 2014 Stellenbosch University

All rights reserved

Stellenbosch University http://scholar.sun.ac.za

Abstract

In modern steelmaking a tundish serves as an important metallurgical reactor to remove inclusions and maintain thermal and chemical homogeneity in the product. In this study the flow behaviour in a four strand tundish was investigated by means of a 1/2 scale water model, based on Froude number similarity, as well as by using numerical modelling. Both the numerical study and physical model were used to characterise residence time distribution (RTD) in the vessel and to calculate properties pertaining to the tundish flow regime.

The three different tundish configurations investigated in this study are: a bare tundish with no flow control devices, a tundish with a turbulence inhibitor and a tundish using a turbulence inhibitor with holes in combination with dams. Preliminary investigations focussed on the framework for obtaining an accurate numerical solution within reasonable computational times. The effect of assuming symmetry and dynamically steady flow in the numerical model was shown to be small relative to the effect of grid size and justifiable by the savings in computational time. The grid independence study indicated the importance of using a finer mesh in areas of high velocity gradients to obtain realistic results and also to limit the number of computational cells. A procedure using gradient adaptation was used to refine the mesh automatically in the required regions for different tundish geometries. Results also showed that the inlet boundary of the numerical model should be selected at the ladle outlet, since assuming a flat velocity profile at the nozzle port resulted in significant changes in the RTD response.

Comparison of the results obtained using the numerical model with those from physical experiments yielded an average error of less than 10%. This was assumed to be a good prediction, considering the assumptions employed in the numerical model. Both the physical and numerical models showed that a tundish without flow control devices was prone to significant short circuiting. The addition of a turbulence inhibitor was shown to be successful in preventing short circuiting and provided surface directed flow, which is thought to aid inclusion removal in the slag. Additionally, the minimum, peak and mean residence times and plug flow volume fraction were increased significantly, while the dead volume fraction decreased. However, using a turbulence inhibitor with holes in combination with dams showed that this configuration may cause increased refractory wear together with increased risk of slag entrainment due to flow patterns with increased surface turbulence. It also showed that the short-circuiting might not be eliminated completely. This indicates that certain design changes to tundish flow control systems can introduce problems that outweigh the benefits of the altered flow patterns.

Furthermore, the numerical method, which was based on the water model, was modified to simulate the high temperature steel process. A very good match was obtained between the results using the two different numerical models. This serves as additional evidence that

Stellenbosch University http://scholar.sun.ac.za

tundish water modelling based on Froude number similarity provides a good representation of the actual industrial process.

Using the numerical model based on the high temperature steel process the effect of turbulence inhibitor shape was studied for four different turbulence inhibitor designs. Results showed the best performance, based on flow characteristic properties and surface turbulence values, was achieved for the design using a rectangular box-like shape with flanges at the top. However, the comparison emphasized the effect of the turbulence inhibitor shape on the flow behaviour, as each design yielded completely different flow patterns. It was also observed that a good turbulence inhibitor provided an optimum amount of turbulent suppression. Insufficient suppression would cause fast flows, which will result in insufficient residence time for inclusion flotation and high surface turbulence values, which may cause slag entrainment. On the other hand, too much suppression may increase the variation between strands.

Stellenbosch University http://scholar.sun.ac.za

Opsomming

Die verdeeltrog speel ‘n belangrike rol in die moderne staalvervaardigingsproses deur inklusies te verwyder en termiese en chemiese homogeniteit in die produk te verseker. In hierdie studie is die vloeigedrag in ‘n verdeeltrog met vier uitlate bestudeer deur middel van ‘n 1:2-skaal watermodel, gebaseer op Froude-getal gelykheid, sowel as deur numeriese modellering. Beide die numeriese en watermodel is gebruik om die verblyftyd-distribusie in die trog te karakteriseer en om waardes te bereken wat die vloeigedrag in die verdeeltrog beskryf.

Drie verskillende verdeeltrog-opstellings is in hierdie studie bestudeer, naamlik: ‘n leë verdeeltrog met geen vloeibeheertoestelle nie, ‘n verdeeltrog met ‘n turbulensie-inhibeerder en ‘n verdeeltrog wat gebruik maak van ‘n turbulensie-inhibeerder met gate, gekombineer met lae damwalle. Vroeë ondersoeke het gefokus op ‘n metode om akkurate numeriese resultate binne aanvaarbare tye te verkry. Die invloed van die aannames van simmetrie en dinamiese gestadigde vloei op die resultate is bepaal om klein te wees teenoor dié van die roostergrootte. Die gebruik van die aannames is dus geregverdig deur die afname in berekeningstyd wat dit meebring. Die roosteronafhanklikheidstudie het getoon dat dit belangrik is om die vloeivergelykings oor klein volume-eenhede op te los in areas van hoë snelheidsgradiënte, beide om realistiese resultate te verseker en om die aantal volume-eenhede te beperk. ‘n Prosedure wat gebruik maak van gradiëntaanpassing is gebruik om die roostergrootte outomaties te verklein in die areas met hoë snelheidsgradiënte vir verskillende verdeeltrog-opstellings. Resultate het ook getoon dat dit belangrik is om die inlaatgrens van die numeriese model by die smeltpot se uitlaat te kies, aangesien noemenswaardige verskille in die verblyftyd-distribusie waargeneem is wanneer ‘n uniforme snelheidsprofiel aanvaar is waar die metaal die verdeeltrog binnegaan.

Daar is gevind dat die resultate by die numeriese en watermodelle verskil met ‘n gemiddelde fout van ongeveer 10%. Dit word beskou as ‘n goeie ooreenstemming, as die aannames wat in die numeriese model gebruik word in ag geneem word. Beide die numeriese en watermodelle het getoon dat die metaalvloei in die leë verdeeltrog geneig is om die kortste roete na die uitlate te kies. Deur van ‘n turbulensie inhibeerder gebruik te maak word hierdie probleem opgelos deur die metaalvloei opwaarts te forseer. In die proses neem die minimum-, piek- en gemiddelde verblyftye, sowel as die propvloei volumefraksie, toe, terwyl die dooievloei fraksie afneem. Die turbulensie inhibeerder met die gate en die lae damwalle is egter meer geneig tot erosie van die vuurvaste materiaal en kan ook vloeipatrone veroorsaak wat metaalskuimdruppels in die metaal kan opneem. Verder volg ‘n klein fraksie van die vloei steeds ‘n kortpad na die uitlaat. Hierdie resultate toon dat sekere veranderings aan verdeeltrog vloeibeerheerstelsels nadelige gevolge kan hê wat enige positiewe gevolge uitkanselleer.

Stellenbosch University http://scholar.sun.ac.za

Verder is die numeriese metode wat tot dusver op die watersisteem gebaseer is, aangepas om die vloei in die hoëtemperatuur staalproses te simuleer. ‘n Baie goeie vergelyking is verkry tussen die resultate wat die twee numeriese modelle voorspel. Hierdie dien as ‘n verdere bewys dat ‘n watermodel, wat op Froude-getal gelykheid gebaseer is, die industriële proses akkuraat kan simuleer.

Deur gebruik te maak van die numeriese model van die hoë temperatuur staalproses, is die effek van die turbulensie-inhibeerder se vorm vir vier verskillende ontwerpe bestudeer. Die studie het getoon dat die beste resultate vir vloeikarakteriserende eienskappe en oppervlak-turbulensie verkry is met ‘n reghoekige ontwerp. Die resultate beklemtoon egter die belangrikheid van die invloed van die turbulensie-inhibeerder se vorm op die vloeigedrag in die verdeeltrog, aangesien elke vorm noemenswaardige verskillende vloeipatrone opgelewer het. Daar is opgemerk dat ‘n goeie turbulensie-inhibeerder ‘n optimale hoeveelheid turbulensie onderdrukking veroorsaak. In die geval van te min onderdrukking is die verblyftye te kort en die oppervlak turbulensie te hoog. Te veel onderdrukking kan egter lei tot groot variasie in die eienskappe van die metaal by die verskillende uitlate.

Stellenbosch University http://scholar.sun.ac.za

Acknowledgements

Firstly, I want to thank my parents for their influence over the years. I do not think a future researcher could have been raised in a better environment. To my dad, Schalk, your example shows that there is no limit to what can be achieved with a combination of hard work and a sincere love for what you are doing. To my mom, Alta, I was certainly lucky to have a mother who is a writer and who is willing to provide free proof reading. Without your help this thesis would certainly have been riddled with silly grammatical errors. Together, the two of you provided the perfect support structure that allowed me to chase my dreams and I will forever be grateful for that.

My thanks to my brother, Schalk, for putting me on the path towards the fascinating field that is CFD and for always being willing to contribute to my limited understanding of this complex topic. Your influence in critically analysing numerical problems has certainly had a large effect on how this study was approached and executed.

A special thanks to Janet Schreuder for sharing the last two years with me. Thank you for always understanding when I had to put in long hours and for the support during the tough times. Without the friendship and the laughter that we shared completing this study would have been a much harder task.

I was also lucky enough to be part of a fantastic group of post-graduate students. You certainly tested my ability to focus at some stages, but it was the seemingly endless laughter in the office that allowed us to keep going to the end. Hopefully we can someday get together again for another pub lunch.

Moving to the more technical aspects, I need to thank several people who contributed to my project. Firstly, to everyone in the workshop, without your advice and help there certainly would never have been a physical model, much less one that is in working order. My gratitude also goes to Harry Delport for showing me around the Cisco steel plant. It certainly helped my understanding of the practical aspects of tundish operation. Also, a big thank you to Deside Chibwe and Mohsen Karimi for sharing your experience of physical and numerical modelling with me.

My gratitude also goes to my co-supervisor, Prof. Bradshaw, whose contributions played a vital role in the refinement of this manuscript. Finally, a special thank you to my supervisor, Prof. Akdogan, who headed this project and ensured that I never lacked the resources I required for my study. I am very grateful that you provided the platform for me to follow my interest in the field of CFD and thus steer my future career in this interesting direction.

Stellenbosch University http://scholar.sun.ac.za

Table of Contents

Stellenbosch University http://scholar.sun.ac.za

Stellenbosch University http://scholar.sun.ac.za

Stellenbosch University http://scholar.sun.ac.za

Stellenbosch University http://scholar.sun.ac.za

Chapter 1: Introduction

Steel is one of the materials on which modern society is built and its production forms an integral part of every industrialized economy. Four decades ago the production of steel underwent a major change with continuous casting rapidly becoming the primary method of creating steel. Currently more than 90% of steel is manufactured through this method (World Steel Association, 2009), compared to only 5.9% in 1971 (International Iron and Steel Institute, 1978). The global annual production of steel through continuous casting now exceeds 800 million tonnes (Thomas, 2004).

1.1. Problem Statement

With the emergence of continuous casting the tundish was developed as an additional vessel in the steelmaking process, serving as a buffer between the batch ladle process and the continuous casting process. However, with the increase in the requirements for high quality steel products the function of the tundish has evolved as well. Many tundish now also serve the purpose of acting as the last metallurgical vessel before casting, where the final steps of temperature and compositional control are performed. In terms of compositional control, the primary focus of the tundish is the removal of non-metallic inclusions. These inclusions are of concern as they can affect the forming process after casting and the properties of the final steel product. Therefore, the presence of large inclusions in sufficient quantities can make a steel product unsuitable to perform its purpose.

Fortunately, since non-metallic inclusions are less dense than molten steel, buoyancy will cause the inclusions to rise in a metallurgical vessel. This allows the removal of these inclusions if sufficient residence time and an accommodating surface slag layer exist for their flotation. In this study the term flotation will refer to the rising of the inclusions due to the buoyancy forces acting upon these lower density particles. Since the tundish must be sufficiently large to perform its purpose as steel reservoir, it also provides a large residence time. With appropriate design, flow behaviour within the tundish can facilitate the flotation and removal process of inclusions. Sahai and Emi (2008) lists a number of important factors to consider when designing for flow that will enhance inclusion removal as: minimum spread of residence times, minimum dead volume, large plug to dead volume fractions and relatively large plug to mixing volume fractions, surface directed flow, a quiescent slag layer and regions of contained mixing. These can be achieved through the correct choice of the design and operating variables that influences the tundish flow behaviour. Some of the important factors are listed as follows:

Stellenbosch University http://scholar.sun.ac.za

- Design variables
  - Tundish shape
  - Volume
  - Aspect ratio
  - Wall angle
  - Number of outlets
  - Outlet position
  - Flow control devices
    - Type
    - Position
    - Size
- Operating variables
  - Throughput rate
  - Melt depth
  - Operating temperature

It is therefore obvious that many factors will influence the performance of the tundish in its role to maximize inclusion removal. The potential of designing the tundish to improve the quality of the steel product through inclusion removal has triggered a large amount of research in the last 25 years, with most of the work done summarised in two review papers (Mazumdar & Guthrie, 1999; Chattopadhyay et al., 2010). These studies used a combination of physical and numerical modelling, as well as industrial experiments, to gather information regarding operation and design of tundish to improve inclusion removal. However, as is the case for most metallurgical processes, the high temperature and opaque nature of the process limits the use of industrial studies in investigating tundish flow behaviour. Additionally, the high operating cost prevents extensive experimentation.

For this reason the most common approach to tundish studies is through physical and numerical modelling. In physical modelling a room temperature water model is used to represent the high temperature, molten steel operation. This model is also frequently of a reduced size to decrease the cost of construction and operation. However, for the water model to behave in a similar manner to the industrial tundish, the physical dimensions and operating conditions should be chosen to meet certain similarity criteria. Possible criteria include geometric, dynamic, kinematic, chemical and thermal similarity. The choice of similarity criteria to be met in the physical model will depend on the aspects of the system that are important to be captured in the physical model.

Numerical modelling, on the other hand, solves the numerical equations governing the behaviour of the system to predict the flow taking place. Since a solution of the flow properties is obtained for the entire flow domain, the information can help to promote understanding of how various factors will influence the flow behaviour. Additionally, once an accurate numerical model is obtained, different design and operating conditions can be

Stellenbosch University http://scholar.sun.ac.za

quickly evaluated at little cost. However, for the numerical model to accurately simulate the real process well-informed choices must be made during the modelling procedure. For this reason, numerical results are often used in conjunction with experimental data in order to validate the predicted results.

Despite the number of published numerical studies of tundish behaviour, detailed information regarding the setup of the numerical models is generally unavailable. This makes repetition of simulations difficult and may prevent understanding of why certain conclusions are reached in literature. Also, due to the nature of numerical modelling of tundish flow, several assumptions are widely applied in tundish studies to reduce the computational times to practical lengths. However, the assumptions of symmetry (Tripathi & Ajmani, 2011; Tripathi & Ajmani, 2005; Jha et al., 2001; Jha et al., 2008), a flat, frictionless surface (Tripathi & Ajmani, 2011; Tripathi & Ajmani, 2005; Jha et al., 2001; Zhong et al., 2007; Kumar et al., 2008; Mishra et al., 2012) and dynamically steady flow (Tripathi & Ajmani, 2011; Tripathi & Ajmani, 2005; Jha et al., 2001; Zhong et al., 2007; Kumar et al., 2008; Mishra et al., 2012) are expected to affect the predicted results. Despite their frequent application, discussion of the extent of the influence of these assumptions on numerical predictions is limited.

Using the tools of physical and numerical modelling, a number of aspects of the tundish have been studied, but the possibilities of topics for investigation have by no means been depleted. A particularly popular topic is the use of flow control devices, which serves to alter the flow from that which would have occurred in a bare tundish. These changes in the flow behaviour may increase the residence time and plug flow volume fraction, which will aid inclusion flotation. They can also create surface directed flow, which will bring the inclusions into contact with the slag for absorption. Different flow control devices that have been shown to aid tundish flow performance are dams (Kumar et al., 2008; Qu et al., 2012; Jha et al., 2008), weirs (Qu et al., 2012; Miki & Thomas, 1999), baffles (Zhong et al., 2007; Merder & Warzecha, 2012) and turbulence inhibitors (Kumar et al., 2007; Jha et al., 2001; Tripathi & Ajmani, 2005; Zhong et al., 2007). Several novel approaches have also been investigated, such as the use of argon bubbling to alter flow and float inclusions (Zhang et al., 2011; Zhong et al., 2008), the use of electromagnetic forces to obtain the desired flow patterns (Ilegbusi & Szekely, 1989; Tripathi, 2011) and the use of a swirling ladle shroud to dissipate turbulence at the inlet (Solorio-Diaz et al., 2004).

One of the methods of flow control in tundish is to use a turbulence inhibitor. Turbulence inhibitors consist of a high density refractory material, which enables them to reduce erosion of the tundish bottom caused by the inlet stream. Additionally, the turbulence inhibitor suppresses the high velocity flow in the inlet region to allow tranquil flow through the bulk of the tundish, which aids the removal of inclusions. A number of studies have discussed the benefits of employing a turbulence inhibitor (Zhong et al., 2007; Kumar et al., 2008), with general observations being the prevention of short circuiting present in a bare

Stellenbosch University http://scholar.sun.ac.za

tundish, increase in residence time and plug flow volume fractions and reduction in dead volume. Several different approaches to turbulence inhibitor design are found in literature (Kumar et al., 2008; Tripathi & Ajmani, 2005; Bolger & Saylor, 1994; Jha et al., 2001). However, information on the relative performance of each design is limited, as well as the influence of the dimensions of the turbulence inhibitor.

Many studies on tundish have focussed on single strand or symmetrical two strand designs, where the properties of the melt are similar at the different strands. Less research has been devoted to multi-strand tundish, where there might be large variations in the composition and temperature of the melt arriving at different outlets. Although the general criteria for good flow performance remain the same, for multi-strand tundish the similarity between different strands becomes important in order to reduce product variability. Several studies have shown that considerable variation occurs between strands in most multi-strand tundish designs. Appropriate tundish design should therefore be able to reduce the variation between strands significantly (Tripathi & Ajmani, 2005; Jha et al., 2001; Zhong et al., 2007; Merder & Warzecha, 2012).

1.2. Scope and Limitations

This study will specifically investigate the effect of different turbulence inhibitor designs on the flow behaviour in a multi-strand tundish. To allow this, other design and operating variables that influences tundish performance will be maintained constant. For this purpose the geometry and operating conditions of the tundish in this study will be based on that used in a previous study by Kumar et al. (2008).

To evaluate the performance of the different tundish designs, residence time distribution (RTD) experiments will be performed. By measuring the time that portions of the tracer spend in the tundish, certain conclusions can be drawn regarding the flow behaviour. Quantities calculated from the RTD response will be used as criteria by which to judge the performance. Such quantities include mean and minimum residence times and plug and dead volume fractions calculated from the modified mixed flow model by Ahuja and Sahai (1986).

Numerical modelling results will reveal further information on the flow patterns forming in the tundish under different design conditions. An aspect of the flow behaviour that will be of particular concern is the turbulence levels near the top surface of the melt, since excessive turbulence can cause the slag to be entrained and large inclusions to be formed. To ensure accuracy of the numerical results, the model will be validated by comparing the predicted RTD response with those obtained in physical experiments. Additionally, aspects such as grid size and the numerical assumptions of symmetry and dynamically steady flow will be analysed in detail to ensure that the numerical model yields accurate results within reasonable computational times. One aspect of the numerical model influencing the accuracy of the predicted flow behaviour, which will not be evaluated, is the choice of

Stellenbosch University http://scholar.sun.ac.za

turbulence model. Instead, previous work on turbulence model selection (Jha et al., 2003; Chattopadhyay et al., 2010) will be used to select an appropriate method for modelling turbulence.

During both the physical and numerical modelling procedures the flow is assumed to be isothermal. In reality heat losses will cause the melt to cool after entering the tundish. Due to the effect of buoyancy the hot incoming melt will tend to rise in the tundish, causing changes in the flow patterns. Previous studies have shown that this effect on the flow behaviour is significant (Miki & Thomas, 1999; Liu et al., 2008). Despite this, isothermal modelling of tundish flow remains a popular approach (Tripathi & Ajmani, 2011; Kumar et al., 2007; Jha et al., 2008), as the isothermal results still aid in understanding the tundish behaviour without having to deal with the challenges presented by including non-isothermal effects in both the physical and numerical model. The scope of this study is therefore limited to isothermal flow to allow efforts to be concentrated on tundish design and the numerical modelling setup.

1.3. Objectives

The main objective of this study will be to contribute to the knowledge available on tundish design and modelling procedure, with emphasis on the use of turbulence inhibitors. This broad objective will be reached through the following steps:

- The design and construction of a ½ scale water model that accurately replicates the flow behaviour in the high temperature steel process, assuming isothermal flow. This model will be based on the geometry used by Kumar et al.(2008)
- Development of a numerical model of the physical model. The effects of several aspects of the numerical model on accuracy and computational time will also be evaluated:
    - Grid size and meshing strategy
    - Symmetry
    - Dynamically steady flow
    - Inlet boundary position
- Validation of the numerical model by comparison with physical model results.
- Analysis of three tundish configurations, using both the water model and the numerical model based on the water model to demonstrate the effect of flow control devices on tundish flow. The three configurations that are used are:
    - A bare tundish with no flow control devices
    - A tundish using a turbulence inhibitor
    - A tundish using a turbulence inhibitor with holes in the sides, in combination with dams

Stellenbosch University http://scholar.sun.ac.za

- Modification of the numerical model for simulating the high temperature molten steel process. This will also serve as additional validation for the physical modelling procedure used.
- Comparison of flow patterns predicted by the numerical model of the industrial process for four different turbulence inhibitor shapes:
    - A rectangular turbulence inhibitor with a flange at the top
    - A round turbulence inhibitor with a flange at the top
    - A rectangular turbulence inhibitor without a flange
    - A rectangular turbulence inhibitor with chamfered flanges

Stellenbosch University http://scholar.sun.ac.za

Chapter 2: The Tundish

2.1. An Introduction to the Tundish

The tundish performs the important role of serving as a buffer tank between the batch ladle process and continuous casting. It is also the last metallurgical vessel before continuous casting; therefore it plays an essential role in delivering steel with the correct composition, quality and temperature. This function has become increasingly important over the last couple of decades with increasingly stringent requirements for the quality of steel products. This section will give a brief overview of the development of the tundish, before investigating important aspects of tundish operation.

2.1.1. Continuous Casting

In modern steelmaking plants, steel is produced using either a basic oxygen furnace (BOF) or an electric arc furnace (EAF). In the BOF pathway molten pig iron and scrap metal are blown with oxygen and flux, such as lime, is used to remove carbon, silicon, sulphur and phosphorous. In the EAF process steel is produced by melting and refining scrap steel, also with oxygen blowing and flux addition. The molten steel is then tapped to a ladle, where it is deoxidised. The deoxidation products, including silica, manganosilicates, alumina, aluminosilicates and aluminates, are removed from the melt by flotation. The melt is then transferred to a tundish, from which it is cast into slabs, blooms or billets. (Pehlke, 2012)

Historically, casting was done in the form of ingots. In this process steel melt is poured into a hollow cast iron mold and allowed to solidify. Pouring can be done by two methods, either from the top or the bottom. During top pouring the stream entering the melt surface entrains reoxidation products and scum, forming macro-inclusions. Splashed metal during filling will adhere to the ingot walls and form surface defects on the product. By using bottom pouring these problems are avoided. However, the steel is fed to the mold through channels lined with refractory bricks. The longer exposure of the melt to refractory materials can cause contamination of the product. Another problem with ingot casting is that during solidification segregation of crystals takes place in the ingot, which may adversely affect the quality of the final product. Several methods exist to overcome these difficulties and ingot casting can be used to deliver products within very stringent quality requirements. However, even for these processes the top and bottom of the ingot has to be cropped, substantially decreasing the yield of the process. (Sahai & Emi, 2008)

An alternative process, called continuous casting, was first proposed in the 19th century, with the first patent for continuous casting lead tubing being granted in 1840 to G.E. Sellars (Irving, 1993). In 1865 H. Bessemer was granted the patent for continuous casting of malleable iron using rotating rolls (Bessemer, 1865). However, industrial advances were limited until the 1940's when the first pilot plants for continuous casting of steel were installed (Irving, 1993). The next 30 years saw the intensive development of the continuous

Stellenbosch University http://scholar.sun.ac.za

casting process, with large scale industrial application following in the early 1970's. Since then, the global average of steel cast through continuous casting has increased to approximately 92.8% in 2008 (World Steel Association, 2009), compared to 5.9% in 1971 (International Iron and Steel Institute, 1978).

Several advantages of continuous casting over ingot casting were the cause for the rapid change in the steelmaking industry (Sahai & Emi, 2008; Irving, 1993). Firstly, since more than three heats of steel can be cast sequentially during continuous casting, only the beginning and ending portions of the strand are generally discarded, allowing a much better yield than in ingot casting. Also, compared to normal ingot casting, continuous casting produces products with much better and more consistent internal and surface quality due to reduced segregation and fewer macro-inclusions. Generally continuously cast strands are more similar in shape to the final products than ingots; therefore the roughing mill can be eliminated in some cases. Further technological advances have made it possible to hot charge as-cast strands into the reheating furnace or to hot roll the strands directly. This reduces yield loss, since both techniques eliminate the need for surface conditioning. By eliminating the need for reheating the energy consumption of casting is also reduced. Finally, modern continuous casting processes allow high withdrawal rates without compromising the quality; therefore continuous casting allows a high throughput rate for the casting process.

2.1.2. The Role of the Tundish

For continuous casting to be possible, an intermediate vessel is required between the ladle and the continuous casting machine to serve as a reservoir, allowing casting to continue while ladles are changed. This is the primary purpose of the tundish. The tundish is a refractory-lined vessel with a variety of possible geometries, but most commonly roughly rectangular in shape. It is designed to deliver molten metal at a designed output rate without major fluctuations in the flow. The flow rate is primarily controlled by the depth of the melt. Further control of the outlet flow can be performed by either stopper rods or slide gates. The number of outlets depends on the type of casting performed. Usually there are 1 to 2 molds for a slab caster, 2 to 8 for a bloom caster and 3 to 8 for a billet caster (Irving, 1993).

Since the tundish is the final stage in the steel making process before casting, it also presents the last opportunity for compositional control of the melt. There is a constant demand for steel with improved properties, such as increased strength, ductility, durability and corrosion resistance, which is required for a large variety of applications. Then there is also the desire to make the steelmaking process more energy and cost efficient and to address environmental concerns. These issues promoted the evolution of the tundish into a metallurgical reactor, with the function of performing final control over the properties of the melt before casting to obtain a final steel product with the desired mechanical properties.

Stellenbosch University http://scholar.sun.ac.za

The main form of compositional control in the tundish is by limiting the number and size of non-metallic inclusions in the melt when casting takes place. Inclusions can cause problems during casting, rolling and heat treating processes and can result in the failure of the steel product during its application. For example, inclusions can cause cracked flanges due to lack of formability in LCAK steel cans and lower fatigue lives in axles and bearings (Sahai & Emi, 2008). This is due to the fact that both fatigue life and formability is highly affected by oxide and sulphide inclusions (Lange, 1988). An example of problems caused during forming is sliver defects, which occur as lines parallel to the rolling direction along the steel grip surface (Sahai & Emi, 2008). Slivers are problematic in LCAK steel sheets used in the automotive industry and originate from aluminates or complex non-metallic inclusions.

Another potential problem caused by inclusions is the clogging of both the nozzle into the tundish and the submerged entry nozzle into the mold (Sahai & Emi, 2008), which can have several detrimental effects on the steelmaking process. Firstly, clogs can dislodge from the nozzle and will either be captured in the steel or in the flux, changing its composition. Both of these cases will cause defects to form in the product. Clogs will also change the flow patterns in the nozzle, which might disrupt flow in the mold. Finally, flow rate control devices may cause interference with level control in the mold when compensating for the clog.

These problems tend to worsen with increased concentration of inclusions, as well as with the maximum size of inclusions present. For different applications there are limits to the maximum size, termed the critical inclusion size, and number of inclusions. Steels with more demanding processing and applications generally have a lower critical inclusion size and number density. Table 2.1, compiled by Emi (1999), shows the critical inclusion size for process upsets and product defects for several steel products.

Table 2.1 - Critical inclusion size of macro-inclusions in cast semis that cause process upsets and product defects (Emi, 1999)

Steel products	Critical inclusion size (µm) in Slabs* or Blooms**
Cold rolled sheet	240*
DI-Can	50*
UOE-Pipe	200*
ERW-Pipe	140*
Cold forgings	100**
Steel cord	30**
Ball bearing	15*

Stellenbosch University http://scholar.sun.ac.za

The number and size of inclusions in the melt exiting the tundish are reduced by preventing the formation and growth of inclusions in the tundish, as well as by removing inclusions that are carried over from the ladle to the tundish. It is therefore also critical that the correct practices must be followed during ladle operation to lower the amount of inclusions contained in the melt being delivered to the tundish.

Another important function of the tundish is to control the temperature of the melt delivered to the continuous casting process (Sahai & Emi, 2008). Since pouring of melt from the ladle can take up to an hour, the temperature of the inlet stream will change with time. Coupled with the heat losses in the tundish itself, the temperature of the melt being cast can therefore be expected to fluctuate during a casting sequence. However, the melt temperature influences the quality and properties of the product, caster operation and refractory wear. It is therefore desired to limit fluctuations and to keep the temperature as close to the optimal value as possible. Since the tundish operates as a buffer tank, fluctuations in the temperature of melt delivered to the caster can be reduced significantly if the mixing in the tundish is sufficient.

2.2. Non-Metallic Inclusions

Non-metallic inclusions include oxides, sulphides, nitrides, carbides and their compounds. Some inclusions, such as sulphides, carbides and nitrides, will form below the liquid temperature of steel. However, mostly large oxides and some sulphides will form in the molten steel. These inclusions will have a negative effect on the product if they are not removed before the casting process. Sulphide inclusions can be minimised by desulphurization in the ladle, therefore oxide inclusions are the most important to consider in the tundish, as they occur in significant quantities in the melt transferred from the ladle to the tundish (Sahai & Emi, 2008).

In the tundish inclusions can have different compositions, shapes and sizes depending on the upstream processes employed during steelmaking. Some typical compositions are Al_2O_3, CaO-(MgO)-Al_2O_3, CaO-Na_2O-SiO_2-Al_2O_3 and CaO-MgO-SiO_2-Al_2O_3 (Emi, 1999). Inclusions can be divided into size categories with macro-inclusions generally larger than 50µm and micro-inclusions smaller than 50µm (Sahai & Emi, 2008). Due to a weaker buoyancy force on a tiny particle, smaller inclusions will have a slower rise velocity and will therefore be more difficult to remove by flotation to the slag layer. The means of origin can also be used to subdivide inclusions. Exogenous inclusions form when the melt re-oxidises when it comes into contact with air or oxidising slag or when the melt entrains slag or refractory materials. Indigenous inclusions form in the melt from the reaction between dissolved oxygen and deoxidising elements added to the melt, such as silicon or aluminium. The nature of the origin of the inclusion will determine the size, which will influence its effect on the product

Stellenbosch University http://scholar.sun.ac.za

and the difficulty of removing it from the melt by flotation. The origin of the inclusion will also determine the method used to prevent its formation.

2.2.1. Exogenous Inclusions

Exogenous inclusions are generally much larger than indigenous inclusions; therefore the prevention of their formation is more important, since they can seriously affect the quality of the product. They are also often formed at a stage that allows little time for flotation before reaching the casting machine, further increasing the importance of their prevention. There are multiple ways in which exogenous inclusions may form (Sahai & Emi, 2008):

- Reoxidation of the melt
    - Reoxidation due to air ingress at the joints of the tundish nozzle, slide gate or the submerged entry nozzle in the caster
    - Reoxidation due to air ingress at the surface of the tundish
    - Reoxidation by oxidation products, such as iron oxide, manganese oxide or silica, that are either carried over from the ladle or formed by the flux added to the tundish
- Entrainment of slag.
    - Entrainment by vortexing or draining of ladle slag into the melt flowing to the tundish
    - Entrainment of the tundish slag by the impinging stream during ladle opening and changeover
    - Entrainment of the tundish slag by turbulent flow at the slag-melt interface
    - Entrainment of the tundish slag due to vortexing to the outlets when the tundish is operated at a low level
- Refractory wear
    - Reoxidation of the melt by less stable oxides contained in the tundish glaze, the nozzle and the tundish lining
    - Erosion of the ladle glaze, ladle nozzle, tundish lining or submerged entry nozzle due to turbulent flow
- Dislodging of deposits
    - Dislodging of alumina clusters deposited on the inner wall of the tundish nozzle and submerged entry nozzle by turbulent flow

2.2.2. Indigenous Inclusions

Indigenous inclusions are formed by the deoxidation reaction and are generally much smaller in size than exogenous inclusions. Indigenous inclusions therefore have a smaller impact on product quality, unless they agglomerate during melt transfer to form larger inclusions.

During the deoxidation reaction, shown in equation 2.1, a deoxidising element (M) dissolved in the melt, such as Mn, Si or Al, reacts with oxygen dissolved in the melt to form an oxide.

Stellenbosch University http://scholar.sun.ac.za

The dissolved oxygen is present due to the use of oxygen injection in the steelmaking process to reduce carbon to the desired concentration. Nucleation and growth of the oxides form liquid inclusions, solid inclusions and clusters of solid inclusions. The reaction often proceeds until thermodynamic equilibrium is reached. The details of these reactions and their thermodynamics will not be discussed here, since they are of little importance to this study. (Sahai & Emi, 2008)

$$n[M] + m[O] \leftrightarrow M_n O_m \qquad [2.1]$$

2.2.3. Methods of Preventing Formation of Inclusions

Throughout the development of the industrial tundish, numerous alterations have been made to the process to prevent inclusion formation. Some of these technologies are briefly discussed in this section, since they will have an effect on tundish design and operation to produce clean steel.

Tundish flux

The tundish flux has several purposes (Irving, 1993), one of which is to prevent the reoxidation of the melt by the atmosphere. It also provides thermal insulation to prevent heat loss from the melt surface and absorbs non-metallic inclusions that rise to the top of the melt. The composition of the flux must be such that it melts quickly in contact with the molten steel, readily absorbs inclusions, remains inert and is not reduced, is not easily entrained into the steel, does not contain oxides which act as a source of oxidation and is gentle on the refractory lining and the ladle shroud (Sahai & Emi, 2008). The properties that govern these factors include the viscosity, melting temperature, interfacial temperature and inclusions solubility. Often, a compromise needs to be made between properties. For example, rice hull, one of the most common tundish fluxes, which contains up to 90% SiO_2, reduces heat loss to a large extent, but is inadequate in accepting inclusions (Sahai & Emi, 2008).

Shrouding during melt transfer from ladle to tundish

To produce clean steel it is important to prevent reoxidation of the melt by the atmosphere when the melt is being poured from the ladle to the tundish. It has been found that reoxidation during pouring can account for 40% of the inclusions in steel and that these inclusions are larger than 100µm in size (Ohno et al., 1974), and will therefore have a significant effect on the product if not removed. Two methods of metal stream shrouding, shown in Figure 2.1, are possible (Sahai & Emi, 2008): physical shrouding by enclosing the stream by a refractory pouring tube or shrouding with argon gas. A combination of the two methods can also be used, where argon is injected into the pouring tube. The injection of argon bubbles will alter the flow patterns in the tundish and can enhance inclusion removal due to particles being captured by the faster rising gas bubbles. However, if argon is present in sufficient quantities it can cause the slag layer to be disturbed. Also, the complicated

Stellenbosch University http://scholar.sun.ac.za

multiphase nature of this process will be difficult to model, therefore most numerical studies are limited to a liquid only system.

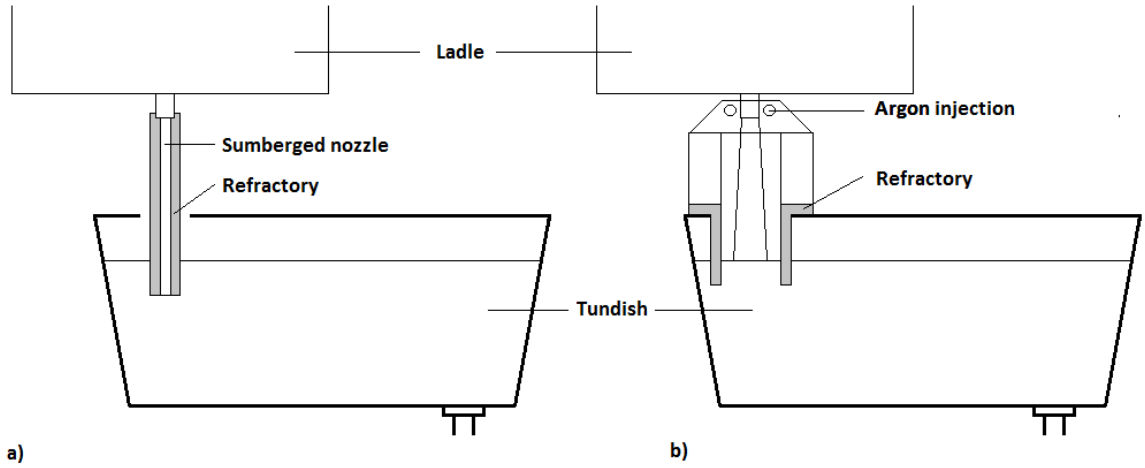

Figure 2.1 - Schematic representation of melt transfer from the ladle to the tundish with a) a long submerged nozzle and b) by enveloping the pouring stream with argon gas

Several studies have proven the usefulness of inlet stream shrouding. At Bao Steel, using a submerged ladle nozzle decreased nitrogen pickup from 24 ppm to 3 ppm (Zhang & Cai, 1997), while at British Steel Ravenscraig Works it was lowered from 14 ppm to 3 ppm (McPherson, 1985). The decrease in nitrogen pickup gives a good indication of the expected decrease in reoxidation of the melt.

Unfortunately there are also some disadvantages associated with the inlet stream shrouding technologies (Sahai & Emi, 2008). The use of a submerged nozzle will increase the erosion rate of the impact pad, especially if the melt depth is insufficient, causing more macro-inclusions to form. It also reduces the filler sand removal and prevents visual detection of ladle slag carry-over. However, the latter two problems can be reduced by altering the composition of the filler sand and by using modern slag sensing devices in the process control system.

Slag sensing technologies

Several technologies exist in modern steelmaking to prevent slag carryover from the ladle to the tundish, by detecting the presence of slag in the melt stream. Methods that have been used include visual observation, optical detection based on emissivity and stream diameter, vibration analysis, weight monitoring using the difference of metal and slag densities and using a slag float valve, which floats at the slag-metal interface (Sahai & Emi, 2008).

However, the most common approach is the use of an electromagnetic sensor to detect the presence of slag. In this method an electromagnetic field is induced in the metal by passing current through a primary coil. Because the electrical conductivity of the slag is significantly lower than that of the metal, the presence of the slag can be detected by measuring the

Stellenbosch University http://scholar.sun.ac.za

eddy currents in a secondary coil. The sensor signal can control the slide gate to stop flow when a predetermined signal strength is detected. (Irving, 1993)

Sealing and argon protection

To prevent inclusions from forming it is of importance that the melt does not come into contact with the atmosphere, making reoxidation possible. During melt transfer from the ladle to the tundish to the mold, there are several places where air ingress can take place. Sealing at the joints of the shrouds should be good. It has been shown that by improving the bayonet system between the ladle nozzle and ladle shroud the nitrogen pickup could be reduced from 8 ppm to less than 1 ppm, while stiffening the SEN holder and increasing the maintenance on it lowered nitrogen pickup from 1.8 ppm to 0.3 ppm (Cameron, 1992). The risk of oxidation by the atmosphere can also be decreased by flooding the joints with argon gas or pressurizing the shrouds with argon (Sahai & Emi, 2008).

Tundish flux is only added once the melt is flowing, therefore when the tundish is filled, the melt is exposed to the atmosphere during this period. Argon flooding can also be used to purge the tundish prior to ladle opening to prevent oxidation of the melt. Oxidation can further be decreased by using a protective tundish cover with carefully sealed edges. (Sahai & Emi, 2008)

2.2.4. Tundish Flow for Inclusion Removal

As mentioned previously, one of the main functions of the tundish is to remove inclusions that form during the upstream steelmaking processes. Since the density of non-metallic inclusions is lower than that of steel, given enough time the inclusions will be floated to the top of the melt. If the correct flux material is used, the inclusions will be absorbed in the slag, preventing them from compromising the steel quality. However, because of the size of some inclusions, the buoyancy force on them is small and they will require a significant period of time to rise. This is especially a problem in applications where the product has a low critical inclusion size, requiring the removal of very small inclusions. There are several principles that can be followed to obtain flow that promotes the flotation of inclusions.

Firstly, a longer residence time will allow more time for inclusions to be floated before exiting the tundish, lowering the average inclusion size in the product. For this reason it is also very important to prevent short-circuiting of flow directly from the tundish inlet to the outlet. In this case a fraction of the flow will spend a very small amount of time in the tundish, allowing even large inclusions to reach the mold.

A shallow melt depth will decrease the distance inclusions must travel to the flux and therefore the residence time required for flotation. However, a melt level that is too low can lead to vortex formation at the outlets, causing the slag to be entrained in the mold, causing severe defects in the product.

Stellenbosch University http://scholar.sun.ac.za

Surface-directed flow will bring inclusions in close proximity with the slag layer for absorption. However, this usually also results in more turbulent flow at the slag/melt interface. The presence of turbulent eddies can entrain the slag into the melt, forming macro-inclusions.

Additionally, flow patterns that have gentle, plug-flow like behaviour will allow the flotation of inclusions, whereas strong mixing flows may entrain some particles and prevent them from rising. However, mixing in the tundish is also required to promote thermal and compositional homogeneity.

Dead volumes as slow moving or completely stagnant regions in the tundish are problematic due to two reasons. Firstly, since the average residence time stays the same at a constant volumetric flow rate, slower moving fluid that spends long periods in the tundish means that an equivalent amount of fluid has a much shorter residence time. Large inclusions in this part of the melt flow may not have sufficient time for flotation. The second problem is that the melt in these areas will cool down significantly due to heat loss and may start to solidify or may influence thermal homogeneity in the product.

2.3. Tundish Modelling Literature

The opaque and high temperature nature of most pyro-metallurgical processes makes it nearly impossible to measure or see what is happening inside the various reactors. Because of this, for many years tundish were designed and operated with little understanding which led to poor performance.

Physical modelling was the first tool available for researchers to gain a better understanding of what was actually taking place inside of these reactors and to use this information to improve the performance by changing design and operating parameters. By performing residence time experiments an approximate idea of the flow pattern could be derived from the time certain portions of the fluid will spend in the tundish. However, it remained difficult and expensive to obtain detailed information about the exact flow patterns. This is where numerical simulation using computational fluid dynamics (CFD) has a vital role to play. CFD has the important benefit that it solves the flow for the entire flow domain, therefore making it possible to view values of various properties, including turbulence values and velocities, in any region of the tundish. Obviously this will provide a much clearer understanding of what exactly is taking place in the tundish, allowing better designs to be proposed and tested.

Over the last couple of decades vast amounts of literature have been published regarding tundish design and operation through modelling, as summarised in two detailed review papers (Mazumdar & Guthrie, 1999; Chattopadhyay et al., 2010). These studies used either physical or numerical modelling, or a combination of the two to investigate various aspects of the tundish. These included subjects such as the effect of tundish design dimensions,

Stellenbosch University http://scholar.sun.ac.za

operating conditions and flow control devices on flow characteristics, flotation of inclusions, temperature distribution and the effect of nozzle clogging. This study will primarily investigate the effect of turbulence inhibitors on the flow behaviour in a multi-strand tundish. Therefore, this section will seek to highlight information that is relevant to the design of a multi-strand tundish with flow control devices.

2.3.1. Turbulence Inhibitors

The melt stream enters the tundish through the submerged nozzle at a relatively high velocity and turbulence. The impact of the incoming stream on the bottom of the tundish can be such that it leads to significant erosion of the refractory. The eroded refractory, in turn, leads to the formation of new inclusions that will be detrimental to the product, as well as an increased operational cost required to repair the refractory. A pour pad of very dense, chemically stable refractory material is typically used to prevent this erosion. Although the pour pad is often only a horizontal slab of different material, various shapes of pour pads have also been introduced to alter the direction of the incoming stream. The diverged incoming stream, upon meeting the surface, then becomes quiescent, hence the name of turbulence inhibitors. The resulting flow is much more suitable for inclusion flotation.

A study pertaining to turbulence inhibitors that is of particular importance to the research in this thesis is that of Kumar et al. (2008), since the same geometry is used in this study. The geometry was selected from literature for use in this study to allow the primary focus to be on the effect of flow control devices in an existing multi-strand tundish design. In the study by Kumar et al. (2008) the authors compared three configurations: a bare tundish, a tundish with dams between the inlet and outlets and a tundish with a turbulence inhibitor with holes in the sides, in combination with low dams. This comparison was done using both physical and numerical modelling. It was found that the use of the dams can prevent the short-circuiting that plagues the bare system. However, the case with the turbulence inhibitor with holes and dams was the superior of the three cases with regards to flow for inclusion removal, yielding a significantly longer mean residence time, a larger fraction plug flow and also less dead volume. Additionally, the variation between strands was significantly lower than for the other two configurations.

The turbulence inhibitor used by Kumar has a simple box-like shape, with a square opening at the top to allow upward flow. The turbulence inhibitor, as well as the general layout of the tundish used in the configuration containing a turbulence inhibitor with holes and dams, is shown in Figure 2.2.

Stellenbosch University http://scholar.sun.ac.za

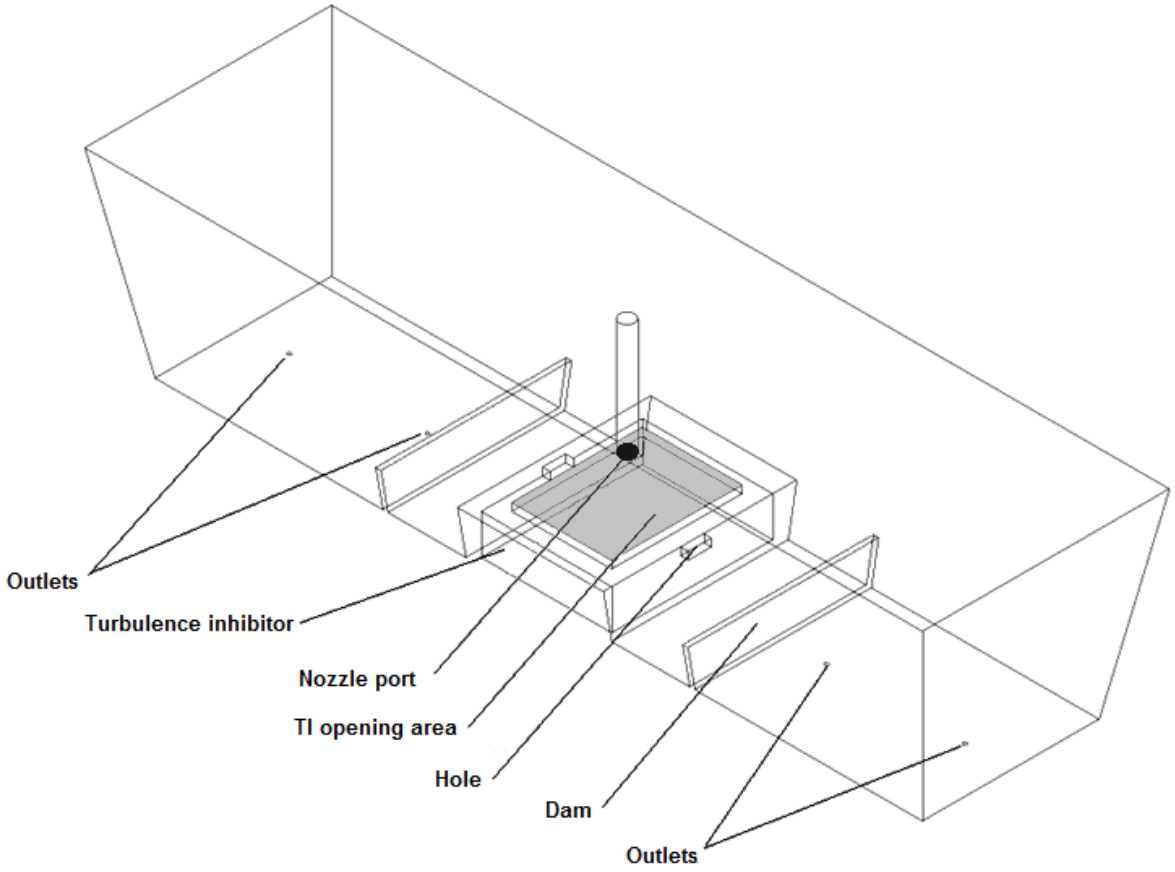

Figure 2.2 - Layout for the tundish with turbulence inhibitor with holes and dams as used by Kumar et al. (2008)

Several other variations of turbulence inhibitors are found in literature. Bolger and Saylor (1994) used a turbulence inhibitor with a circular wall, with an inward facing flange at the top. The walls of turbulence inhibitors are often sloped inward, as shown in Figure 2.3, for the design used by Tripathi and Ajmani (2005). In this study, based on a six strand, curved shape, billet tundish, it was found that the contoured design of the turbulence inhibitor increased the mean residence time and plug flow fraction over the case with sharp edges.

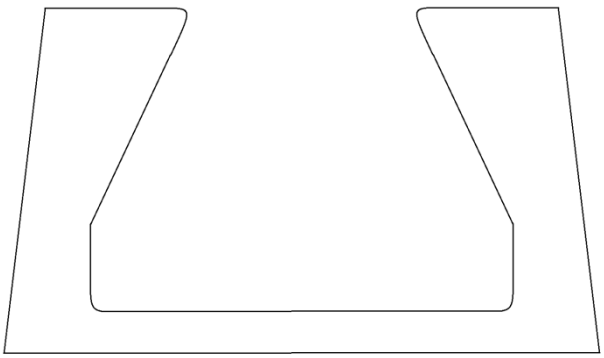

Figure 2.3 - An approximate sketch of the turbulence inhibitor shape along the longitudinal plane of the design used by Tripathi and Ajmani (2005)

Stellenbosch University http://scholar.sun.ac.za

From a comparison of two different turbulence inhibitors, Tripathi and Ajmani (2011) concluded that the amount of turbulence suppression can be increased by increasing the height of the pouring chamber or by reducing the opening area. However, increased suppression did not necessarily lead to superior flow characteristics. Therefore, it was concluded that the turbulence suppression produced by the design should be optimised with regards to the flow characteristics.

Using a simple turbulence inhibitor design consisting of a square arrangement of vertical walls, Jha et al. (2001) found that in a six strand billet caster, there is an optimum combination of the turbulence inhibitor height, outlet position and inlet nozzle submersion depth.

It is therefore clear from literature that several shapes of turbulence inhibitors can be used, all reducing the turbulence and promoting upward flow. It is also apparent that some shapes will have benefits over each other with regards to the resulting flows. However, a comprehensive comparison of several different designs is not available in the available literature. Also important to note is that the optimal turbulence inhibitor design would depend on the shape and size of the tundish, the nozzle depth and the outlet positions of the specific case.

2.3.2. Multi-strand Tundish

Depending on the type of steel being produced, casting may be performed simultaneously from one to eight outlets. The number of strands being cast will influence the design of the tundish geometry. Figure 2.4 compares the geometry for three different casting operations. The first two figures show a single-strand and a symmetrical two-strand tundish. For the two-strand tundish the melt arriving at the two outlets are expected to have similar residence times and temperatures due to the symmetry of the geometry. However, for the four-strand tundish, and other multi-strand tundish designs, the melt arriving at the two outlets in each symmetrical halve will arrive through significantly different pathways. This can cause the melt at the different outlets to differ in composition and temperature.

Stellenbosch University http://scholar.sun.ac.za

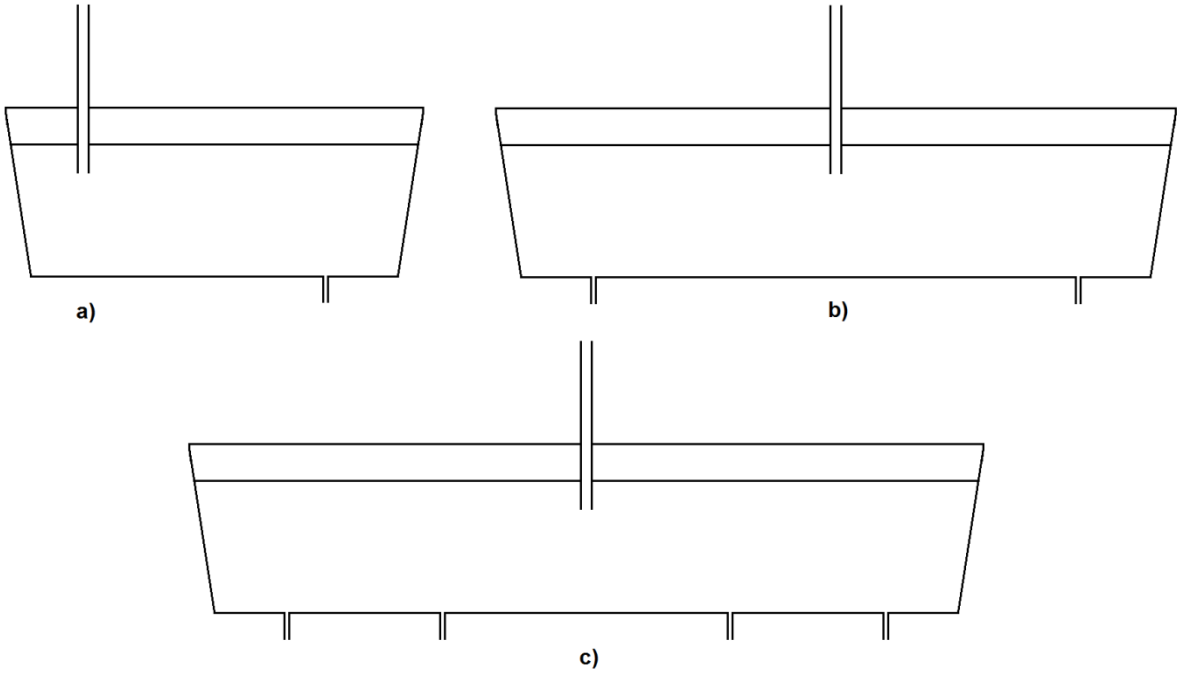

Figure 2.4 - Side views for a) a single strand tundish, b) a symmetrical two-strand tundish and c) a four-strand tundish

Multi-strand tundishes have been the subject of fewer investigations than single strand and symmetrical two-strand tundishes. In general the criteria for flow that will enhance the flotation of inclusions remain the same for multi-strand tundish. However, similarity between strands also becomes important to allow similar melt, in terms of temperature and composition, to be delivered at the different strands. This is essential to allow the different strands to undergo the same forming processes and to prevent unacceptable variation in quality between the products.

Several multi-strand tundish studies were performed on six-strand billet casters. Such a study by Tripathi & Ajmani (2011) indicated that very large differences will occur between the residence time distributions of the three individual strands in each symmetrical half of the tundish. Similarly large variations between strands were observed for a six-strand billet caster in a study by Jha (2001). Numerical simulations for different turbulence inhibitors and distances between the strands indicated that the relative positions of the individual strands are significantly impacted by these factors. Therefore, it should be possible to increase strand similarity through determining the optimal turbulence inhibitor design and outlet positions.

Investigation of a four-strand bloom caster, using a baffle with holes by Zhong (2007), showed variation between the two strands in each symmetrical half, with the C-curve of the inner strand showing a higher and earlier peak value. The addition of a square turbulence inhibitor and optimization of the position of the holes in the baffle decreased the variation in the individual C-curves substantially.

Stellenbosch University http://scholar.sun.ac.za

2.4. Summary

In this chapter the operation of the tundish was discussed. It was seen that although the primary purpose of the tundish is still to serve as a link between the ladle process and continuous casting, it can also aid in producing clean steel by promoting the removal of inclusions and preventing new inclusions from forming. Inclusion removal takes place through the buoyancy force acting on the less dense inclusions in the more dense molten steel, causing them to rise. When reaching the surface, these inclusions will be absorbed in the slag layer, if the correct slag material is used. To maximise the removal of inclusions the flow conditions in the tundish should be such that a large residence time, small dead volumes, large plug flow volumes and surface directed flow occurs. The buoyancy force will be less on smaller inclusions, therefore longer residence times will be required to reduce the maximum inclusion size in the melt leaving the tundish. The size of the inclusions present in the melt depends on the mode through which it had formed. Flow patterns can also play a role in the forming of new inclusions, as turbulent flow at the slag layer may cause the slag to be entrained in the molten steel, forming new inclusions.

It is therefore clear that for both inclusion removal and slag stability the tundish should be designed and operated to produce the desired flow patterns. This can be achieved through the use of flow control devices placed in the tundish. The turbulence inhibitor is an important option as it has been shown in previous studies (Kumar et al., 2008; Tripathi & Ajmani, 2005) that it provides surface directed flow, eliminating short-circuiting, and reduces the turbulence of the incoming melt stream, increasing the residence time and plug flow volume. However, the benefit of the turbulence inhibitor will depend on its size and shape. However, in the available literature a comparison of different turbulence inhibitor shapes have not been made. It was also noted that in multi-strand tundish the similarity of the melt leaving different strands becomes an important factor to consider. In conclusion, better tundish performance can therefore be achieved by controlling the flow taking place through turbulence inhibitor design, keeping in mind inclusion flotation, slag layer stability and strand similarity.

Stellenbosch University http://scholar.sun.ac.za

Chapter 3: Flow Characterization

To fulfil its function of delivering steel with the desired cleanliness, composition and temperature, the tundish must be designed and operated in a way to generate flow patterns that will aid in achieving this purpose. However, it is difficult and expensive to acquire detailed information about the flow throughout the entire system using physical experiments. An alternative approach is to obtain information regarding how long portions of the fluid will remain in the vessel. This information is simple to acquire experimentally and can, in most cases, satisfactorily account for the flow pattern in the vessels. Also, as is the case in this study, this information can be used to validate a CFD model, which can provide detailed information about the flow in the system.

The method used to gain the information about the time fluid spends in the reactor is called the stimulus-response technique. The stimulus is provided by adding a tracer material to the inlet stream and the response is determined by measuring the concentration of the tracer at the outlets. Several different types of materials can be used as tracer, including dyes, salts, acids and radioactive material. Factors that will determine the selection of the tracer are the cost of the tracer and the ease and accuracy of measuring its concentration. It is also desirable that the tracer should behave as similarly as possible to the fluid being used in the system, so that it accurately models the fluid flow. The response is plotted as dimensionless time against dimensionless concentration and is called the Residence Time Distribution (RTD) of the fluid.

Two methods are frequently used to input the tracer to obtain a stimulus. The first option is to change the concentration of the tracer in the inlet flow and maintaining it at that concentration for the duration of the experiment. The concentration of tracer at the outlet will continue to rise until it reaches the inlet concentration. An example of such a response is shown in Figure 3.1 for a tundish CFD experiment. RTD responses obtained from a pulse input and plotted on a dimensionless scale are called F-curves. However, this approach is not practical for this study, because of the high cost of maintaining the tracer concentration in the inlet flow.

Stellenbosch University http://scholar.sun.ac.za

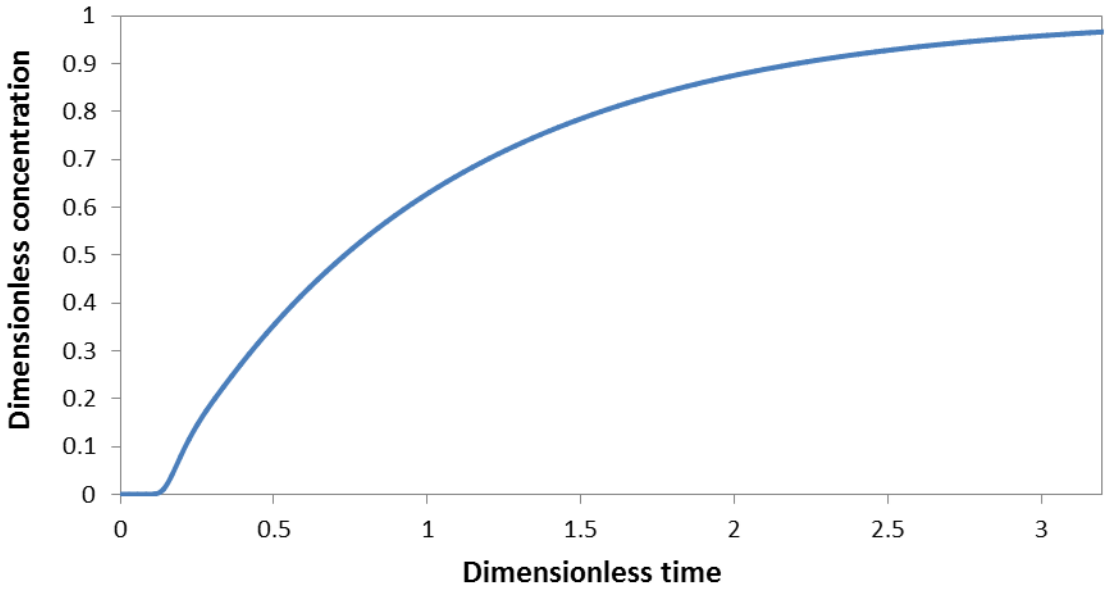

Figure 3.1 - Dimensionless residence time distribution for a step input

The second approach is to inject the tracer as a pulse over a short time and measure the response at the outlet. The response, in dimensionless form, is called the C-curve. An example, shown for the same CFD experiment as for the F-curve, is shown in Figure 3.2. Another advantage of the pulse approach is observed in the example. The response obtained using this method has a much more definitive shape, because of the peak being formed. This is beneficial when comparing the RTD curves visually for different cases. This is the approach that will be followed for this study and will be discussed in more detail.

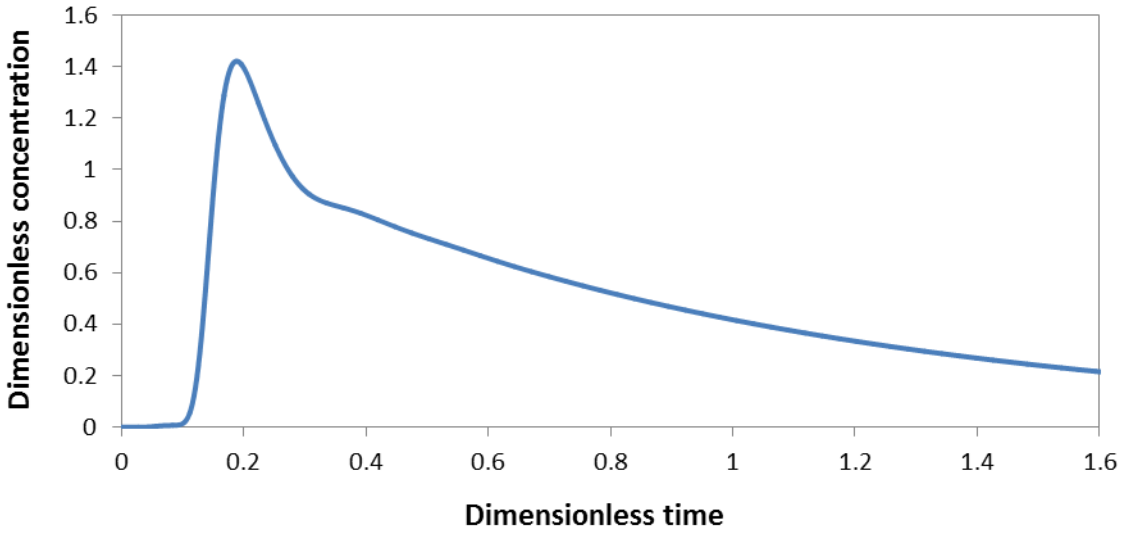

Figure 3.2 - Dimensionless residence time distribution for a pulse input

Stellenbosch University http://scholar.sun.ac.za

3.1. The Dimensionless C-curve

The theoretical average residence time gives an indication of the average time spent by fluid in the tundish. It is defined as follows, where V is the volume of the tundish and Q is the volumetric flow rate:

$$t_{ave} = \frac{V}{Q} \quad [3.1]$$

To obtain the dimensionless time for the RTD curve, the time is divided by the theoretical average residence time, denoted as θ.

$$\theta = \frac{t}{t_{ave}} \quad [3.2]$$

For a pulse input, the dimensionless concentration is defined as:

$$C = \frac{c}{\frac{m}{V}} \quad [3.3]$$

The ratio of $\frac{m}{V}$ gives the average concentration of the mass of tracer added, m, is dissolved in the entire volume of fluid, V.

Using these three equations, the concentration measurement at each of the tundish outlets can be converted to a dimensionless value. Since the outlet flow is driven by gravity, the flow rates at each of the outlets are essentially the same. Therefore, the overall dimensionless concentration can be simply calculated as the average value of the separate outlets for that specific time. In this study C-curves for individual outlets will often be compared to give an indication of strand similarity for a particular tundish design, while the overall C-curves will be used to assess the overall tundish flow performance.

3.2. Mean and Variance of the RTD

To get an idea of the amount of time a fluid element can be expected to spend in the tundish, the mean residence time can be calculated. This is of significance to inclusion removal since it can be expected that the larger the mean residence time, the more time will be available for flotation and the smaller the average inclusion size in the product. The mean residence time for a pulse input is defined as:

$$\bar{t} = \frac{\int_0^\infty tcdt}{\int_0^\infty cdt} \quad [3.4]$$

When the concentration is measured at equal time intervals, equation 3.4 can be simplified as follows:

$$\bar{t} = \frac{\sum_{i=0}^{\infty} t_i c_i \Delta t}{\sum_{i=0}^{\infty} c_i \Delta t} = \frac{\sum_{i=0}^{\infty} t_i c_i}{\sum_{i=0}^{\infty} c_i} \quad [3.5]$$

Stellenbosch University http://scholar.sun.ac.za

For the dimensionless form of the RTD curve this becomes:

$$\bar{\theta} = \frac{\sum_{i=0}^{\infty} \theta_i C_i}{\sum_{i=0}^{\infty} C_i} \qquad [3.6]$$

To get a measure of the spread of the residence time distribution about the mean, the statistical variance can be calculated:

$$\sigma_t^2 = \frac{\int_0^{\infty} (t - t_{mean})^2 c dt}{\int_0^{\infty} c dt} \qquad [3.7]$$

Similarly to the mean, this can be rewritten for equal time intervals and be converted to dimensionless from:

$$\sigma_t^2 = \frac{\sum_{i=0}^{\infty} (t_i - t_{mean})^2 c_i \Delta t}{\sum_{i=0}^{\infty} c_i \Delta t} = \frac{\sum_{i=0}^{\infty} t_i^2 c_i}{\sum_{i=0}^{\infty} c_i} - t_{mean}^2 \qquad [3.8]$$

$$\sigma^2 = \frac{\sum_{i=0}^{\infty} \theta_i^2 C_i}{\sum_{i=0}^{\infty} C_i} - \theta_{mean}^2 \qquad [3.9]$$

3.3. Ideal Flow Models

There are two models for ideal flow in a reactor: plug flow and well-mixed flow, each based on assumptions of the flow behaviour. Since these ideal cases do not exist in reality, more realistic models derived from these ideal flow models have also been derived. To obtain a description of the type of flow dominant in a reactor, it is often assumed that the flow volume consists of different flow regions, each based on one of the flow models, with flow exchange taking place in and around these regions. The simplest of the combined models, which has frequently been used successfully in tundish studies, assumes the flow to consist of plug flow regions, well-mixed regions and dead regions. This section will describe the properties of each of these regions.

3.3.1. Plug Flow

Ideal plug flow

The ideal plug flow model assumes that there is no longitudinal mixing in the system, while transverse mixing may occur. For this case each flow element will have the same residence time in the reactor. This type of flow is shown schematically in Figure 3.3.

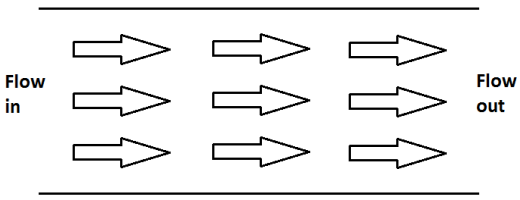

Figure 3.3 - Schematic representation of flow in the ideal plug flow model.

Stellenbosch University http://scholar.sun.ac.za

Since each flow element spends the same time in the reactor, the entire response will take place at the theoretical average residence time, $\theta = 1$, and produce an RTD response as shown in Figure 3.4.

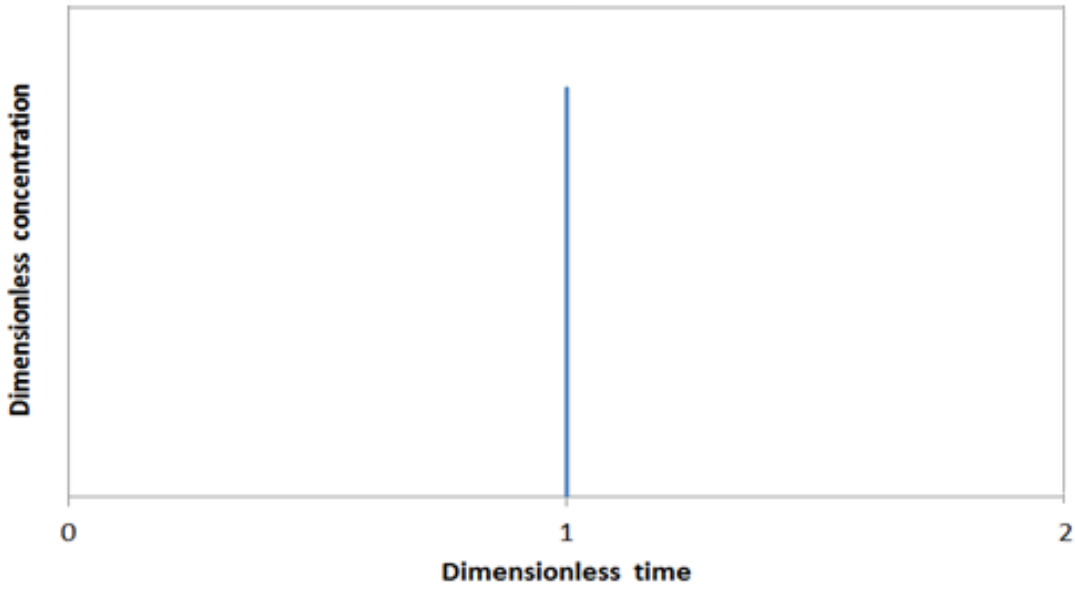

Figure 3.4 - RTD response for a pulse input, assuming ideal plug flow

Dispersed Plug flow

In reality some extent of longitudinal mixing will occur in most applications due to different flow velocities and turbulent and molecular diffusion. The dispersed plug flow model accounts for the longitudinal mixing by using a dimensionless group, called the vessel dispersion number. The vessel dispersion number ranges from values of zero to infinity, with the behaviour approaching ideal plug flow as the vessel dispersion number approaches a zero value. The change in the RTD nature with increased dispersion number is shown in Figure 3.5. Although the dispersed plug flow model is not used explicitly in this study, it does explain why a difference between minimum and peak residence times may occur in real systems, such as the tundish. Knowledge of this behaviour is used to adapt the calculation of the plug flow volume fraction for such systems in Section 3.4.2. A more detailed description of the dispersed plug flow model is given by Levenspiel (1972).

Stellenbosch University http://scholar.sun.ac.za

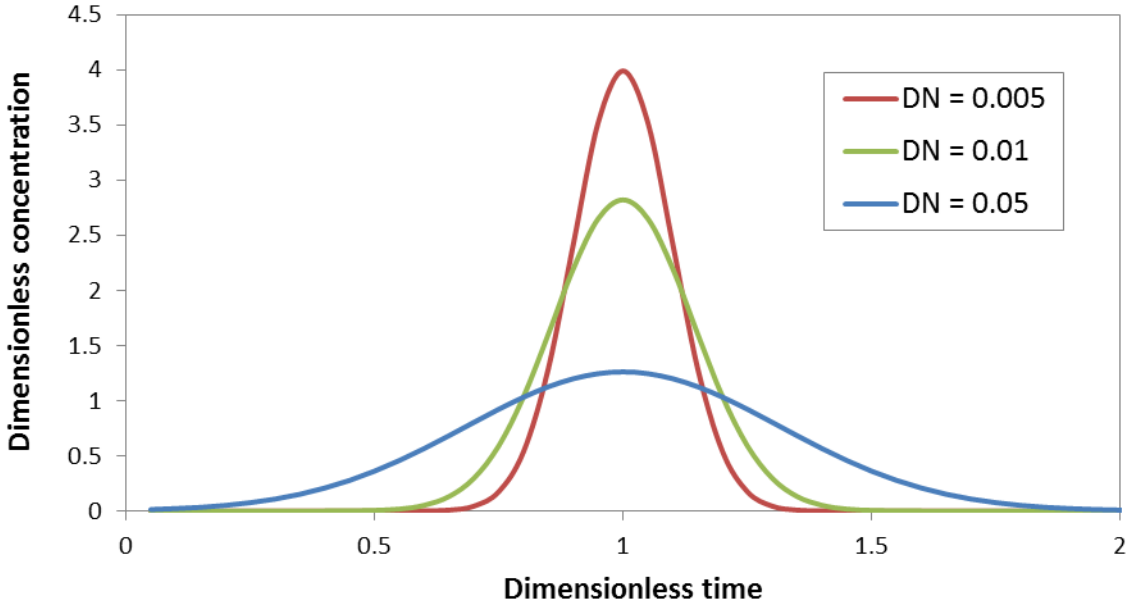

Figure 3.5 - C-curve for dispersed plug flow with different values of the dimensionless dispersion number

3.3.2. Well-mixed Flow

The well-mixed model assumes the flow to be highly mixed, thus the tracer concentration is identical at any position in the reactor at any moment of time. The outlet tracer concentration will therefore also be the same as the concentration in the bulk fluid.

Considering a mass balance over the reactor, the following expression for the dimensionless concentration with time can be derived, integrating over the boundary conditions of $c = m/V$ at $t = 0$ and $c = c$ at $t = t$:

$$\dot{m}_{in} - \dot{m}_{out} = \frac{dm}{dt} \quad [3.10]$$

$$Q(0) - Qc = \frac{d}{dt}Vc \quad [3.11]$$

$$\frac{dc}{c} = -\frac{Q}{V}dt \quad [3.12]$$

$$c = e^{-\theta} \quad [3.13]$$

The RTD response for this ideal flow is shown in Figure 3.6. Since the tracer is assumed to be uniformly dispersed through the reactor at $t = 0$, the initial dimensionless concentration is equal to one. With time the outlet concentration decreases, following an exponential decay.

Stellenbosch University http://scholar.sun.ac.za

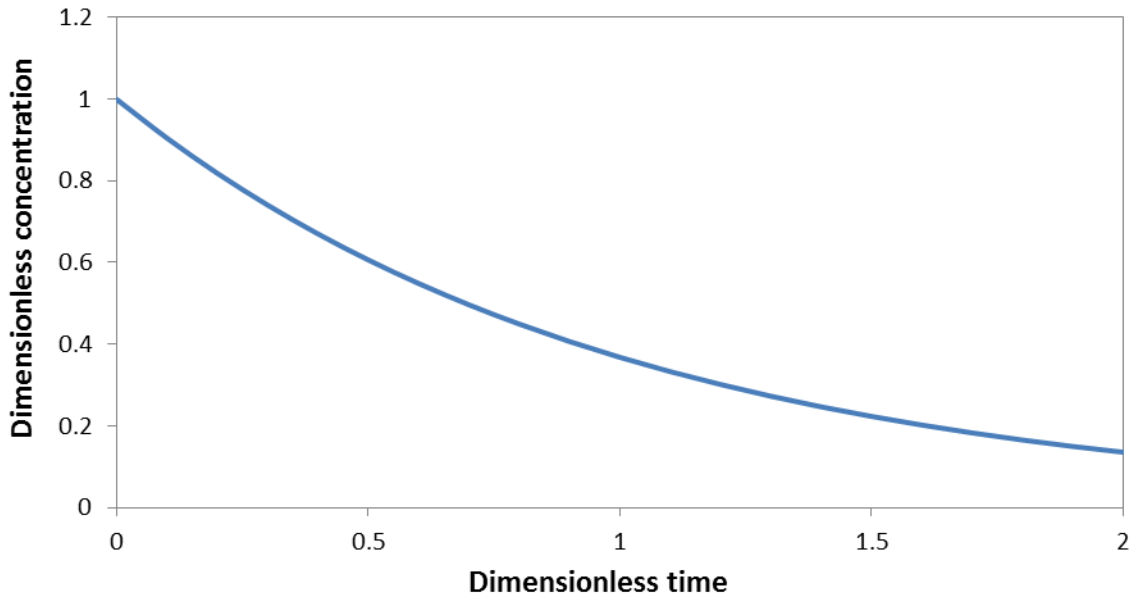

Figure 3.6 - RTD response for a pulse input, assuming ideal well-mixed flow

3.3.3. Active and Dead Regions

The active region is defined as any region in the reactor where a combination of plug flow and well-mixed flow occurs. Placing two ideal reactors in series, one with plug flow and the other with well-mixed flow, the response shown in Figure 3.7 is obtained, regardless of the order of the reactors. For this ideal case the minimum residence time is equal to the plug volume fraction ($\frac{V_p}{V}$).

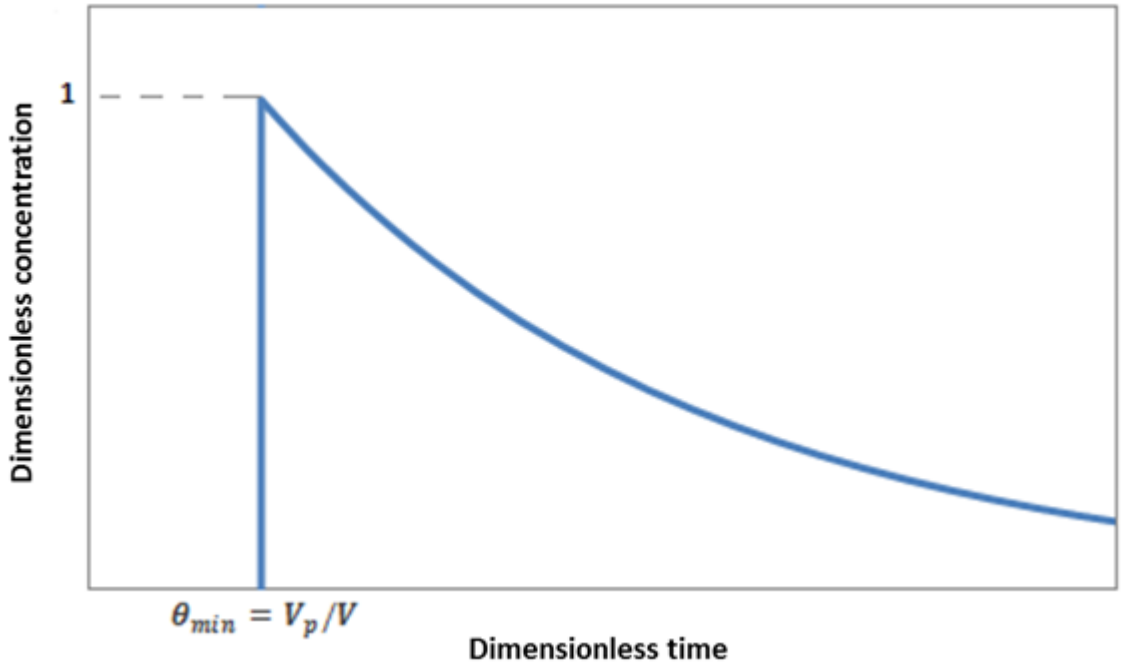

Figure 3.7 - Residence time distribution for ideal plug flow and ideal well-mixed flow reactors in series

Stellenbosch University http://scholar.sun.ac.za

Any tracer that arrives at the outlets after a specified cut-off time is attributed to the dead volume, while the rest is attributed to either plug flow volume or well-mixed volume. This is based on the assumption that for the fluid element to have such a lengthy residence time it had to have passed through one of the slow moving dead volumes. The dead volume can behave in two different ways. Firstly, it may be completely stagnant, with no flow entering or leaving the region. Alternatively, the flow can move very slowly through this region, causing some fluid elements to remain in the reactor for longer than expected.

Most tundish studies apply the arbitrary selected cut-off time of $\theta = 2$. Kumar et al. (2008, 2007) used a cut-off time of $\theta = 2.5$ based on a suggestion by Zong (1999) that part of the long tail can be attributed to the exponential edge caused by intensive mixing. However, for this study the more commonly accepted value of $\theta = 2$ will be used as the cut-off time.

3.4. Combined Models for Tundish Application

As mentioned previously, the simplest form of the combined model assumes that the volume of the reactor can be subdivided into three volumes: mixed volume, plug flow volume and dead volume. This approach has been used for several decades in reactor design and is applied in most flow analysis studies based on the tundish. However, several variations of the combined model have been proposed and there seems to be little consistency in how the equations to calculate the different flow volumes are applied in literature regarding the tundish. This section will give a brief overview of the different approaches used in literature and highlight the methods used in this study.

3.4.1. Dead Volume Fraction

Using the mixed model of Kemeny et al. (1981), the dead volume fraction is calculated as the fraction of the difference in the theoretical mean residence time (equation 3.2) and the mean residence time (equation 3.4) calculated up to the cut off time of $\theta = 2$, as shown in equation 3.14. This is also the method most commonly used in literature regarding the flow analysis of tundish systems (Tripathi & Ajmani, 2005; Jha et al., 2001; Mishra et al., 2012).

$$\frac{V_d}{V} = \frac{\bar{t} - t_{av}}{\bar{t}} = 1 - \bar{\theta}_{cut-off} \qquad [3.14]$$

However, this approach is criticised by Sahai and Emi (1996a) since equation 3.14 is based on the assumption of completely stagnant dead zones. However, it is clear that in the tundish there will always be an exchange of mass between the active and dead regions, since the dead volumes are generally slow moving and not completely stagnant. They went ahead to show that the correct expression for the dead volume fraction is in fact equation 3.15. This is the approach that will be used in this study, applying the most commonly used cut-off time of $\theta = 2$.

Stellenbosch University http://scholar.sun.ac.za

$$\frac{V_d}{V} = 1 - \frac{Q_a}{Q} \times \bar{\theta}_{cut-off} \quad [3.15]$$

Equation 3.15 can be derived by assuming that the vessel, with volume V, is divided into an active volume, V_a, and a dead volume V_d. Of the total volumetric flow rate Q, Q_a flows through the active region, while Q_d flows through the dead volume. Then:

$$\bar{\theta}_{cut-off} = \frac{\bar{t}_{cut-off}}{t_{ave}} = \frac{V_a/Q_a}{V/Q} = \frac{V_a}{V} \times \frac{Q}{Q_a} = \left(1 - \frac{V_d}{V}\right) \times \frac{Q}{Q_a} \quad [3.16]$$

The equation can then be rearranged to form equation 3.15. $\frac{Q_a}{Q}$ is the fractional volumetric flow rate through the active region and is equal to the area under the C-curve up to the cut-off time. In the case of completely stagnant dead volumes the volumetric flow rate through the active region will be equal to zero and equation 3.14 will become valid.

3.4.2. Plug Flow Volume

For the calculation of plug flow volume there are also different approaches that are being used. The simplest one, and most widely used in literature, is based on the combination in series of an ideal plug flow reactor and an ideal mixed reactor for which the response is shown in Figure 3.7. In this case the plug volume fraction is simply equal to the dimensionless minimum residence time.

$$\frac{V_p}{V} = \theta_{min} \quad [3.17]$$

This approach is based on the fact that for the case of ideal plug flow and mixed reactors in series, the minimum residence time and the peak residence times are equal. For tundish, however, this is not the case, as can clearly be seen from the example C-curve shown in Figure 3.2, where the peak residence time is more than double the minimum time. This is due to considerable longitudinal diffusion taking place in the system. To overcome this problem a 'modified combined model' was proposed by Ahuja and Sahai (1986), which have subsequently been used by several authors (Kumar et al., 2007; Tripathi & Ajmani, 2011). In the combined model the plug flow volume is replaced by a dispersed plug flow volume and calculated as in equation 3.18. This is the approach that will be used in this study, wherever the plug flow volume fraction is calculated, unless specifically stated otherwise.

$$\frac{V_p}{V} = \frac{\theta_{min} + \theta_{peak}}{2} \quad [3.18]$$

One of the problems with the combined model approach is the slightly arbitrary definition of the plug flow volume and the highly arbitrary specification of the cut-off time in calculating the dead volume. To overcome this problem, Zong et al. (1999) proposed another modified combined model specifically to calculate the plug volume fraction as a design variable for continuous refining vessels. This modified model has the advantages that it is suitable for use with reactors with a variety of RTD curves and is very useful for treating tail data, since the calculated value is insensitive to the cut-off point chosen. However, this

Stellenbosch University http://scholar.sun.ac.za

approach imparts no physical meaning to the other two volumes in the combined model, the mixed volume and the virtual dead volume. This definition of plug flow will be used as a supplementary criteria in parts of this study, using equation 3.19 to calculate the plug volume fraction, applying the author's cut-off time at $\theta = 2.5$ for calculating the mean residence times and variance.

$$\frac{V_p}{V} = \theta_{mean}(\theta_{mean} - \sigma) \qquad [3.19]$$

3.4.3. Mixed Volume

The combined model by Kemeny et al. (1981) equates the mixing volume fraction to the inverse of the peak concentration, as shown in equation 3.20.

$$\frac{V_m}{V} = \frac{1}{C_{peak}} \qquad [3.20]$$

However, one of the problems with the combined model by Kemeny is that if the values of the plug, mixed and dead volumes are calculated from equations 3.14, 3.17and 3.20, the values do not add to one. For this reason, the most common approach in calculating the well-mixed volume is to simply assume that the well-mixed volume accounts for the volume not attributed to plug flow or dead volume. Therefore:

$$\frac{V_m}{V} = 1 - \frac{V_p}{V} - \frac{V_d}{V} \qquad [3.21]$$

In the case of using the combined model by Ahuja and Sahai, the plug flow volume fraction is simply replaced by the dispersed plug flow volume, as is done in this study.

3.4.4. Short-circuiting Volume

Another modification of the combined model that is used in literature (Kumar et al., 2007) is to add a fourth volume type to the model, namely the short-circuiting volume. This approach is suitable for cases where a large degree of short-circuiting takes place and two or more peak concentrations are formed and is calculated as the area bounded by the first peak in the C-curve (Singh & Koria, 1996). However, this study will mostly deal with designs that will eliminate short-circuiting and therefore this approach will not be considered.

3.5. Summary

Residence time distribution techniques are a good way of inferring information regarding flow behaviour from the response to a stimulus. In this study a pulse injection of tracer will be used as stimulus. In tundish literature the common approach is to assume that the volume consists of regions of plug flow, well-mixed flow and dead volumes. Calculating the fractions of the different regions of these combined models allows a method for quantifying tundish performance. However, several different approaches are used for calculating these values by various authors. From literature it was found that the best approach is to calculate

Stellenbosch University http://scholar.sun.ac.za

the dead volume as described by Sahai & Emi (1996a) and the plug volume fraction from the minimum and peak residence times, as suggested by Ahuja and Sahai (1986). This is the approach that will be used in this study to evaluate the performance of different tundish configurations. The RTD responses and combined model parameters will also be used during the validation of the numerical model.

Stellenbosch University http://scholar.sun.ac.za

Chapter 4: CFD Theory

4.1. An Introduction to CFD

CFD is the science of solving the governing equations in a process numerically to predict the flow behaviour, heat transfer, mass transfer, chemical reactions and other processes taking place. It provides an alternative to physical modelling as a way to obtain information about high temperature refining processes. The big difference between using CFD and RTD physical modelling for flow analysis, however, is that while RTD experiments allow the researcher to make certain inferences about the internal workings based only on what is measured at the outlets, CFD transports the investigator into the reactor. The benefits of this are obvious. Now the researcher can see precisely, in three dimensions, how the melt will move over a flow control device or how the flow patterns will change when changing the length/width ratio of the tundish. This allows a much better understanding of what is happening inside the reactor, which allows the researcher to much easier propose improvements to the system.

CFD modelling is therefore an extremely powerful tool for use in flow analysis of any system. However, a number of choices regarding turbulence models, grid size, discretization methods and time step size can influence the results. Therefore, without careful consideration of each choice, requiring an understanding of the relevant theory and testing of the effects of selecting different options, the numerical results are not necessarily representative of the real system. Therefore, it is clear that for CFD to remain the powerful tool that it is, it must be used with careful consideration, clear understanding and proper validation processes to fulfil its potential.

The second important advantage of the CFD approach over physical modelling is that once an accurate numerical model has been developed, the solution procedure can be applied in a timely fashion to test the effect of various designs and operating conditions.

4.2. Governing Equations

In a closed system the flow is governed by the conservation equations for mass and momentum. For flows involving compressibility or heat transfer the equation for conservation of energy is also considered. When multiple species are present, the species conservation equations are solved.

4.2.1. Conservation of Mass

The general form of the mass conservation equation (or continuity equation) is shown in equation 4.1 as applied in FLUENT (ANSYS, 2011):

$$\frac{\partial \rho}{\partial t} + \nabla \cdot (\rho \vec{v}) = S_m \qquad [4.1]$$

Stellenbosch University http://scholar.sun.ac.za

In equation 4.1, the operator ∇ represents the partial derivative of a property with respect to all directions in the chosen coordinate system. S_m is a source term that can either be due to mass transfer from a dispersed phase to the continuous phase or due to user defined sources and is not used in this study. Also, for incompressible flow, such as the flow considered in this study, the transient term falls away and ρ becomes constant; therefore the continuity equation is applied as:

$$\nabla \cdot \vec{v} = 0 \qquad [4.2]$$

4.2.2. Conservation of Momentum

In Fluent the momentum conservation equation is applied as follows (ANSYS, 2011):

$$\frac{\partial}{\partial t}(\rho\vec{v}) + \nabla \cdot (\rho\vec{v}\vec{v}) = -\nabla \mathrm{p} + \nabla \cdot (\bar{\bar{\tau}}) + \rho\vec{g} + \vec{F} \qquad [4.3]$$

In equation 4.3, p represents the static pressure, $\rho\vec{g}$ the gravitational body force and $\bar{\bar{\tau}}$ the stress tensor. The calculation for the stress tensor is shown in equation 4.4, where I is the unit tensor.

$$\bar{\bar{\tau}} = \mu[(\nabla\vec{v} + \nabla\vec{v}^T) - \frac{2}{3}\nabla \cdot \vec{v}I] \qquad [4.4]$$

In the momentum conservation equation, $\vec{F}$ represents external body forces, arising from interaction with a dispersed phase, which will not be present in this study. Also, for the incompressible flow considered in this study, ρ becomes constant; thus for transient flow the momentum equations are applied as in equation 4.5.

$$\rho\frac{\partial\vec{v}}{\partial t} + \rho\nabla \cdot (\vec{v}\vec{v}) = -\nabla \mathrm{p} + \nabla \cdot (\bar{\bar{\tau}}) + \rho\vec{g} \qquad [4.5]$$

However, in most of the simulations considered in this study the momentum equations are solved for steady state, therefore the transient term falls away and equation 4.5 simplifies further:

$$\rho\nabla \cdot (\vec{v}\vec{v}) = -\nabla \mathrm{p} + \nabla \cdot (\bar{\bar{\tau}}) + \rho\vec{g} \qquad [4.6]$$

4.2.3. Conservation of Species

Separate species are specified in order to track tracer moving through the tundish when simulating RTD experiments. For this reason the species model is activated, in which case the conservation of species equations will be solved, as shown in equation 4.7 for species i (ANSYS, 2011).

$$\frac{\partial}{\partial t}(\rho Y_i) + \nabla \cdot (\rho\vec{v}Y_i) = -\nabla \cdot \vec{J}_i + R_i + S_i \qquad [4.7]$$

In equation 4.7, $\vec{J}_i$ is the diffusive flux due to gradients in concentration and temperature.

$$\vec{J}_i = -\rho D_{i,m}\nabla Y_i \qquad [4.8]$$

Stellenbosch University http://scholar.sun.ac.za

Since the movement of tracer with time must be tracked, the momentum equation will always be solved transiently. Considering incompressible flow, the conservation of species equation can therefore be simplified as follows:

$$\rho \frac{\partial Y_i}{\partial t} + \rho \nabla \cdot (\vec{v} Y_i) = -\nabla \cdot \vec{J}_i \qquad [4.9]$$

4.3. Turbulence

Turbulent flow is present in most flows encountered in industrial practice and is characterised by fluctuations in velocity and highly disordered motion. These fluctuations in velocity occur on various length scales and increase the transfer rate of momentum, species and energy in the system. To accurately simulate the real system, it is therefore essential that the effect of turbulence should be incorporated into the numerical model.

There are two main approaches to doing this: Reynolds-averaged formulations, where no structures are solved directly, and eddy-resolved formulations, where some or all structures are resolved directly. Some of the length scales over which turbulence occur are so small that they require an impractically small mesh to be resolved directly. The high computational requirement for solving turbulence through this approach, called Direct Numerical Simulation (DNS), makes it practical only for very simple problems with small amounts of turbulence. An alternative approach is that of Large Eddy Simulation (LES), where only the larger eddies are resolved directly and the effects of the smaller eddies are modelled. The alternative to resolving the turbulent eddies is the use of the Reynolds-averaged Navier-Stokes models.

The averaging effect introduced by using RANS modelling generally provides a smoother solution than the behaviour predicted when the eddies are resolved. However, it allows very large decreases in the required computational time (Loth, 2006). Fortunately, in most applications, accurate solution of the finer details of the very small eddies do not significantly impact the bulk flow, which is the part that is of practical significance to most engineering problems. This clearly favours the Reynolds-Averaging approach, which explains why nearly all numerical studies of tundish flow have been performed using the Reynolds-averaging approach. Further discussion of the turbulence models is therefore required.

4.3.1. The Reynolds-Averaged Navier Stokes (RANS) Models

The RANS models are based on the assumption that the velocity at any given time can be divided into a mean component and a fluctuating component, therefore:

$$u_i = \bar{u}_i + u_i' \qquad [4.10]$$

By substituting this expression into the instantaneous continuity and momentum equations and applying a time (or ensemble) average, the Reynolds-averaged Navier Stokes equations are obtained. They are similar in form to the instantaneous Navier-Stokes equations, except

Stellenbosch University http://scholar.sun.ac.za

that the velocity now represents a time (or ensemble) averaged value and additional terms represent the effect of turbulence. The Reynolds stresses, $-\rho\overline{u_i'u_j'}$, must be modelled to close the equation. The RANS equations are implemented by FLUENT as follows (ANSYS, 2011):

$$\frac{\partial \rho}{\partial t} + \frac{\partial}{\partial x_i}(\rho u_i) = 0 \qquad [4.11]$$

$$\frac{\partial}{\partial t}(\rho u_i) + \frac{\partial}{\partial x_j}(\rho u_i u_j) = -\frac{\partial p}{\partial x_i} + \frac{\partial}{\partial x_j}\left[\mu\left(\frac{\partial u_i}{\partial x_j} + \frac{\partial u_j}{\partial x_i} - \frac{2}{3}\delta_{ij}\frac{\partial u_l}{\partial x_l}\right)\right] + \frac{\partial}{\partial x_j}(-\rho\overline{u_i'u_j'}) \qquad [4.12]$$

A common method of modelling the Reynolds stresses is to use the Boussinesq hypothesis, where the Reynolds stresses are related to the mean velocity gradients as follows (ANSYS, 2011):

$$-\rho\overline{u_i'u_j'} = \mu_t\left(\frac{\partial u_i}{\partial x_j} + \frac{\partial u_j}{\partial x_i}\right) - \frac{2}{3}\left(\rho k + \mu_t\frac{\partial u_k}{\partial x_k}\right)\delta_{ij} \qquad [4.13]$$

This hypothesis is applied in the $k-\epsilon$, $k-\omega$ and Spalart-Almaras models. The major advantage is the low computational time associated with calculating the turbulent viscosity, μ_t. However, its assumption that μ_t is an isotropic value is not strictly true, but holds for many practical engineering flows.

$k-\epsilon$ Models

The most frequently used group of RANS turbulence models calculate the turbulent viscosity as a function of k, the turbulent kinetic energy and ϵ, the turbulent dissipation rate.

The standard $k-\epsilon$ model, proposed by Launder and Spalding (1974) has primarily been used in practical engineering flow simulations due to its robustness, low computational requirements and relatively good accuracy. However, the RNG and, most recently, the realizable $k-\epsilon$ model offer some advantages over the original $k-\epsilon$ model. The realizable $k-\epsilon$ model will be applied in this study due to the improved accuracy it offers when the flow includes strong streamline curvature, rotation and vortices. The modelled transport equations for k and ϵ for the realizable $k-\epsilon$ model are:

$$\rho\frac{\partial}{\partial x_j}(ku_j) = \frac{\partial}{\partial x_j}[(\mu + \frac{\mu_t}{\sigma_k})\frac{\partial k}{\partial x_j}] + G_k - \rho\varepsilon \qquad [4.14]$$

$$\rho\frac{\partial}{\partial x_j}(\varepsilon u_j) = \frac{\partial}{\partial x_j}[(\mu + \frac{\mu_t}{\sigma_\varepsilon})\frac{\partial \varepsilon}{\partial x_j}] + \rho C_1 S\varepsilon - \rho C_2\frac{\varepsilon^2}{k+\sqrt{\nu\varepsilon}} \qquad [4.15]$$

Stellenbosch University http://scholar.sun.ac.za

In these equations, G_k represents the generation of turbulence kinetic energy due to the mean velocity gradients and C_1 is a function of S, the mean strain rate. The eddy viscosity is calculated from:

$$\mu_t = \rho C_\mu \frac{k^2}{\varepsilon} \qquad [4.16]$$

The difference between the realizable k-ε model and the standard k-ε model is that C_μ is a variable for the realizable model, not a constant. The standard model constants for the realizable k-ε model are used (Shih et al., 1995): $C_{1\varepsilon} = 1.44$, $C_2 = 1.9$, $\sigma_k = 1.0$ and $\sigma_\varepsilon = 1.2$.

4.3.2. Near Wall Regions

The presence of walls has a large influence on the behaviour of turbulence. Therefore another choice regarding turbulence must be made when deciding how to treat the modelling of turbulence near the walls. Figure 4.1 shows a typical profile for turbulence near a wall.

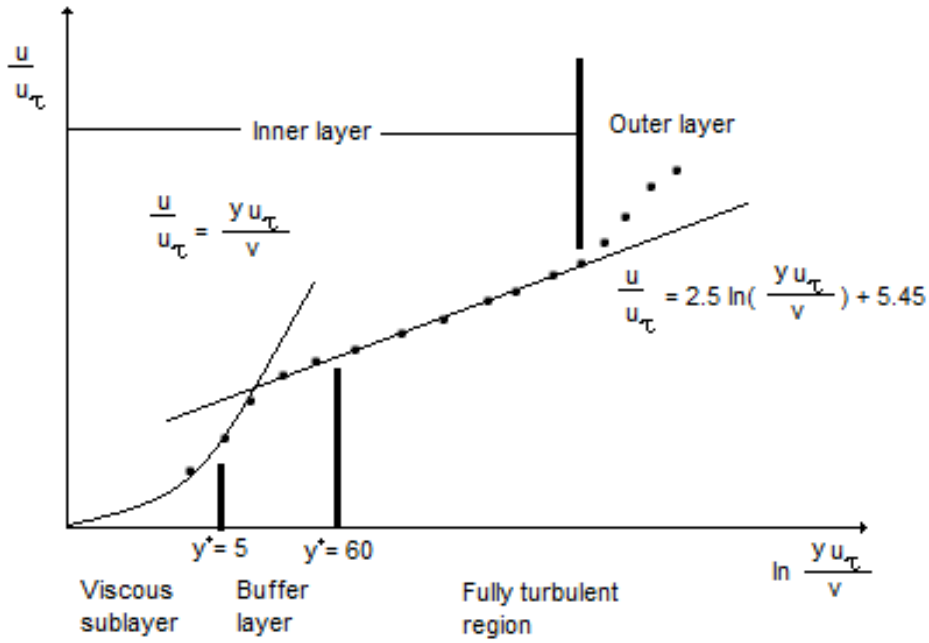

Figure 4.1 - Boundary layer regions in the near wall turbulent flows (redrawn from ANSYS(2011))

In the viscous sublayer the flow is almost laminar and viscosity plays a large role in momentum transfer. In the fully turbulent region, turbulence dominates momentum transfer. However, in the buffer layer both the viscosity and turbulence play a role.

Stellenbosch University http://scholar.sun.ac.za

There are two methods to approach the near-wall region. The first is to resolve the viscous sublayer. This requires very fine grid cells and will therefore require more computational power. This method is used when the wall forces are vital for the simulation, for example in aerodynamic drag applications.

The second method uses a wall function and does not require such small cells. A wall function is a semi-empirical equation that links the flow variables in the near-wall cells to their corresponding cells at the wall. A wall function consists of a law-of-the-wall for the mean velocity close to the wall and some additional formulas for near wall turbulent qualities, such as turbulence kinetic energy and the turbulence dissipation rate. This approach is generally used when the mixing in the middle of the domain is more important than the forces at the wall, which will clearly be the case in the present study.

4.4. Gradient Adaptation

The simplest case for meshing a CFD problem is when a constant mesh size can be specified throughout the flow domain. A grid independence study can then be performed by gradually decreasing the mesh size until the solution no longer changes significantly with decreasing mesh size. And indeed, there are several applications where it is in fact as simple as that to obtain an accurate CFD solution for the aspect of the system investigated. However, in many systems, for example where complicated flows with steep gradients occur or when multiphase models are used to track complex phase interactions, the computational time will become impractically large due to the increase in the total number of cells before grid independence is reached. In these cases an efficient numerical model will require the mesh to be locally refined in the areas where a high resolution grid is needed for an accurate solution, while maintaining a coarser mesh in the rest of the flow volume.

FLUENT offers several criteria by which to adapt the mesh in localised regions. Specific cells are marked, either for refinement or coarsening, based on these criteria. Since only refining will be used in this study, it will be discussed in more detail. In three dimensions, each parent cell is divided into eight child cells for tetrahedral and hexahedral meshes, as illustrated in Figure 4.2.

Stellenbosch University http://scholar.sun.ac.za

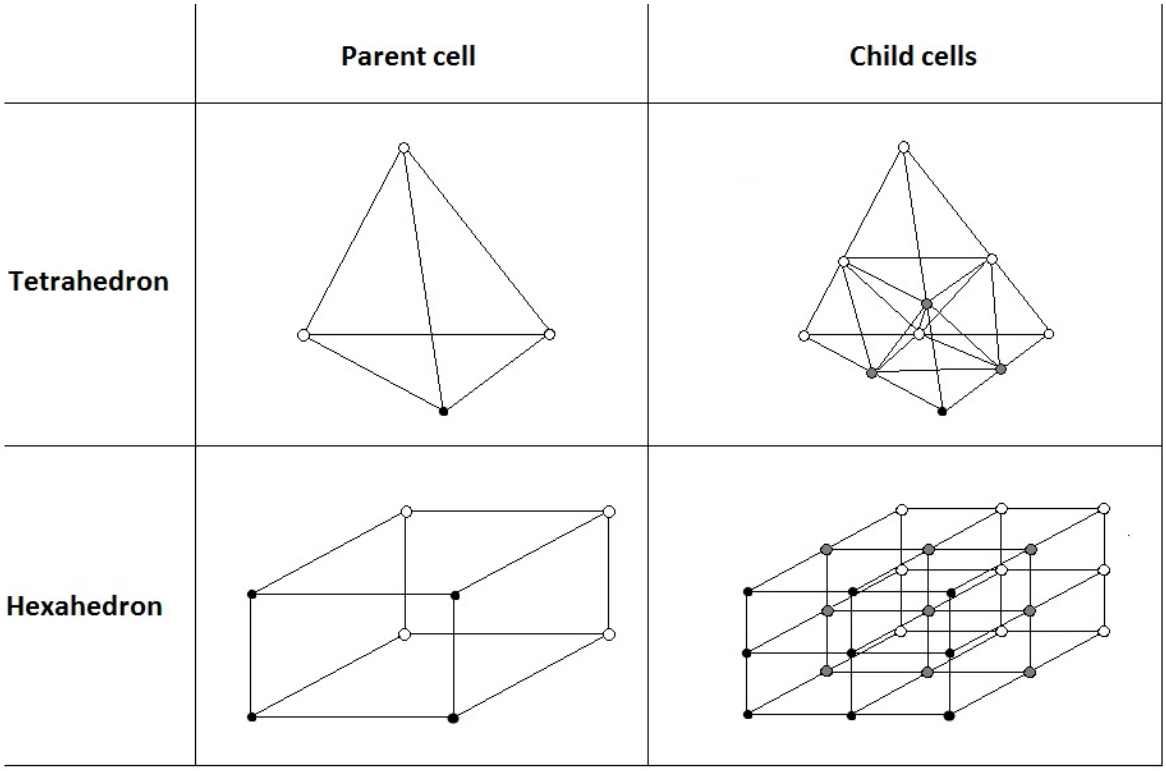

Figure 4.2 - Schematic representation of refinement of tetrahedral and hexahedral cells

One of the simplest adaptation criteria, which is utilised in this study, is boundary adaptation. Using this tool, all cells within a specified distance or number of cells from the specified boundaries are marked for refinement. This approach is useful, since the no-slip condition at walls frequently causes some of the largest gradients in the fluid domain to be formed near walls. These boundary flows can have an important effect on the overall solution, in which case it is necessary for them to be solved accurately, using a sufficiently fine mesh.

The second adaptation technique, which is primarily used in this study, is called gradient adaptation. This approach uses an initial solution to refine the mesh in areas where a large numerical error is expected, assuming the error to increase with increased gradients. This is a very useful approach, since it allows a more accurate numerical solution with minimal computational cost. It also allows a more automated approach to adapting the mesh for different geometries. For example, consider two tundish designs with different flow control device configurations, both meshed by a combination of a coarse mesh and a refined mesh. However, depending on the designs, the high gradient areas, which will require the refined mesh, can be in completely different parts of the tundish. Instead of having to manually find and refine these areas, a solution can be obtained using the coarse mesh and the mesh can be refined in the desired areas by specifying a value of the error indicator based on the gradient of a flow variable.

Stellenbosch University http://scholar.sun.ac.za

Three different approaches are used in calculating the error indicator in FLUENT for gradient adaptation. Firstly, the isovalue approach calculates the error indicator from a specified isovalue of the selected variable. This approach is suggested in cases where the derivative is not helpful, for example when the mesh must be adapted in regions with a high reaction rate. Secondly, the gradient approach is based on the Euclidean norm of the gradient of the selected variable and is suggested for problems involving strong shock, for example where supersonic flows occur in an inviscid fluid. However, the flows in this study are expected to have relatively smooth solutions. For flow of this nature, the curvature approach is suggested, which is based on the undivided Laplacian of the selected variable. The equation for calculating the error indicator, e_i, as used in FLUENT, is shown in equation 4.17, where $|\nabla^2 f|$ is the undivided Laplacian of the selected variable. (ANSYS, 2011)

$$|e_i| = (V_{cell})^{\frac{r}{3}} |\nabla^2 f| \qquad [4.17]$$

It can be seen than in calculating the error indicator, the Laplacian is multiplied by a characteristic length scale, $(V_{cell})^{\frac{r}{3}}$. This is based on the assumption that for a smaller existing cell, the error will be smaller for the same gradient. By changing the gradient volume weight, r, from 1 to 0 the effect of the volume weighting can be reduced. In the case of a volume weighting of 1, the characteristic length scale simply becomes the cube root of the volume of the cell.

Stellenbosch University http://scholar.sun.ac.za

Chapter 5: Physical Modelling

5.1. Model Similarity

The main objective of physical modelling is to create a system, referred to as the model, which is a realistic representative of the real operation to be studied, termed the prototype, but allows the properties of the system to be measured in an easier manner and experiments to be performed at a lower cost. In the case of a steelmaking tundish, it is desirable for the model to operate at a lower temperature than the real steelmaking process, to facilitate easy measurement. Also, even if the researcher has access to a real industrial process to perform plant trials, the cost of operating the plant is too high to allow casual experimentation. Using water as the modelling material reduces the cost of experimentation and makes extensive experimentation more feasible.

However, it seems obvious that for water at room temperature to behave in the same manner as steel at 1700°C, strict rules must be followed. In physical modelling there are several similarity criteria that must be met to achieve this. Possible similarity criteria include geometric, kinematic, dynamic, thermal and chemical similarity. Since the physical modelling for this study will assume isothermal, non-reactive flow, thermal and chemical similarity will not be considered for this study.

5.1.1. Geometric Similarity

Geometric similarity simply requires that the prototype and the model must have the same shape. Therefore every dimension in the model must be scaled from the prototype by a fixed factor, termed the scale factor. Therefore,

$$\mathrm{L_m} = \lambda\, \mathrm{L_p} \qquad [5.1]$$

For this study a scale factor of ½ was chosen, thus every dimension was reduced to half the size in the prototype. For the case of the tundish, using a smaller scale factor will lead to a smaller model, which will be less expensive to construct and will require lower flow rates to operate. Full scale models may also be impractical for some experimental areas due to the large amount of space they will consume. However, full scale models do offer an advantage in tundish modelling, as will be discussed under the section regarding dynamic similarity.

5.1.2. Dynamic Similarity

Dynamic similarity implies that forces in corresponding locations must be scaled by a fixed ratio between the model and prototype. The forces that are important will vary depending on the system being investigated. In the case of the tundish, the forces that are normally considered are the inertial, viscous and gravitational forces, each defined as follows:

$$F_{inertial} = \rho v^2 L^2 \qquad [5.2]$$

Stellenbosch University http://scholar.sun.ac.za

$$F_{viscous} = \mu v L \quad [5.3]$$

$$F_{gravitational} = \rho g L^3 \quad [5.4]$$

In physical modelling these forces are usually expressed at dimensionless numbers representing ratios of these forces. The Reynolds number represents the ratio of the inertial forces to the viscous forces, while the Froude number represents the ratio of the viscous forces to the gravitational forces.

$$Re = \frac{\rho v D}{\mu} \quad [5.5]$$

$$Fr = \frac{v^2}{gL} \quad [5.6]$$

To maintain Reynolds number similarity at the inlet of the tundish between the model and the prototype (therefore maintaining the same ratio of inertial to viscous forces), the velocity at the inlet of the model needs to be correctly selected. Assuming the kinematic viscosities of steel at 1600°C and water at 25°C to be equal (they are within 10% of each other), the prototype inlet velocity can be expressed in terms of the scale factor and the prototype velocity as follows:

$$Re_m = Re_p \quad [5.7]$$

$$\left(\frac{\rho v D}{\mu}\right)_m = \left(\frac{\rho v D}{\mu}\right)_p \quad [5.8]$$

$$v_m = \frac{D_p}{D_m} v_p \quad [5.9]$$

$$v_m = \left(\frac{1}{\lambda}\right) v_p \quad [5.10]$$

A similar process can be completed for similarity based on the Froude number:

$$Fr_m = Fr_p \quad [5.11]$$

$$\left(\frac{v^2}{gL}\right)_m = \left(\frac{v^2}{gL}\right)_p \quad [5.12]$$

$$v_m = \sqrt{\frac{L_m}{L_p} \times v_p^2} \quad [5.13]$$

$$v_m = \sqrt{\lambda} \times v_p \quad [5.14]$$

From equations 5.10 and 5.14 it can immediately be observed that when using a reduced scale model Reynolds number similarity will lead to a higher velocity in the model, while Froude number similarity will cause a reduced velocity for the model. Therefore, the only method of maintaining both Reynolds number and Froude number similarity is to use a full

Stellenbosch University http://scholar.sun.ac.za

scale model. However, in many circumstances it is impractical to use a full scale model due to increased construction and operating cost, as well as the increased requirement of space.

Therefore, for a reduced scale tundish model, a choice needs to be made between Reynolds and Froude number similarity. This decision will depend on the nature of the flow and the relative importance of the forces in the system being studied. The Froude number will be important when both inertial and gravitational forces are important. However, because isothermal flow is considered, buoyancy will not affect the flow and the gravitational force becomes unimportant. Despite this, Froude similarity gives a useful relationship between the model and prototype in terms of the scale factor.

Since the flow in a tundish is normally turbulent, the inertial forces are much larger than the viscous forces. In such turbulent flows, diffusive momentum transfer can take place over relatively large distances due to turbulent eddies. Therefore in turbulent flow the diffusive momentum transfer is dependent on the combined effect of turbulent eddies and molecular viscosity, termed the effective viscosity. The contribution of turbulent eddies to diffusive momentum transfer in such conditions may be orders of magnitude larger than that caused by molecular viscosity. For this reason, Reynolds similarity is very important for laminar flow, but less so for turbulent flow.

However, for turbulent flow the ratio of inertial forces, resulting in convective flow, and effective viscous forces, resulting in diffusive momentum transfer, is important. This ratio, termed the turbulent Reynolds number, is defined as follows:

$$Re_T = \frac{\rho v D}{\mu_{effective}} \qquad [5.15]$$

It has been shown that the effective viscosity is directly proportional to the fluid velocity over a large range of flow rates in turbulent flow (Sahai & Burval, 1992). Thus the turbulent Reynolds number is generally constant and similarity between the model and the prototype automatically obtained.

The conclusion is that for turbulent flow, neither the Reynolds or Froude numbers are essential similarity criteria, but both provide useful relations to scale the flow between the model and prototype. To verify this, Sahai and Emi (1996b) performed both physical and numerical experiments on physical models with scales factors of 1 and 0.6 respectively. The results showed that the dimensionless RTD curves did not change significantly over a large range of flow rates (0.13 l/s to 0.88 l/s for the smaller model and 0.25 l/s to 0.88 l/s for the larger model). It also showed similar average residence time distribution curves over a large range of flow rates for the larger and smaller models.

The choice of similarity criterion is concisely summarised by Sahai and Emi (2008):

"In summary, for isothermal water modelling of melt flow in a tundish, which is generally turbulent, the geometric similarity should be maintained and the model may be operated at

Stellenbosch University http://scholar.sun.ac.za

any flow rate within the turbulent range. The turbulent Reynolds number similarity criterion is naturally satisfied if one operates in the turbulent regime. In a reduced scale model, it is not necessary to satisfy the Froude similarity criterion for melt flow modelling. However, it provides relationships for parameters relating melt flow and inclusion behaviour between the model and the prototype tundish. Thus it is common to use the Froude similarity criterion in a reduced-scale water model of a tundish"

For this reason, Froude number similarity was selected to scale the flow rates for this study, since it would allow inclusion modelling in future work.

5.1.3. Kinematic Similarity

Kinematic similarity implies the similarity of motion. Therefore, the velocity in corresponding locations in the prototype and model should be in the same fixed ratio. Also, the time intervals between corresponding events should be in a fixed ratio, known as the time scale factor. Assuming Froude number similarity, the following relationship for the time scale factor can be deduced from equation 5.14:

$$\frac{L_m}{t_m} = \sqrt{\lambda} \times \frac{L_p}{t_p} \qquad [5.16]$$

$$\frac{t_m}{t_p} = \sqrt{\lambda} \qquad [5.17]$$

5.2. Model Selection

The prototype used for this study was selected from literature based on the following criteria:

- Simple geometry, simplifying in depth analysis of factors such as symmetry, dynamically steady numerical solving, grid independence and turbulence inhibitor design.
- Multiple strands to allow the study of variation between strands
- Literature data associated with it to allow additional comparison for model validation.

The tundish design that was chosen is based on that used by Kumar et al. (2008). It is a simple, four-strand, trough-shaped tundish with walls inclined by 10°. However, it was decided to use a scale factor of 1/2, instead of 1/3, as used by Kumar, to reduce any possible errors resulting from the scaling down of the model. The dimensions of the model are shown in Figure 5.1.

Stellenbosch University http://scholar.sun.ac.za

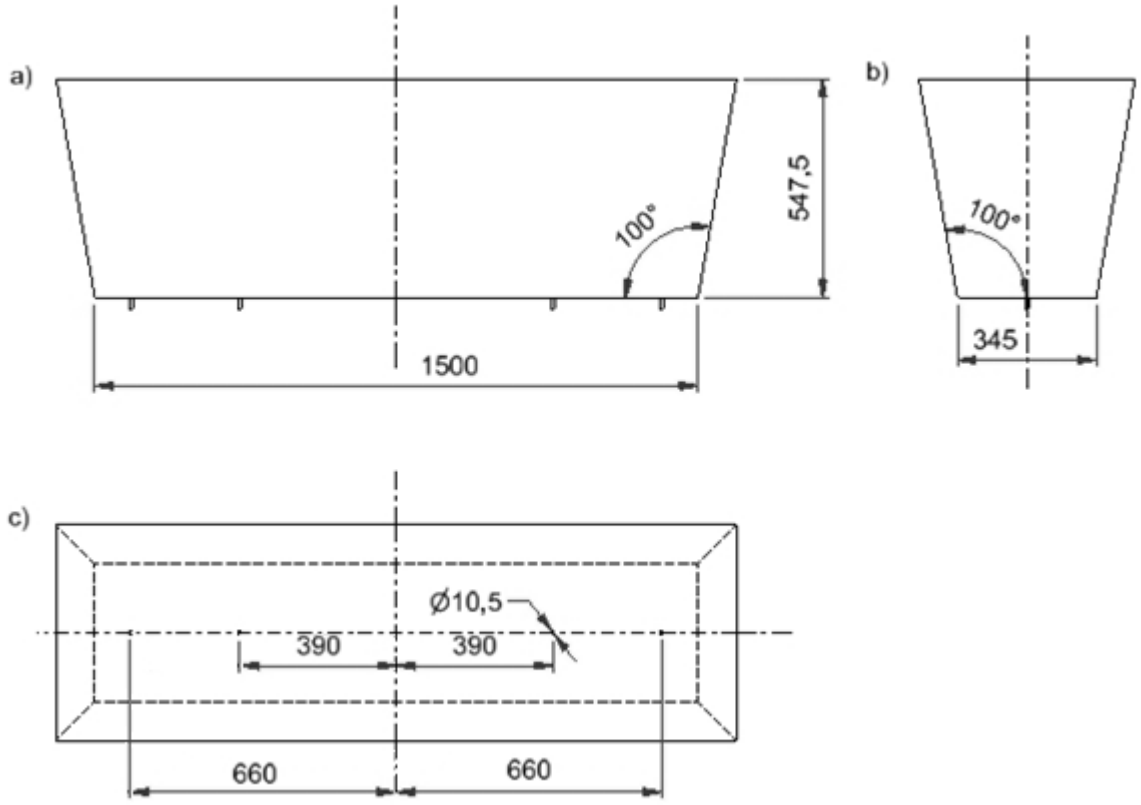

Figure 5.1 - Dimensions of the tundish model (in mm) shown from a) the front view, b) the side view and c) the top view

Using Froude similarity and a length scale of ½, the dimensions and inlet flow rate for the model was determined. A comparison of the prototype and water model is shown in Table 5.1.

Table 5.1- Comparison of design and operating variables of the industrial tundish and the 1:2 water model

Property	Industrial tundish	Water model
Length at base(m)	3	1.5
Volume (l)	2000	250
Mass flow rate (kg/min)	1015	25.6
Volumetric flow rate (l/h)	8 700	1 540
Bath height (m)	0.78	0.39
Froude number	1.24	1.24

Stellenbosch University http://scholar.sun.ac.za

5.3. Physical Model Description

5.3.1. General Setup

The physical model of the tundish was constructed from clear, 6mm PVC. A turbulence inhibitor based on the design proposed by Kumar et al. (2008) was constructed from 15mm thick grey PVC. The dimensions of the turbulence inhibitor are shown in Figure 5.2. The turbulence inhibitor was fixed in position and sealed by using silicon. The holes in the sides could also be closed by inserting correctly sized PVC blocks in them and sealing them with silicon.

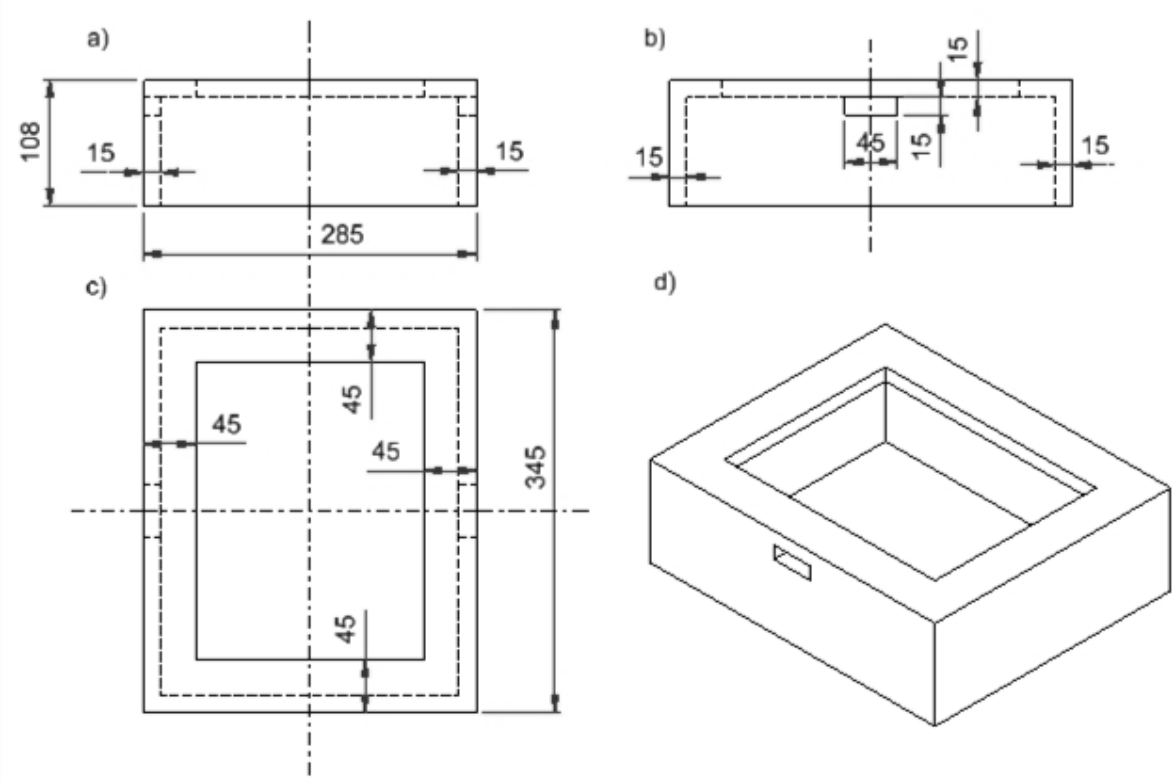

Figure 5.2 - Dimensions of the turbulence inhibitor (in mm) shown from a) the front view, b) the side view, c) the top view and d) the isometric view

Figure 5.3 shows a schematic representation of the entire physical model setup. Water is fed from the mains to a feed tank, which is kept at a fixed level by a float valve. From the feed tank the water is pumped to the tundish. The inlet flow rate is controlled by a gate valve (V-3) and a rotameter (3). Four ball valves (V-3, V-4, V-5 and V-6) can be closed to stop outlet flow, which is driven by gravity, and allow the tank to fill up. The water from the outlets is fed back to a storage tank. From here the water is either fed to sewage, when there is tracer present in the water, or recycled back to the feed tank. Individual aspects of the physical model will be discussed in detail in the following sections.

Stellenbosch University http://scholar.sun.ac.za

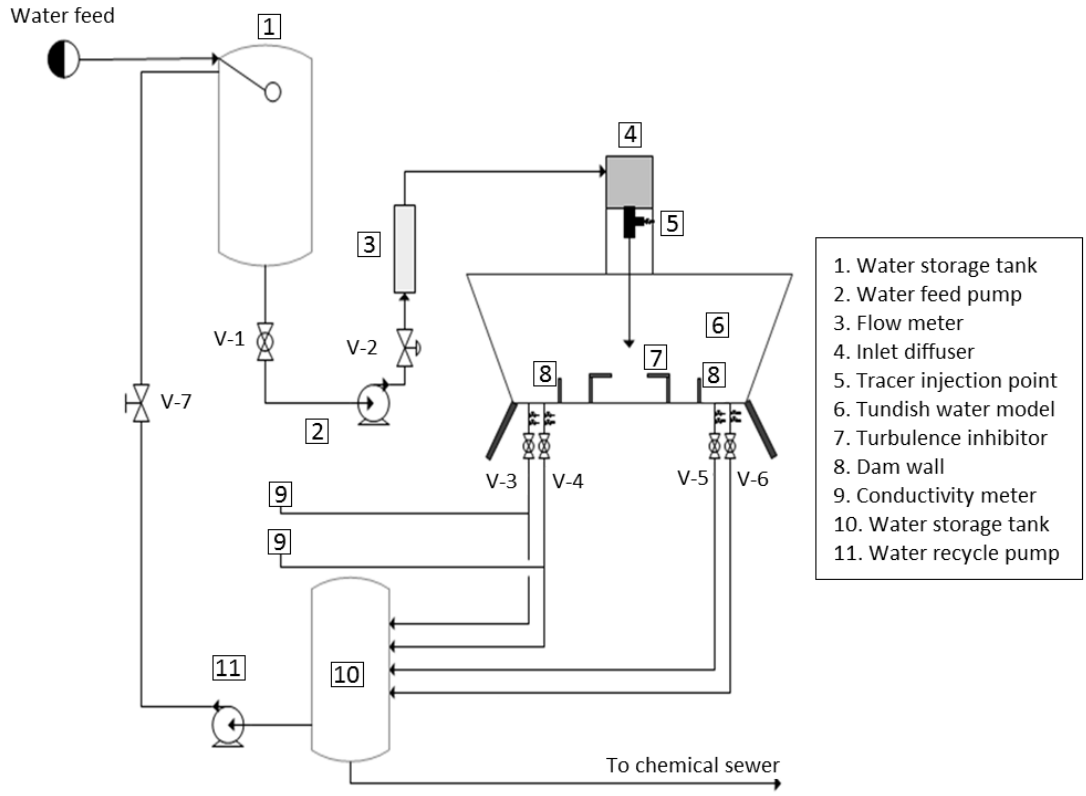

Figure 5.3 - Schematic representation of the physical model setup

5.3.2. Inlet Configuration

Since the feed tank is placed to the side of the tundish model the pipe leading to the inlet of the model will need to turn 90° above it. Figure 5.4 shows that even for a smooth bend the velocity profile is disrupted significantly and requires a considerable distance to recover. In this case the profile is still skewed with 0.5m of pipe length after the bend. Given a long enough length of pipe a fully developed profile will form, but having the bend high above the bath will complicate construction.

Stellenbosch University http://scholar.sun.ac.za

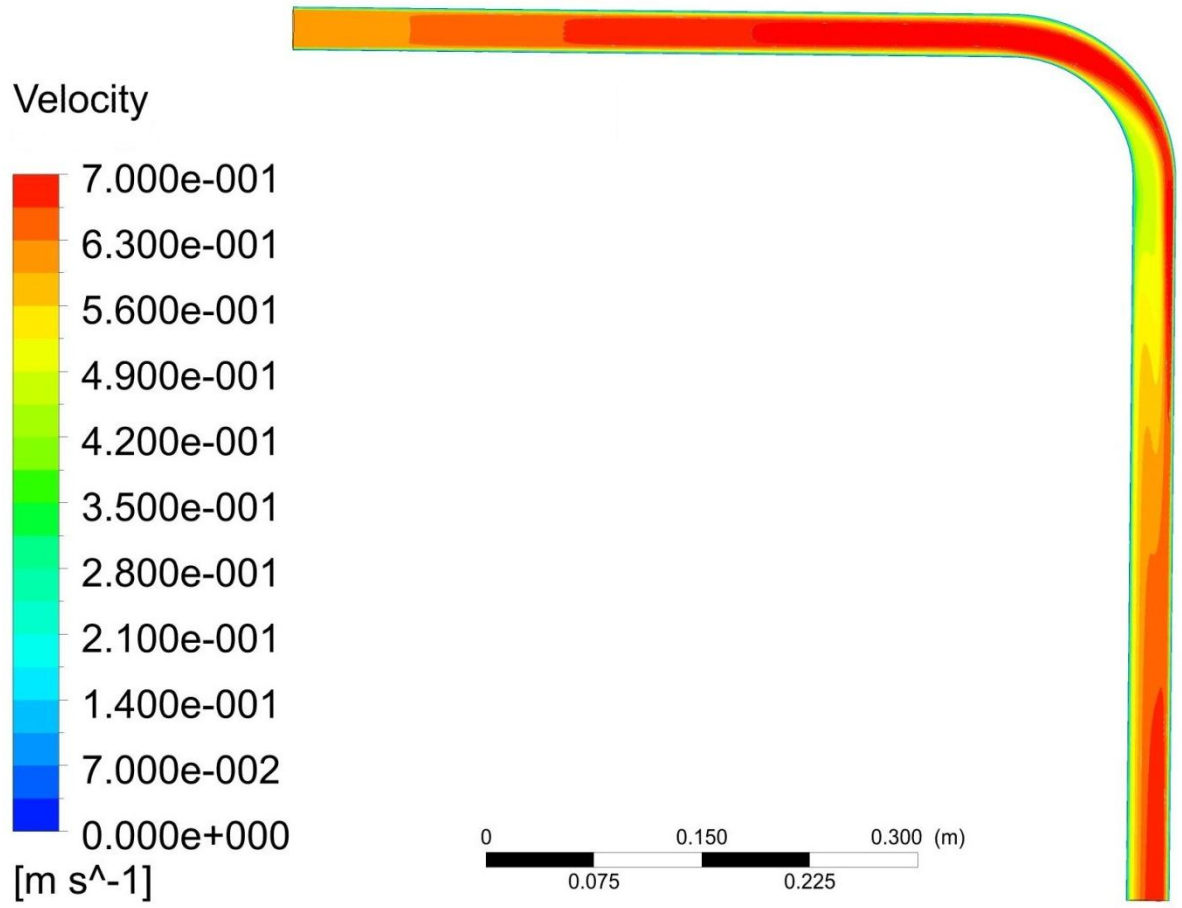

Figure 5.4 - Velocity contours in a curved pipe

To solve this problem an 8L ($0.02m \times 0.02m \times 0.02m$) cubic vessel was constructed with the inlet at the side and the outlet at the bottom. Figure 5.5 shows the velocity contours along the centre plan for a cube with side of 0.01m generated through numerical simulation. After the inlet flow strikes the opposite wall, it spreads throughout the rest of the inlet vessel. This allows the flow to converge on the outlet from all sides, allowing a fully developed profile to develop in a much shorter length of pipe. Any possible effect on the final results caused by a skewed inlet velocity should therefore be eliminated in the final physical model setup.

Stellenbosch University http://scholar.sun.ac.za

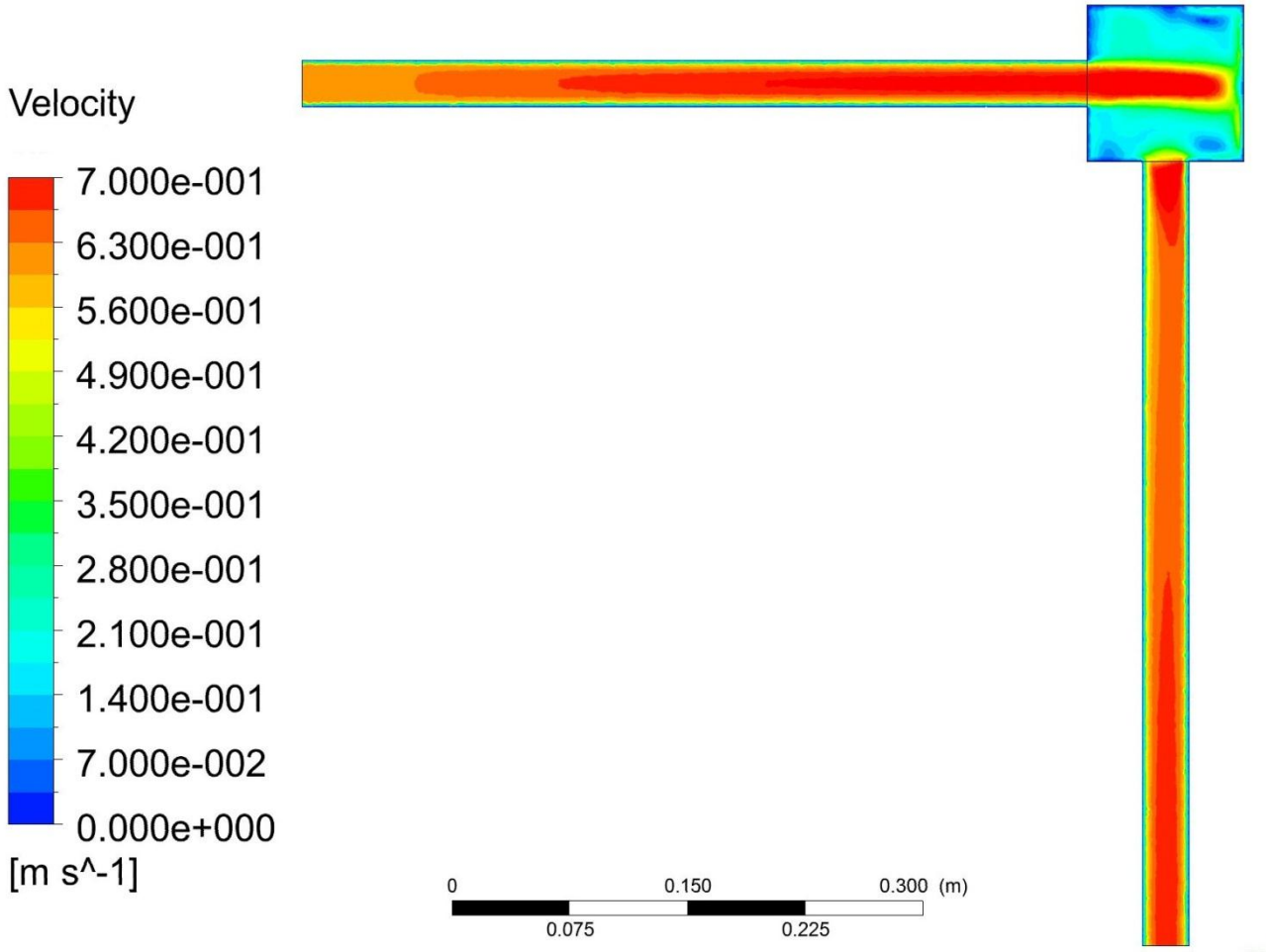

Figure 5.5 - Velocity contours for the inlet design with the cubic vessel

Another aspect of the inlet design was the method used for tracer injection. To make tracer injection possible, a T-shaped piece of stainless steel pipe was welded to the bottom of the inlet vessel. The T-piece ended in a small pipe, over which a plastic tube could be fitted. Tracer was injected through the tube using a syringe. A micro-valve in the tube could be closed to prevent air from entering the system. Since the injection tube is small, the tracer will enter the system at a relatively large velocity. For this reason the T-piece was placed as close to the inlet vessel as possible, to reduce any effect this may have on the velocity profile where the flow enters the tundish model. Figure 5.6 shows a schematic representation of tracer injection in the T-piece.

Stellenbosch University http://scholar.sun.ac.za

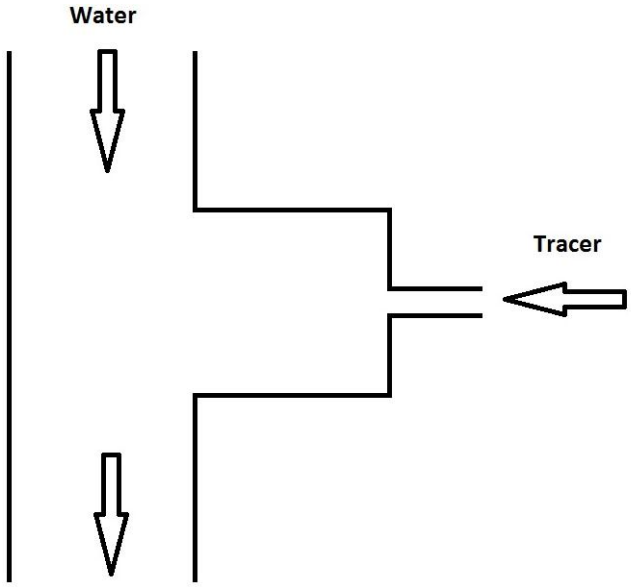

Figure 5.6 - Schematic representation of tracer injection in the T-piece

A section of pipe was inserted at the bottom of the T-piece. The length of the pipe was chosen so that the fluid exits the pipe at a height of 165mm from the bottom of the tundish model. The pipe used has an inner diameter of 28.5mm, the closest to 30mm available. This will cause a slightly raised inlet velocity from the desired model parameters, but the effect on the residence time distribution will be small, due to the insensitivity of the model to the Reynolds and Froude numbers discussed in section 5.1.2. The inlet vessel was mounted on a stand that fits over the tundish model and can be placed in the centre of the tundish model.

5.3.3. Outlet Configuration

The ball valves in the outlet pipes of the physical model only served the purpose of stopping flow when filling the tundish model, not controlling the flow rate. The outlet flow rates, driven by gravity, were fixed to be equal to the inlet flow rate by controlling the outlet diameter at a certain bath height. The outlet velocity for a chosen bath height, h, could be calculated from the following equation, derived from Bernoulli's equation:

$$v = \sqrt{2gh} \qquad [5.18]$$

For the calculated velocity, the diameter was then selected to deliver the desired volumetric flow rate at the outlet. This diameter was achieved by placing a PVC insert with the desired inner diameter in the outlet hole. The top edge that prevents the insert from falling into the hole was kept to a minimum height to prevent interference with the flow.

For equation 5.18 to be valid, certain requirements had to be reached. Firstly, the pressure at the outlets had to be atmospheric, the same as at the top of the liquid. However, in reality the pipe going down to the storage tank caused a vacuum to form below the outlets, causing higher than expected flow. This was rectified by placing micro-valves in the outlet

Stellenbosch University http://scholar.sun.ac.za

pipes, just below the tundish model. This allowed air to enter the pipe and establish atmospheric pressure.

The second condition was that the frictional losses through the insert must be minimised. Friction losses associated with the type of orifice used can cause significant deviations from equation 5.18. The pressure drop over the insert was minimised by rounding the upper edge of the insert and by giving it a length several times longer than the inner diameter.

To test that the outlet flows were correct, the volumetric flow rate was measured three times for each outlet by determining the volume of water exiting the outlet in sixty seconds. The results are shown in Table 5.2 and indicate that all outlet flow rates were within 2% of the desired rate.

Table 5.2 - Results for three runs testing the deviation of flow rates of the four outlets from the desired value

Outlet	Volumetric flow rate (m3/s)				% Error
	Run 1	Run 2	Run 3	Average	
1	0.107	0.106	0.104	0.106	1.90
2	0.107	0.107	0.106	0.107	0.969
3	0.108	0.110	0.108	0.109	0.995
4	0.107	0.108	0.110	0.108	0.530

5.3.4. Measurement Vessels

A method had to be designed to measure conductivity with the available field instrument, without interfering with the flow or producing a long delay between the time the tracer exits the tundish and the time of measurement. For this purpose two measurement vessels were constructed to be placed below the PVC pipe at the two outlets designated for measurement. The vessel volume was limited to the minimum required to insert the conductivity sensor in order to minimise the residence time. Assuming that the flow in the tundish is symmetrical, measurement was only done for one half of the tundish.

5.4. Experimental Procedure

To start experimentation the tundish model was first allowed to fill with the outlets closed. The flow was then stopped. A small period of time was allowed for the remaining flow patterns to dissipate before the inlet flow was turned on again, the flow rate was adjusted to the desired value and the outlet valves were opened. The micro-valves in the outlet pipes were then also opened to obtain the desired outlet flow rate. Approximately 15 minutes were allowed for the flow pattern in the tundish to develop before experimentation started.

The experiment was begun by injecting 50mL of potassium chloride tracer, with a concentration of 200g KCl per 1L water, through a syringe into the inlet pipe. The injection

Stellenbosch University http://scholar.sun.ac.za

was done gradually over a period of 5 seconds to minimise the effect on the inlet flow. This period was argued to be small enough compared to the minimum and average residence times of the tundish to make this approach acceptable. To confirm this argument a numerical experiment was used to investigate the effect of the 5 second injection in the tundish with a turbulence inhibitor. This was done by comparing the RTD response for a case where the tracer was injected over 5 seconds and for a case where a volume of tracer was defined below the nozzle port at the start of the simulation. Figure 5.7 shows the 5 second injection causes a small delay in the response at the outlet. However, the effect was considered to be small enough to justify the injection approach.

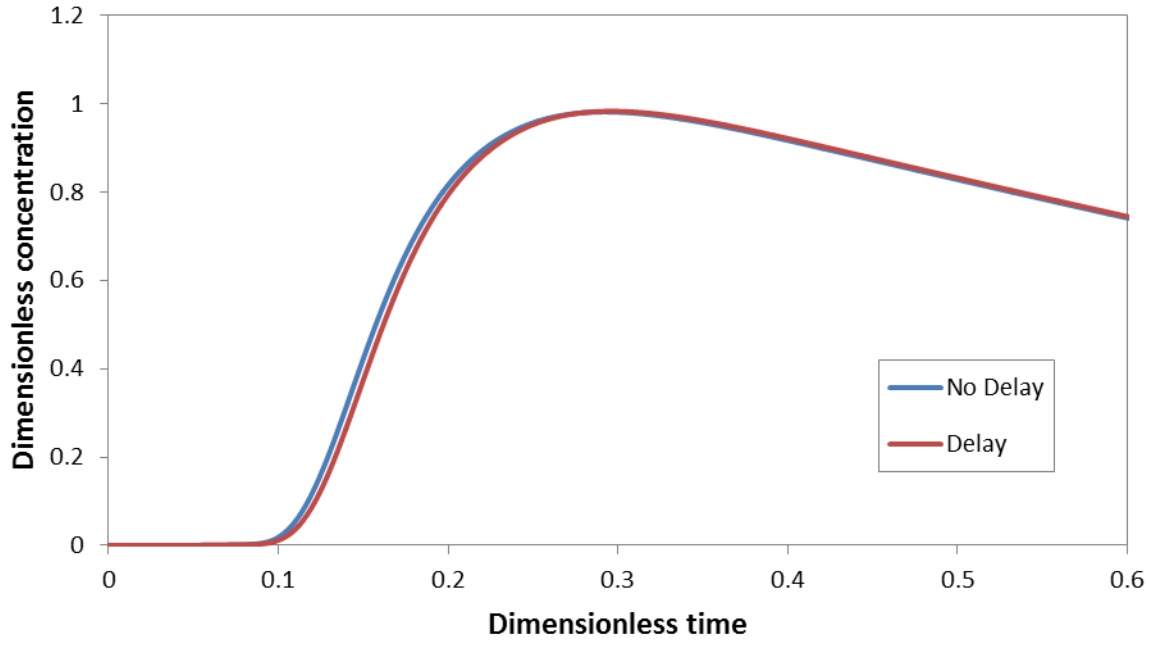

Figure 5.7 - Comparison of RTD curves using numerical simulation for a pulse tracer injection and injection of a period of 5 seconds

The concentration of the tracer in the outlet flow was then monitored on a computer for the duration of the experiment using a conductivity meter. The meter was calibrated using a 0.01M conductivity standard. The experiment was allowed to continue for a period of 35 minutes, approximately 3.5 times the theoretical residence time of the tundish, after which the data was saved to file for further analysis. Since only one conductivity meter was available the process had to be repeated twice, once for each outlet.

Stellenbosch University http://scholar.sun.ac.za

Chapter 6: Physical model results

The physical model setup was used to analyse the flow using three different tundish configurations. The flow rate, bath height and nozzle outlet position are maintained at the levels specified in Section 5.3. The first case considered is a bare tundish with no flow control devices. The second case employs the turbulence inhibitor with holes in combination with low dams (TID case), as recommended by Kumar et al. (2008). The third case utilizes only a turbulence inhibitor, with the holes closed to prevent short circuiting (TI case). This case serves the purpose of analysing whether the use of holes and dams, which is expected to increase the operational cost due to refractory wear, offers significant improvements in the flow characteristics to validate their use.

6.1. Repeatability of Results

Some degree of variability is expected in the experimental results, due to experimental error and the natural variability caused by the transient behaviour of the process. Possible sources of experimental errors include the inlet flow rate, the amount of tracer injected, the rate of injection and the outlet flow rates. To account for variability in the results, replicate runs were performed for each setup and the average values used in calculating the flow characteristics using the combined model. To form an idea of how many replicates should be performed to obtain a representative average value, five replicate runs were carried out for the case using the TID setup. Figure 6.1 compares the RTD curves for the five runs up to $\theta = 2$ and from visual inspection the variability seems to be generally low.

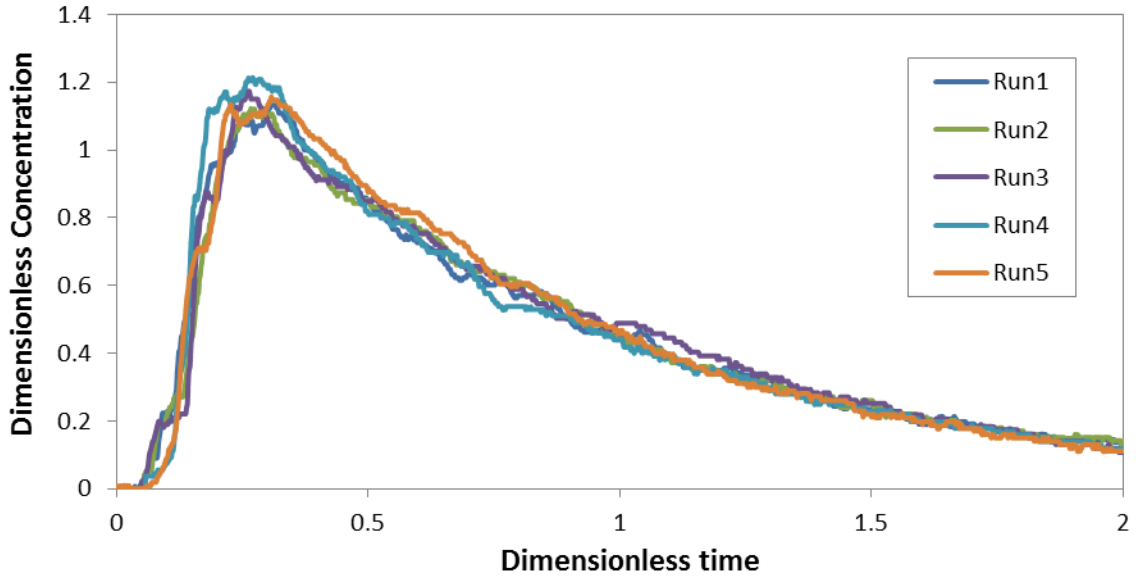

Figure 6.1 - Residence time distributions for five replicate runs using the TID setup

By comparing important flow characteristic properties for the five replicates, the repeatability can be analysed more accurately. These results are summarised in Table 6.1

Stellenbosch University http://scholar.sun.ac.za

and shows that the repeatability of the experiment is relatively high. For all values, excluding the minimum residence time (θ_{min}), the coeffiecient of variation (CV) is lower than 0.07. The relatively high variation in the value of the minimum time is due to the short time after which breakthrough occurs. Compared to this small value of time the slight experimental errors in tracer injection, flow rate setup and measurement become more significant. Based on this evidence it seemed reasonable that three runs would be sufficient to obtain averaged results for the TID case.

Table 6.1 - Comparison of flow characteristic properties for five replicate runs performed using the TID setup

	Run 1	Run 2	Run 3	Run 4	Run 5	Average	Variance/average
$\boldsymbol{\theta_{min}}$	0.039	0.051	0.045	0.059	0.059	0.050	0.173
$\boldsymbol{\theta_{peak}}$	0.295	0.271	0.263	0.269	0.306	0.281	0.066
$\boldsymbol{\overline{\theta}}$	0.846	0.866	0.847	0.830	0.826	0.843	0.019
$\boldsymbol{C_{peak}}$	1.13	1.12	1.17	1.20	1.13	1.150	0.029
$\boldsymbol{V_{dp}}$	0.167	0.161	0.154	0.164	0.182	0.166	0.063
$\boldsymbol{V_d}$	0.287	0.300	0.288	0.318	0.304	0.299	0.042
$\boldsymbol{V_m}$	0.546	0.539	0.558	0.518	0.513	0.535	0.035

However, for the bare case, where the peaks occur at an earlier time, this variance is expected to increase. This is because the minimum and peak residence times are much shorter than for the cases including the turbulence inhibitor. Therefore, experimental errors will have a larger effect on these values. Comparing five replicate runs for the bare setup in Figure 6.2, it can be clearly seen that significant variation occurs, especially in the region of the second peak. For this reason, it was decided that five replicates would be used for each case.

Stellenbosch University http://scholar.sun.ac.za

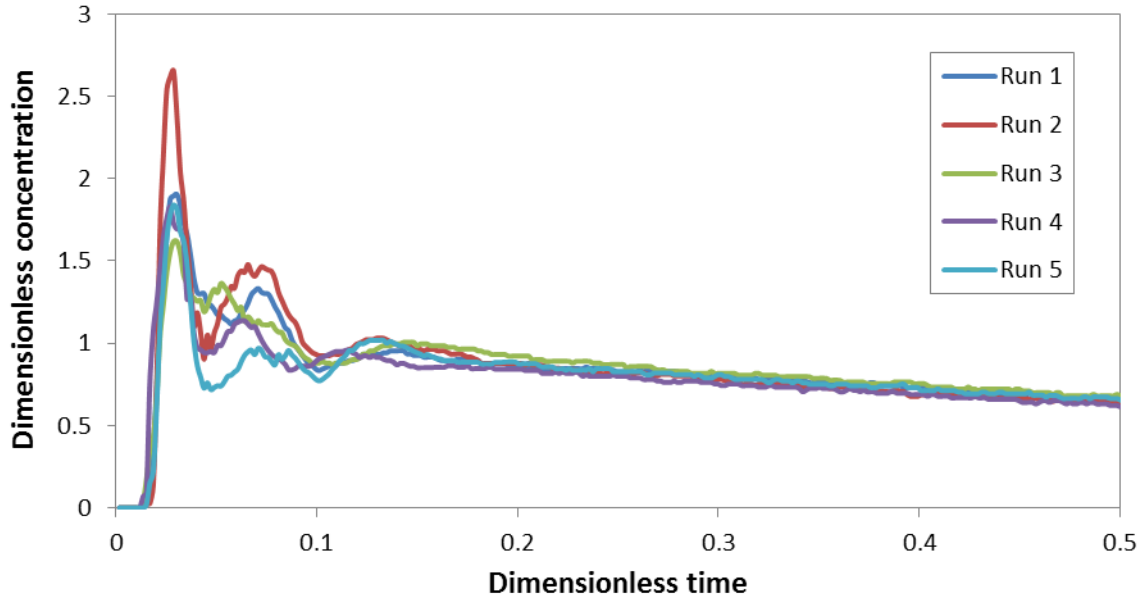

Figure 6.2 - Comparison of RTD curves for the 5 runs performed on the physical model for the bare setup

6.2. Comparison of the C-curves for the Different Setups

By plotting the overall RTD curves for each of the three tundish configurations on the same axes, some conclusions can be drawn regarding the flow behaviour of each and the expected relative performance can be derived. Such a comparison is shown in Figure 6.3.

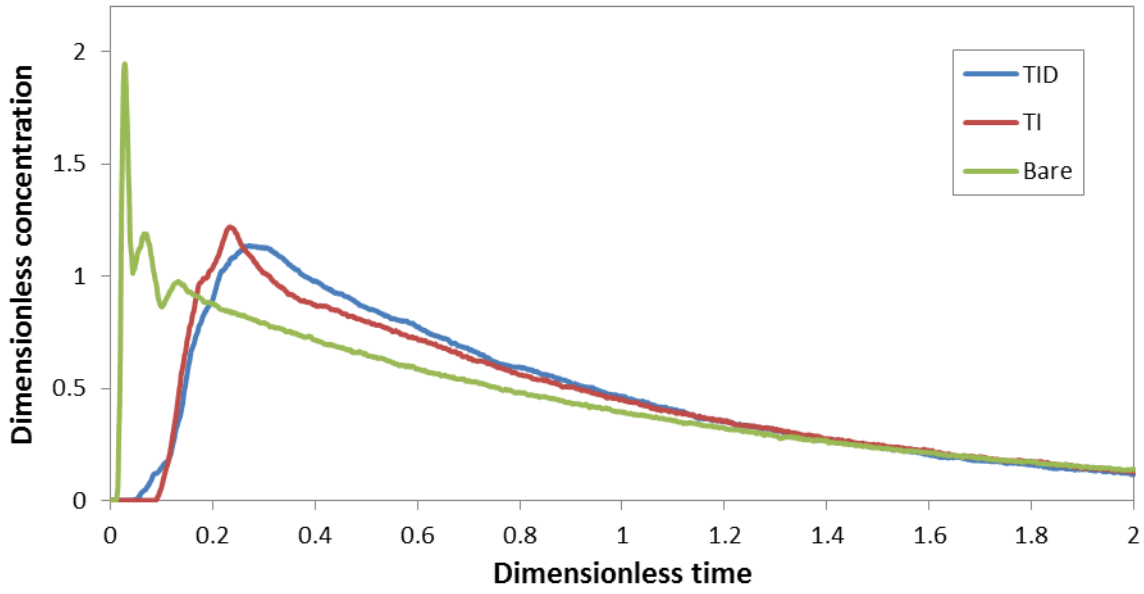

Figure 6.3 - Comparison of RTD responses for three different tundish configurations, as obtained from the average values of the physical experiments

The first observation that is immediately apparent is how much the bare configuration differs from the two cases with flow control devices. The minimum residence time is nearly

Stellenbosch University http://scholar.sun.ac.za

zero and a relatively large fraction of the flow will spend a very small time in the tundish. Since smaller inclusions require larger residence times to rise to the slag layer, these short residence times may not be sufficient for the removal of some of the larger inclusions. These large inclusions will pass directly to the mold, lowering the quality of the steel product produced. This short circuiting behaviour can be logically expected, since it is obvious that a portion of the melt flowing down from the nozzle port will flow directly to the outlet after striking the bottom of the tundish.

However, for the cases with the turbulence inhibitors present, the short-circuiting is prevented since the flow is forced upwards. This leads to a much larger minimum residence time than for the bare case and also causes a clear shift of the peaks in the RTD curves to occur later. It can therefore safely be assumed that the maximum inclusion size present in the mold for the TI and TID cases will be smaller than for the bare case. The upward directed flow from the turbulence inhibitor can also benefit inclusion removal, as it will help to bring inclusions in contact with the slag for absorption. However, care should be taken that the flow making contact with the slag layer does not generate sufficient turbulence to cause slag entrainment, which can have seriously detrimental effects on the product quality.

When comparing the C-curves for the TID and TI cases, the responses are fairly similar. Nonetheless, two observations can be made. Firstly, the minimum residence of the TID case (21.0 s) is considerably lower than that of the TI case (53.0 s). The most likely explanation for this is that the height of the dams is insufficient to completely prevent the flow passing through the holes from short-circuiting to the outlets. Although only a very small fraction of the flow experiences this short circuiting, it might allow some large inclusions into the product. The second observation is that the addition of the holes in the turbulence inhibitor and the dams causes a slightly later peak concentration, which means that apart from the small fraction that short-circuits, the first portion of fluid to arrive at the outlets spend a slightly longer time in the tundish, which implies more flotation time for large inclusions.

6.3. Comparison using the Modified Combined Model

A more quantitative method of comparison between the three different cases is to compare the values of the important dimensionless times (minimum, peak and mean times) and the parameters calculated using the modified combined model, as discussed in Section 3.4. This comparison is summarised in Table 6.2.

Stellenbosch University http://scholar.sun.ac.za

Table 6.2 - Comparison of the dimensionless minimum, peak and mean residences times, as well as the dispersed plug flow volume, dead volume and well-mixed volume fractions for the three tundish configurations, as calculated from the physical experiments

Configuration	θ_{min}	θ_{peak}	θ_{mean}	V_p	V_d	V_m
Bare	0,0101	0,067	0,687	0,039	0,370	0,591
TID	0,0354	0,264	0,747	0,150	0,299	0,551
TI	0,0892	0,234	0,756	0,162	0,306	0,532

The bare tundish is clearly inferior to both the other cases based on these values. The significantly lower minimum, peak and mean residence times will all mean less time for inclusions to be removed. Additionally, the lower plug volume fraction implies flow that is less suitable for inclusion removal, while the higher dead volume fraction will lower thermal and compositional homogeneity.

When comparing the TI and TID cases, the values are much closer to each other. The most significant difference lies in the minimum residence times, where the breakthrough time for the case with the holes and dams is less than half of that of the case with only the turbulence inhibitor. The only possible advantage of the TID case lies in a slightly larger peak residence time. Therefore, from the physical experimental results alone, there is no clear evidence that the addition of the holes and dams provided any significant improvement to flow behaviour in the tundish.

As a matter of interest, a comparison was made between the plug volumes calculated in the three different ways described in Section 3.4.2: the normal plug flow volume of the combined model by Kemeny et al. (1981), the dispersed plug flow of the modified combined model by Ahuja & Sahai (1986) and the alternative method suggested by Zong et al. (1999). Figure 6.4 shows that with all three methods the plug flow volume for the bare case is predicted to be much lower than the other. The main limitation of the combined model method by Kemeny et al. (1981) using only the minimum residence time in the calculation, can be observed by looking at the very low plug flow volume predicted for the TID case. This is because of the short-circuiting over the dam that causes a much lower minimum residence time than for the TI case. However, this short-circuiting only takes place for a very small fraction of the flow, otherwise the flow behaviour for the TID and TI cases are very similar. Therefore, the relative values for the other two methods, which suggests only slightly more plug flow like behaviour for the TI case than for the case with the holes and dams added, seems much more reasonable. Comparatively, the dispersed plug flow of the modified combined model and the plug flow proposed by Zong et al. (1999) show similar trends for the three cases investigated with the physical model. This is of interest, since the method of Zong et al. (1999) is proposed to be applicable to a large variety of reactors, with very different C-curves. The dispersed plug flow, which is calculated only from the minimum

Stellenbosch University http://scholar.sun.ac.za

and peak residence times, will be less likely to be an accurate measure of flow performance for a large variety of designs, although more so than the method based only on the minimum residence time. However, the advantage of the dispersed plug flow from the modified combined model over the method proposed by Zong et al. (1999) is that it gives physical meaning to the dead and mixing volumes, which can serve as additional criteria by which to measure tundish performance. It is therefore encouraging to note that for the three configurations discussed the same conclusions could be drawn from the two different methods and it would be interesting to note whether this applies for a variety of tundish configurations.

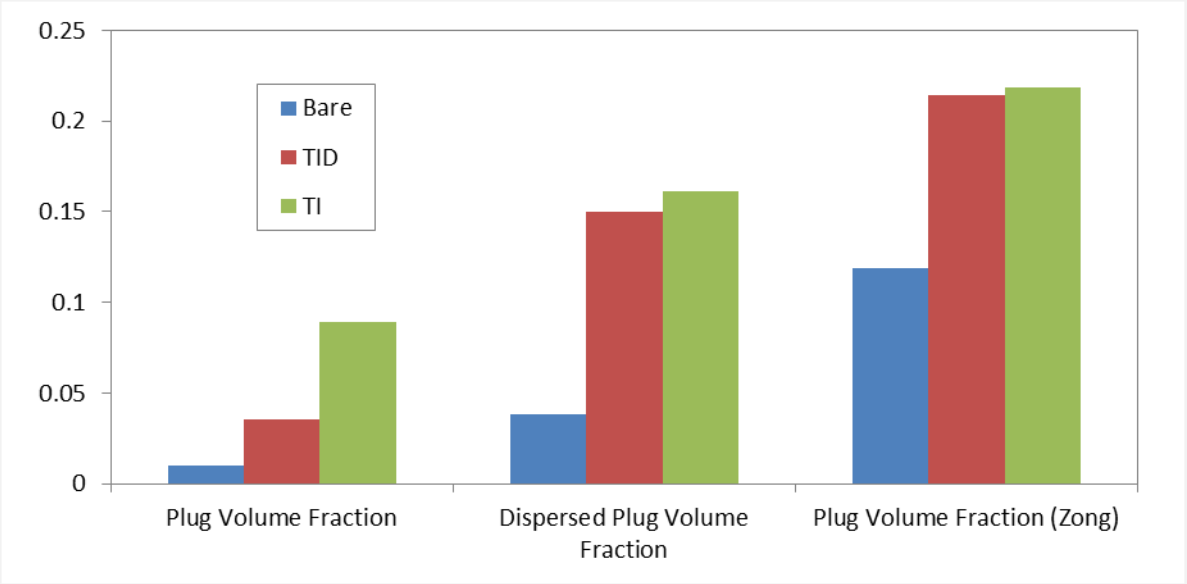

Figure 6.4 - Comparison of plug volume fractions by using three different methods

6.4. Comparison of Variation Between Strands

Another method of analysing the performance of a multi-strand tundish is to compare the C-curves for the individual strands. This is of practical importance to industrial practice since the melt arriving at the different outlets can have significantly different temperatures and compositions, most important being the size and quantity of inclusions, if the melt reaching these outlets have spent different times in the tundish. This will affect the way that the casting process is controlled, since either the casting in each strand will have to be operated under different conditions or a compromise has to be found between two strands, with both operating at non optimal conditions. One method of doing such a comparison is to calculate the parameters of the modified combined model for each outlet and compare the values. Such a comparison is summarised in Figure 6.5, by plotting the difference between each of the important properties for the outer and inner strands for the three configurations studied with the physical model. For all three cases it is apparent that the outer strand performs better than the inner strand, with the minimum, peak and mean residence times and the plug for volumes being higher and the dead volume being lower.

Stellenbosch University http://scholar.sun.ac.za

The outer strand is therefore likely to have fewer and smaller inclusions in the mold for all three configurations.

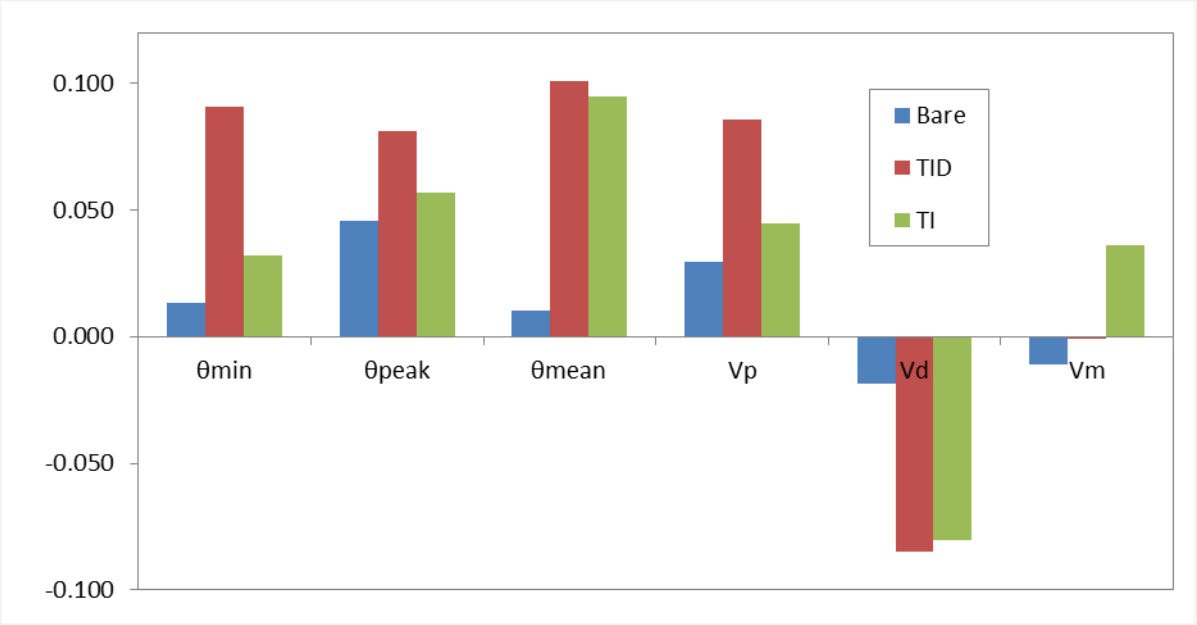

Figure 6.5 - Comparison of RTD parameters for the difference between in the outer and inner strands of the three configurations discussed

Comparing the different configurations, the variation between strands for the bare case is clearly much lower than for the two configurations using the turbulence inhibitor. However, it must be put into perspective by looking at the values summarised in Table 6.3. For all the properties the performance of inner strands of the cases using the turbulence inhibitor is still superior to the outer strand of the bare case. Nonetheless, it does show that the two cases using the turbulence inhibitor are not as superior to the bare case as would be concluded from the overall properties, since the performance of their inner strands are significantly inferior to their outer strands. There is clearly room to improve the design of the turbulence inhibitor and enhance the performance of the inner strand. Lastly, it can be noted that the TI case shows slightly better strand similarity than the TID case. This negates one of the arguments for the addition of holes and dams to the case using only the turbulence inhibitor (Kumar et al., 2008).

Table 6.3 - Comparison of RTD parameters for the outer and inner strands of the three configurations compared in the physical experiments

Configuration	Outlet	θ_{min}	θ_{peak}	θ_{mean}	V_p	V_d	V_m
Bare	Inner	0.010	0.0842	0.682	0.047	0.380	0.573
	Outer	0.024	0.13	0.692	0.077	0.361	0.562
TID	Inner	0.040	0.232	0.697	0.136	0.342	0.522
	Outer	0.131	0.313	0.797	0.222	0.257	0.521
TI	Inner	0.086	0.179	0.709	0.132	0.346	0.521
	Outer	0.118	0.236	0.804	0.177	0.266	0.557

Stellenbosch University http://scholar.sun.ac.za

An alternative method that might be useful to quantify the variation between strands, is to calculate the ratio of the area between the C-curves of the two individual strands to the area under the overall C-curve. This value will give a measure of the difference in the RTD response at two different outlets. Calculating the ratio by integrating from the beginning of the experiment to $\theta = 2$, the strand variation for the bare tundish, the TI case and the TID case are 0.165, 0.222 and 0.254, respectively. This method therefore ranks the strand variability of the three configurations in the same order as was found when comparing the different RTD parameters. For this case, this ratio appears to be a good method of estimating the variation between strands while only using one parameter. Nonetheless, its validity over a range of applications should be tested further.

These comparisons, however, only give an estimate of the overall difference between the RTD responses at the outlets. For a more specific indication of where the variation occurs, the individual C-curves should be plotted on the same axis for each case. For the bare tundish, it can be seen in Figure 6.6 that the peak for the outer strand occurs at approximately double the time as for the inner outlet. However, it only takes a very short time for the concentrations of the tracer to become very similar at the two outlets.

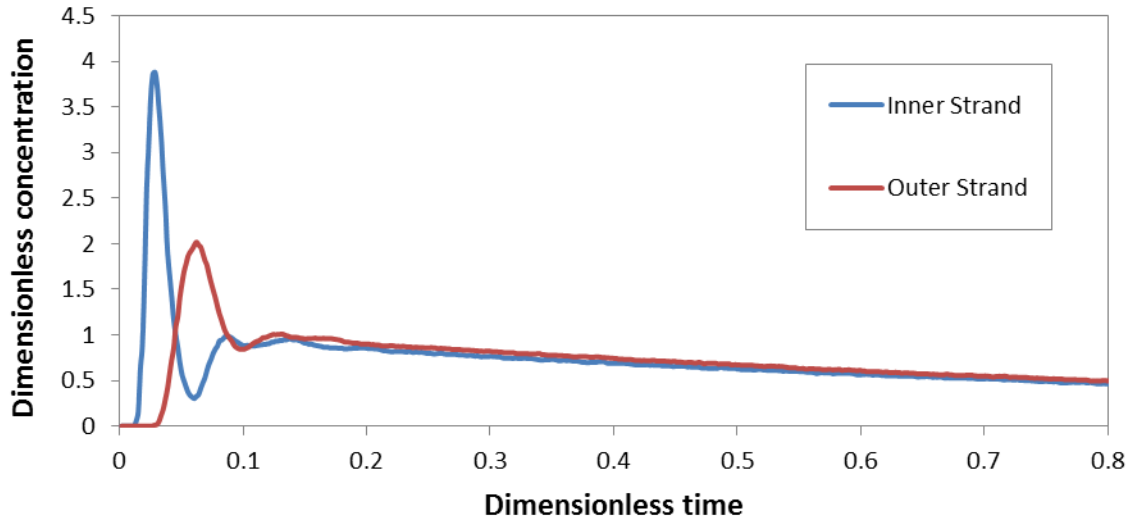

Figure 6.6 - RTD responses for the individual strands for the bare tundish, as obtained from the physical experiments

Such a comparison for the TID, shown in Figure 6.7, shows that although the peaks are much closer to each other, the curves take much longer to establish a similar concentration.

Stellenbosch University http://scholar.sun.ac.za

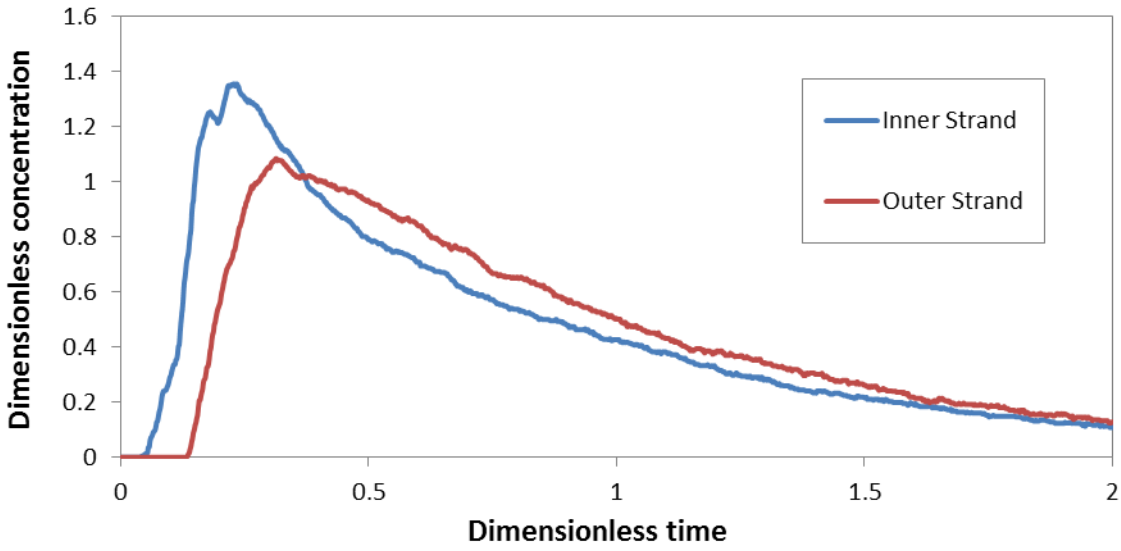

Figure 6.7 - RTD responses for the individual strands for the TID tundish, as obtained from the physical experiments

For the TI case, the comparison in Figure 6.8 shows that the behaviour is very similar to that of the TID case, the main difference being slightly closer concentration values after the curves have crossed.

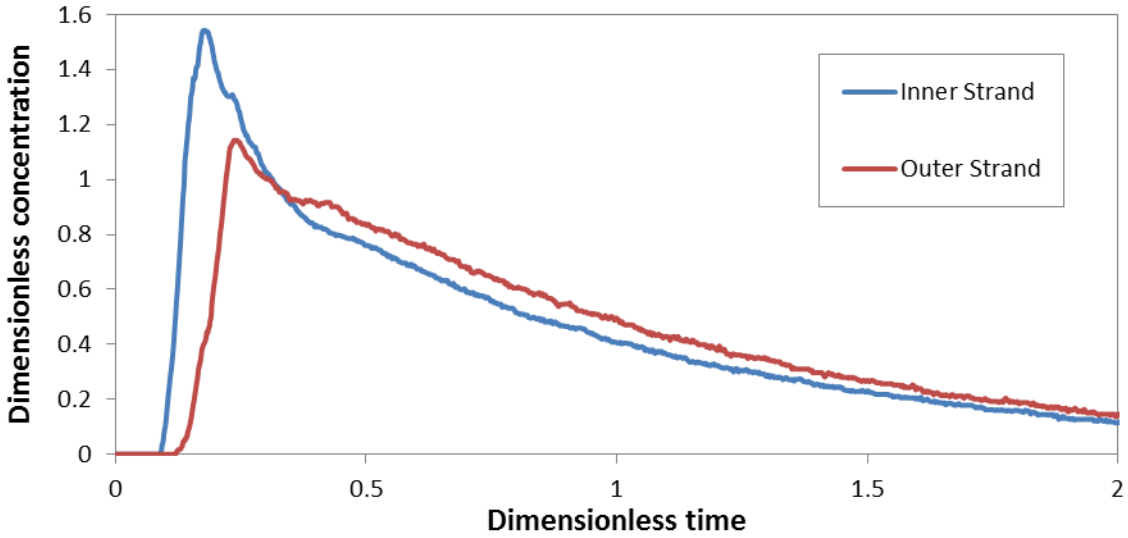

Figure 6.8 - RTD responses for the individual strands for the TI tundish, as obtained from the physical experiments

It can therefore be concluded that the strand similarity is much more for the bare tundish than for the two cases with turbulence inhibitors, with the TI case being the superior of the two by a small margin. Strand similarity should be improved by increased mixing in the tundish. The strand variations compare reasonably well with the calculated mixing volume fractions, shown in

Stellenbosch University http://scholar.sun.ac.za

Table 6.2, where the well-mixed fraction of the bare tundish is significantly higher than that of the two turbulence inhibitor cases. Unfortunately, this trend does not hold for the comparison of the TI and TID cases, where the variation between strands is less for the TI case, but the mixed volume fraction calculated from the overall C-curve is lower. However, when looking at the well-mixed volume fractions for the individual curves, the fractions are higher for the TI case. Therefore, generally, designing for a larger well-mixed volume fraction should decrease the variation between strands. However, the design should be done in such a way that the mixed volume is increased at the expense of the dead volume, instead of the plug flow volume, in order to still promote flow that is beneficial for inclusion removal.

Stellenbosch University http://scholar.sun.ac.za

Chapter 7: Numerical Model Setup

When attempting to obtain a numerical solution using CFD, several important decisions need to be made regarding the setup of the numerical model, each of which will have an effect on the computational time required to obtain the solution, as well as the accuracy of the solution acquired. A clear understanding of the problem being modelled and the theory regarding each choice will therefore help to ensure that accurate results are obtained without requiring unnecessarily long computational times. Unfortunately, very few numerical studies regarding the tundish contain detailed information about the numerical setup and validation of the assumptions used. This situation is problematic for two reasons. Firstly, it can sometimes cause uncertainty regarding the accuracy of the results if the conclusions appear unlikely. Secondly, it also makes it difficult to duplicate the method when a similar problem has to be solved. For this reason, this chapter will attempt to clearly justify and explain all choices made regarding the numerical model setup, using experiments and literature.

7.1. Initial Grid Independence

To begin an investigation of the numerical assumptions employed in the CFD study, a rough idea had to be formed regarding the effect of the grid size on the numerical solution. Several simulations were performed using uniformly sized meshes of tetrahedral cells, except for automatic refinement at curved surfaces to obtain good mesh quality. Tetrahedral cells were necessary for acceptable mesh quality with the presence of the submerged inlet nozzle, small outlets and flow control devices. The sizes of the cells were chosen so that each smaller size approximately doubles the number of cells. It is also important to note that the sizes that are used in this study were based on the element sizes as specified in ANSYS Meshing. The element size is defined as the maximum edge or face length allowable for each cell. Also, for the model development studies, it is important to note that only the first 400 seconds, which corresponds to approximately two thirds of the theoretical residence time, was usually simulated. This is because the long tail is much less sensitive to changes in the numerical setup. The effect of various assumptions and mesh sizes could therefore be best observed by looking at the peak time and concentration, which are more sensitive to changes in the model. This is most likely caused by the fact that the first portion of the tracer to reach the outlets will be that moving through the higher velocity areas of the tundish, where higher gradients will occur, making it more susceptible to numerical error. Therefore, to test whether an assumption or simplification has a significant effect on the numerical solution, it is sufficient to compare the first portion of the RTD responses. However, longer times must to be simulated for when RTD parameters such as the dead volume fraction and the mean residence must be obtained.

Stellenbosch University http://scholar.sun.ac.za

Figure 7.1 shows the dependence of the RTD solution on grid size for the TID case and compares the results with the results from the physical experiments. It can be seen that decreasing the size down to 8mm has a major effect on the solution. After that the effect becomes smaller, with grid independence effectively being reached at 5mm. However, it can still be seen that the solution differs significantly from that of the physical modelling.

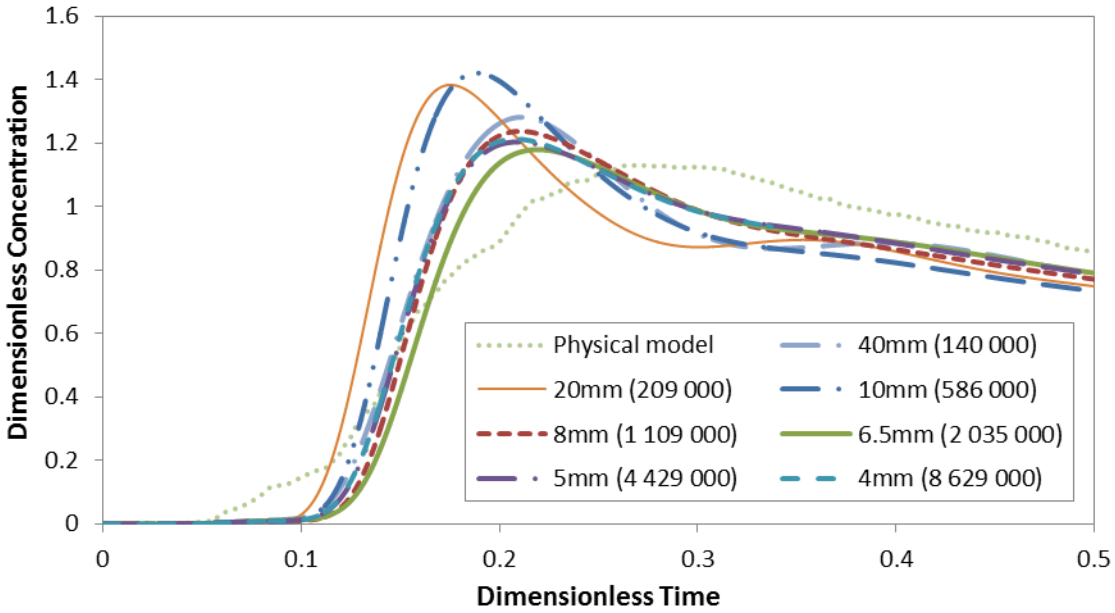

Figure 7.1 - Solution dependence on grid size for uniformly sized meshes, using the overall RTD curves.

The difference can be seen more clearly when comparing the C-curves for the individual outlets in Figure 7.2. Generally, the numerical model predicts much greater strand similarity than the physical model. Two important differences are not accurately predicted by the numerical simulation: Firstly, the significantly shorter minimum and peak residence times for the inner outlet and secondly, the higher concentrations at the outer outlet after the curves have crossed.

Stellenbosch University http://scholar.sun.ac.za

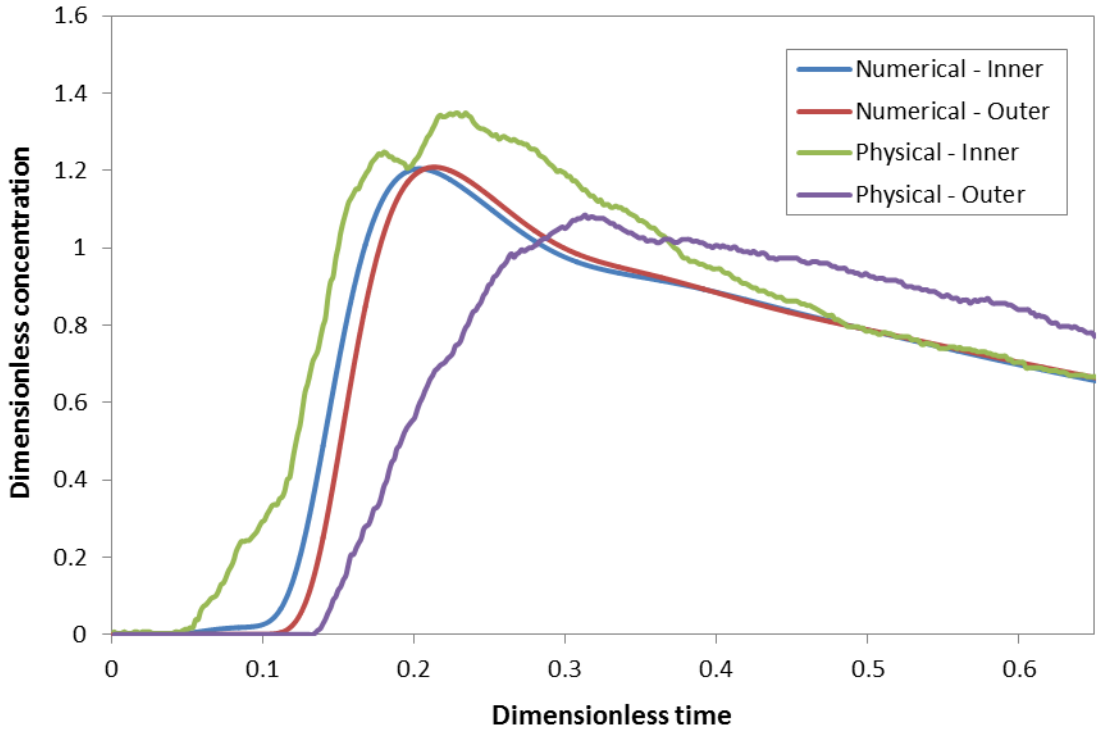

Figure 7.2 - Comparison of individual outlet residence distributions for the physical model and the numerical simulations using a constant mesh size of 5mm

It was revealed that using a mesh adapted in high gradient areas and near surfaces, the numerical solution compares better with the results obtained from the physical model. This approach will be discussed in detail in the following chapter. What is important to note from this section of the study, is that the solution is very dependent on mesh size and that even when using very high density meshes (up to 8 million cells) a uniformly sized mesh does not give accurate solutions.

7.2. Dynamically Steady Flow and Symmetry

When considering the numerical simulation of a tundish there are two simplifying assumptions frequently used in literature that can greatly reduce the computational times required. By employing symmetry planes it is assumed that when the geometry is symmetrical, the flow fields will also be symmetrical over the symmetry planes. Since the geometry used in this study has two symmetry planes, the volume that has to be solved is decreased to a quarter of the size. This effectively also reduces the number of mesh cells required, and therefore also the computational time, by four times.

The dynamically steady concept assumes that the velocity and turbulence fields in the tundish do not change with time. This allows the user to solve the momentum and turbulence equations using a steady-state equation and activate the transient solver only when tracking the tracer movement through the steady flow field. The benefit of this is that the species equations converge much faster than the momentum and turbulence equations.

Stellenbosch University http://scholar.sun.ac.za

This in turn allows a single iteration per time step to be performed, instead of the approximately 8 required when solving the momentum and turbulence equations transiently. This effectively reduces the computational time required for the transient portion of the simulation by eight times, which is very useful considering the long residence time of the tundish. The time required to achieve a steady solution is very small compared to the time required to solve the transient movement of the tracer for three times the mean residence time to obtain a RTD response.

Thus, using these two assumptions in combination basically causes the difference between the same simulation taking a day or taking a month. However, it is inevitable that both of these assumptions will introduce error to the numerical results. Although many researchers have used the assumptions of symmetry (Tripathi & Ajmani, 2011; Tripathi & Ajmani, 2005; Jha et al., 2001; Jha et al., 2008) and dynamically steady flow (Tripathi & Ajmani, 2011; Tripathi & Ajmani, 2005; Jha et al., 2001; Zhong et al., 2007; Kumar et al., 2008; Mishra et al., 2012), no studies were found where the effects on these assumptions on the numerical model had been tested.

For this reason it was decided to investigate the effect that these assumptions will have on the numerical solution. However, from the initial grid independence study, it was apparent that this comparison would not be possible using a grid independent solution, since the combination of a high number of cells and a non-simplified solution procedure would lead to unrealistic computational times with the available processing power. In the end it was decided that a uniform mesh of 14mm cells would be used, as this was the finest mesh that seemed practical. Although the results are not expected to be accurate, due to the coarse grid, it should still serve as a valid comparison between the simplified and non-simplified solution procedures.

To analyse the assumptions, three different cases were compared: using both symmetry planes and the dynamically steady assumption, applying the dynamically steady assumption on the full geometry and neglecting both simplifying assumptions. The reason it was decided to investigate the case ignoring both assumptions, despite it being the most computationally expensive, is that the effect of ignoring symmetry will most likely be most clearly seen when the momentum and turbulence equations are solved transiently. This is because the changing flow patterns may cause unsymmetrical flow to develop.

Two observations were made during the course of this experiment, before comparing the residence time distributions of the three different setups. Firstly, the repeatability of the numerical experiments was much lower than expected for all three cases, when a new mesh was generated for each run. For this reason three simulations were run for each case and an average RTD calculated. A comparison of the C-curves at the same strand for three runs without symmetry and dynamically steady assumptions are shown in Figure 7.3. It is clear that the shape of the responses is significantly different in each case.

Stellenbosch University http://scholar.sun.ac.za

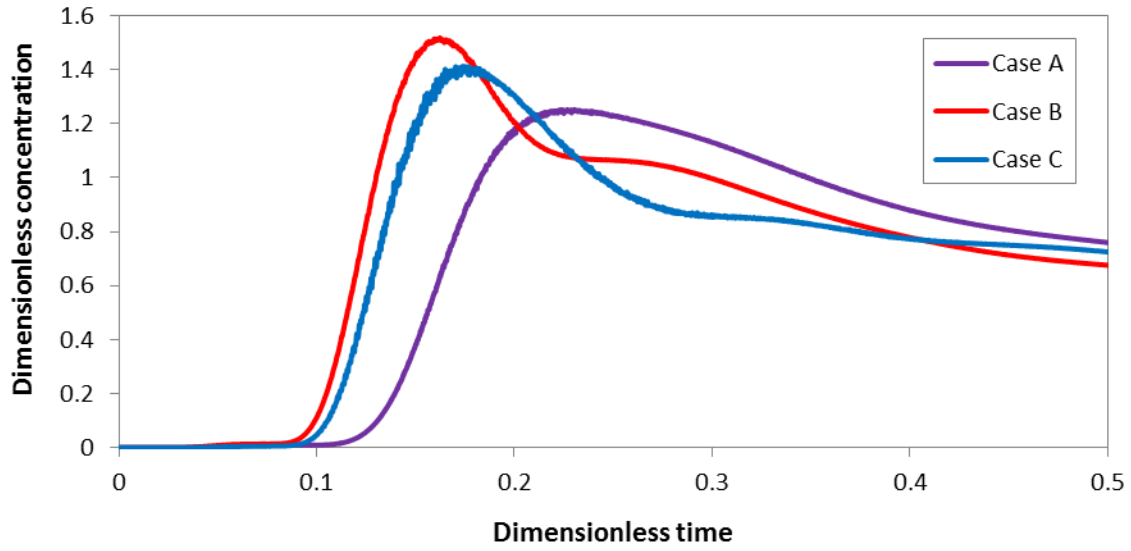

Figure 7.3 - Comparison of the RTD curves for three replicate runs without symmetry and dynamically steady assumptions for the TID case

The second observation is regarding symmetry. Figure 7.4 shows the variation between the RTD responses at the different outlets when neglecting both assumptions. It is seen that the symmetrically placed outlets have very different C-curves for both the outer (1 & 4) and inner (2 & 3) outlets.

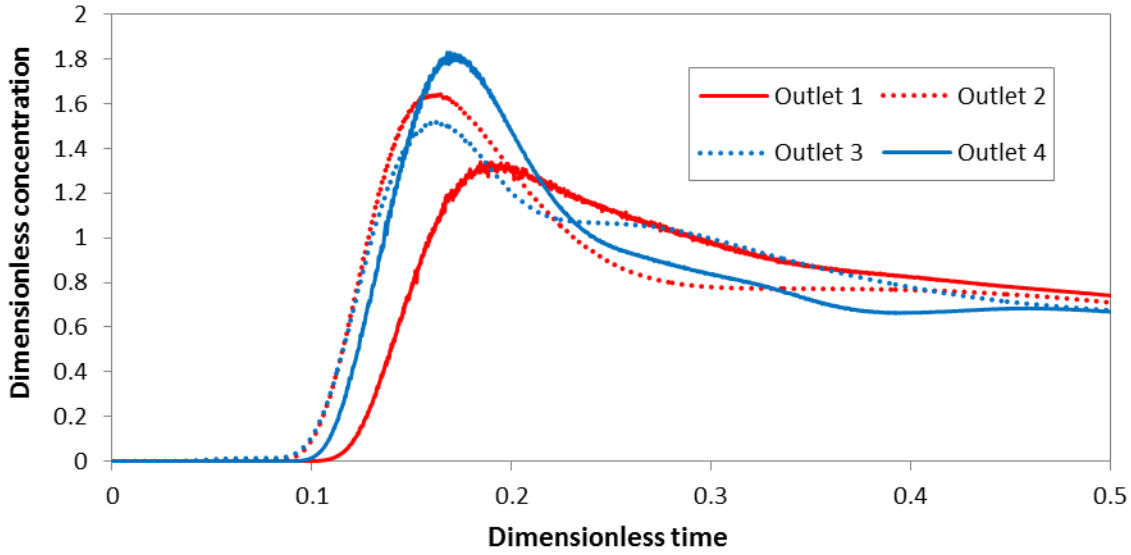

Figure 7.4 - Individual C-curve at the four outlets for a simulation of the TID case without assuming symmetry or dynamically steady flow

Both of these observations seem to suggest that solving the numerical model without applying symmetry or dynamically steady flow will lead to more variation in the RTD curves and non-symmetrical flow. However, the physical experiments definitely do not show such large variations in the same outlet between runs. An alternative suggestion is that the variation between runs and symmetrical halves can be explained by the coarse mesh being

Stellenbosch University http://scholar.sun.ac.za

used. This is because the numerical error introduced by the inaccurate mesh will change every time a new mesh is generated between runs and will also differ in the symmetrical sections. This hypothesis seems likely to be true when looking at the average values of the three replicate simulations. A comparison of the averaged RTD curves for the two symmetrical halves of the tundish is shown in Figure 7.5. The fact that the two curves are nearly identical suggests that the flow is indeed highly symmetrical.

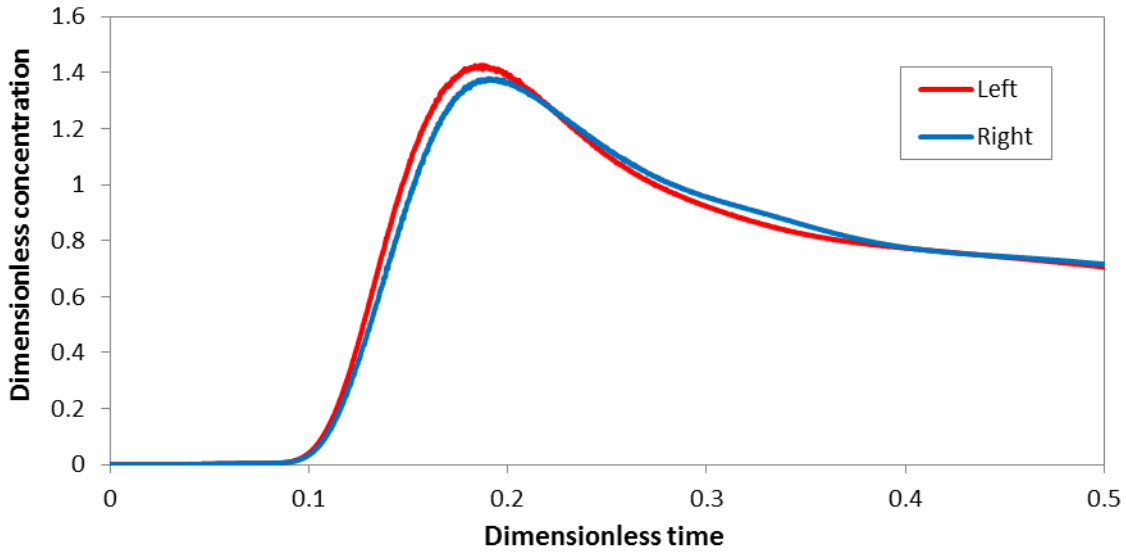

Figure 7.5 - Comparison of averaged RTD responses for the separate halves when simulating the TID case without symmetry or dynamically steady flow assumptions

When comparing the averaged curves for the inner and outer outlets, as shown in Figure 7.6, more realistic RTD shapes are obtained, with the minimum and peak times being smaller for the inner outlets.

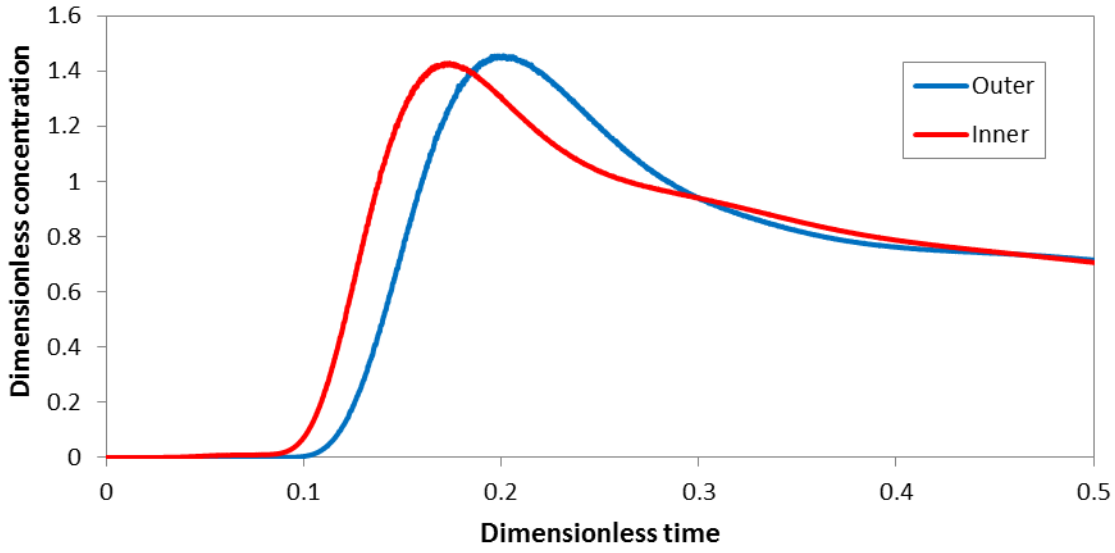

Figure 7.6 - Comparison of averaged RTD responses for the inner and outer outlets when simulating the TID case without symmetry or dynamically steady flow assumptions

Stellenbosch University http://scholar.sun.ac.za

Although this discussion focussed on the fully transient case with no symmetry assumptions, the same general observations can be made for all three numerical setups, with the variations being greater for the two cases where the full volume is modelled. It therefore seems likely that the variation between runs can be explained by the coarse grid and that a valid comparison between the three numerical setups can be made using average values of several replicate runs. However, a similar comparison using a grid independent mesh is suggested for future investigation.

When comparing the average RTD responses for the three different numerical setups being considered, the results appear promising. Figure 7.7 shows that there is nearly no difference between the fully transient and dynamically steady simulations when considering the full geometry. A bigger deviation is seen for the two dynamically steady cases, with the model employing both symmetry planes having peak values that is approximately 17% higher. It therefore appears that the effect of assuming symmetry is significant and that solving the full volume is advisable for accurate results. However, from knowledge gained from further grid investigations, as discussed in Chapter 8, it was seen that the effect of accurately resolving the mesh is much more important than solving the full geometry. Unfortunately, a grid independent mesh for the full geometry would require a high density mesh and very long computational times. For this reason it was decided to use the model applying both symmetry planes and dynamically steady flow and focus on obtaining a grid independent solution.

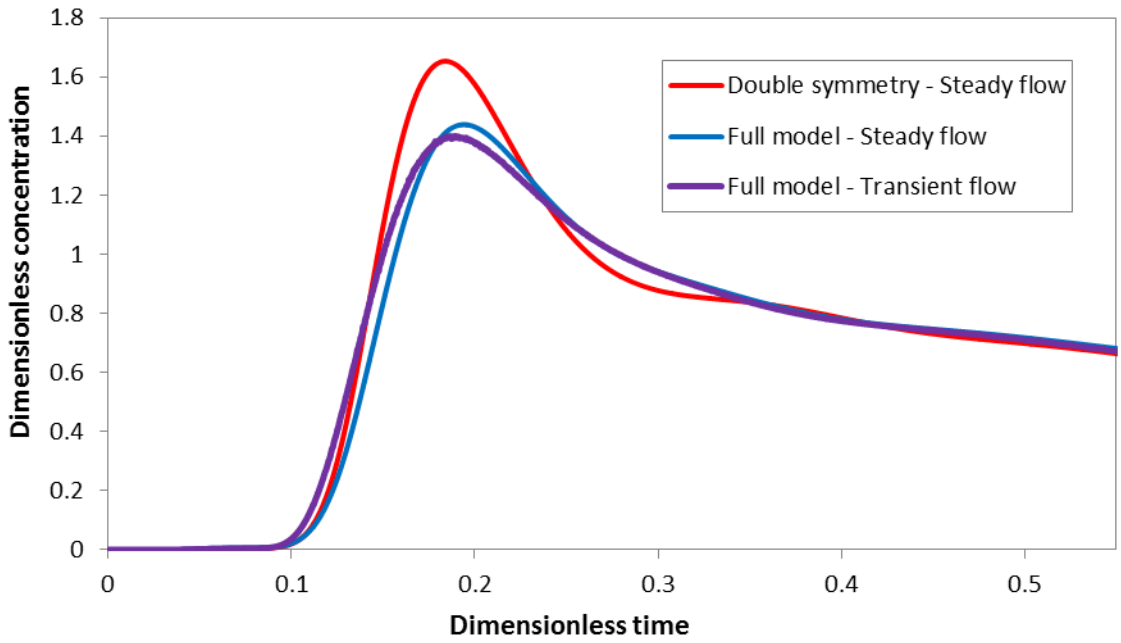

Figure 7.7 - Comparison of average RTD curves for the three different numerical setups: applying both symmetry and dynamically steady flow, applying dynamically steady flow to the full geometry and neglecting both assumptions

Stellenbosch University http://scholar.sun.ac.za

7.3. Turbulence Modelling

The use of turbulence models in the numerical simulation of tundish flow has been the subject of several investigations in literature. This is due to the fairly complicated nature of turbulence in the tundish. Flow near the inlet and outlet of the tundish is highly turbulent, while it may be weakly turbulent in other areas. For this reason the κ-ϵ turbulence models may not be strictly applicable to all regions of the tundish, since they require fully turbulent flow.

The majority of studies, however, have used the standard κ-ϵ model (Tripathi & Ajmani, 2005; Zhong et al., 2007; Kumar et al., 2008; Jha et al., 2008). However, a study by Schwarze et al. (2001) compared the standard and RNG κ-ϵ turbulence models in a V-shaped tundish and found that although the velocity fields did not differ much, the standard κ-ϵmodel over predicted the turbulent kinetic energy. Comparing the results with experimental data, they concluded that the RNG model approximates the turbulence better in situations with high streamline curvature. Another study, by Hou and Zou (2005) using a swirling tundish, found that the RNG κ-ϵ model converges faster than the standard κ-ϵ model.

Due to the presence of low turbulence areas in the tundish some authors have also looked at using the RSM turbulence model, which does not have the same limitations as the κ-ϵ models. Kumar et al. (2004) compared the standard κ-ϵ and the RSM models for a bare tundish and found that the results using RSM compared slightly better with physical experiment results. However, the author recommends further work on the accuracy of the RSM model for tundish modelling. Another study (Solorio-Diaz et al., 2004) compared the standard κ-ϵ, standard κ-ω (which incorporates modifications for low Reynolds numbers) and RSM model results to PIV measurements in a swirling shroud tundish. The RSM model delivered the results that compared the best with the physical model results. The disadvantage of the RSM model is, however, that it requires longer computational times than the RANS models and may therefore not be practical for all studies.

The most comprehensive study regarding turbulence models in the tundish was done by Jha et al. (2003), where the effect of several different turbulence models on the predicted residence time distribution was compared. It was concluded that models such as the standard κ-ϵ model, the RNG κ-ϵ model, the Chen-Kim κ-ϵ model and the LES model predict gross flow properties fairly well, but that others, such as the Lam-Bremhorst low Reynolds number κ-ϵ model, predicts initial transient tracer variation better. The author concludes that for most applications the standard κ-ϵ or Chen-Kim κ-ϵ models remain the best option for calculation of overall flow properties, due to the low computational times.

It is therefore apparent that literature cannot clearly suggest a best approach for turbulence modelling in the tundish and that an investigation to determine the most accurate model would be beyond the scope of this thesis and would merit a body of study on its own. It was therefore decided that a κ-ϵ would be used for this study. However, the more recent

"realizable κ-ϵ" was chosen over the standard κ-ϵ model due to the improvements it offers, as discussed in Section 4.3.

7.4. Boundary Conditions

The numerical solution is highly dependent on the way the boundary conditions are defined. For this reason careful selection of the boundary conditions is required to obtain realistic numerical results. Each of the boundaries will now be addressed separately:

7.4.1. Inlet

The first decision regarding the inlet boundary is to select its position. Three locations have commonly been used: the nozzle port (Tripathi & Ajmani, 2011), the meniscus (Jha et al., 2008) and the ladle boundary (Kumar et al., 2008). Since the melt arrives in the tundish through a relatively long nozzle from the ladle in the industrial system, it can be assumed that a non-uniform profile will develop, which may impact the flow in the tundish. Specifying the inlet at the meniscus will not provide sufficient time for the correct profile to develop, while selecting the boundary at the port assumes a flat velocity profile. Numerical simulations by Kumar et al. (2004) have shown that the different possible locations for the inlet boundary do have a significant impact on the RTD response for a bare tundish setup. Simulation with the current numerical setup, applying the same approach of three averaged simulations using a 14mm mesh, confirms that including the nozzle in the model will significantly influence the C-curve for the TID case. This is shown in Figure 7.8.

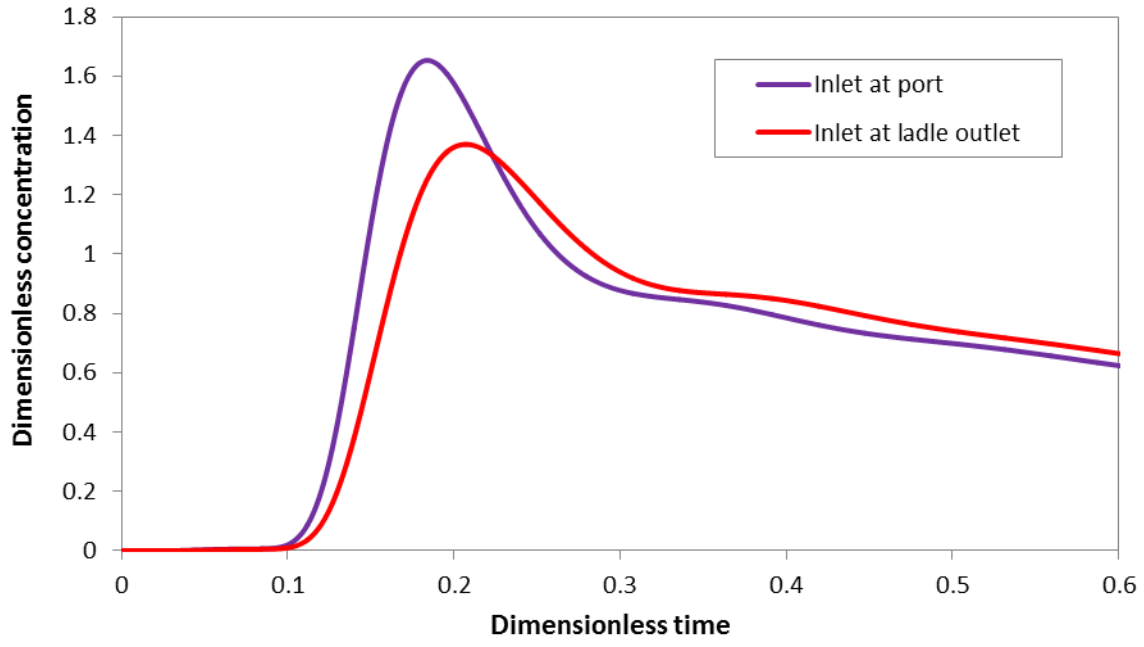

Figure 7.8 - Comparison of C-curve for the TID setup depending on the inlet boundary position

For this reason a section of the inlet nozzle will be included in the numerical model. The boundary at the top of the nozzle is specified as a uniform velocity inlet, the velocity

Stellenbosch University http://scholar.sun.ac.za

calculated from the nozzle diameter and tundish throughput rate. The length of the nozzle is selected so that a fully developed profile forms at the port, as shown in Figure 7.9.

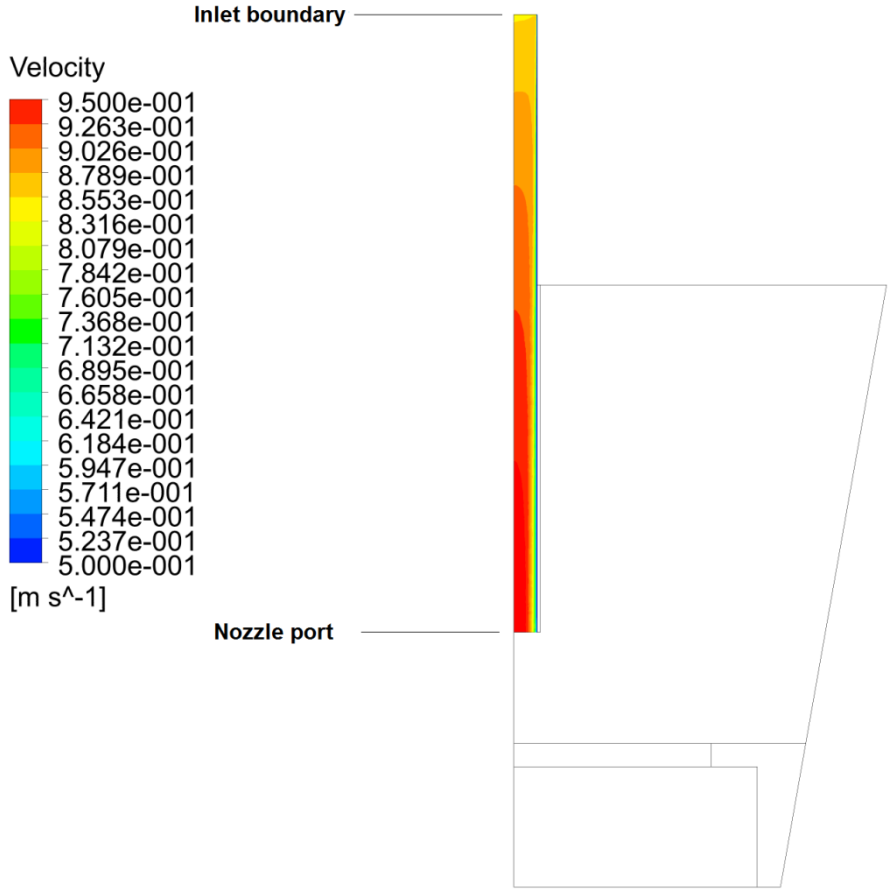

Figure 7.9 - Contour plot showing the development of the velocity profile in the nozzle from the inlet boundary to the nozzle port

The quantities of the turbulent properties at the inlet boundaries were calculated from equations 7.1 and 7.2, which have been used by several authors (Kumar et al., 2008; Hou & Zou, 2005; Solorio-Diaz et al., 2004) to obtain a good correlation between numerical and experimental results. It is also expected that due to the addition of the nozzle in the simulation, the results should be insensitive to the turbulent boundary conditions, since the turbulent properties will also develop along the nozzle.

$$\kappa = 0.01 u_{inlet}^2 \qquad [7.1]$$

$$\varepsilon = \frac{2k^{1.5}}{d} \qquad [7.2]$$

During the transient portion of the simulation, when the species solver is activated, the mass fraction of tracer at the inlet is specified as 1 for the duration of tracer injection.

Stellenbosch University http://scholar.sun.ac.za

7.4.2. Outlets

Two approaches are used for specifying the outlet boundary: using a specified outlet velocity (Liu et al., 2008; Raghavendra et al., 2013) or applying a pressure outlet (Ilegbusi & Szekely, 1989; Jha et al., 2001). A review by Mazumdar and Guthrie (1999) stated that the predicted flow patterns were insensitive to the method used for specifying the outlet boundary. For this study a pressure of 1 atm was used as the outlet boundary condition, since the pressure gradient from the bottom of the melt to atmospheric pressure at the outlet is what drives the flow in the physical model.

7.4.3. Walls

The no-slip boundary condition was applied to the tundish walls, flow control device surfaces and the faces of the nozzle.

7.4.4. Tundish Surface

Nearly all numerical studies of the tundish in literature (Jha et al., 2008; Mishra et al., 2012; Kumar et al., 2008; Tripathi & Ajmani, 2005; Zhong et al., 2007) neglect the presence of a slag layer at the top of the model and assume a flat surface, with zero shear stresses specified at the boundary. The only exceptions are studies that look specifically at modelling the slag behaviour (Li et al., 2012). The reason for the widespread use of the flat surface assumption is that including the slag or melt-air interface requires multiphase modelling. Not only does this increase the complexity of modelling decisions and add to the computational time, it also eliminates the possibility of solving for a steady solution of the momentum and turbulence equations. As discussed in Section 7.2, having to solve the momentum and turbulence equations transiently will drastically increase the required computational time. Unfortunately, no information regarding the effect of the assumption could be found in the available literature. It can be assumed that the presence of a slag layer would cause some dissipation of the energy of the melt flow. Based on the widespread use of the assumption it is assumed that its effect on the numerical results is small. Therefore, the assumption of a flat, frictionless surface will be employed in this study as well.

7.4.5. Symmetry

As discussed in Section 7.2, two symmetry planes will be employed in this study. The location of the planes is shown in Figure 7.10. The symmetry boundary condition specified at these planes requires zero gradients of all properties of the surface.

Stellenbosch University http://scholar.sun.ac.za

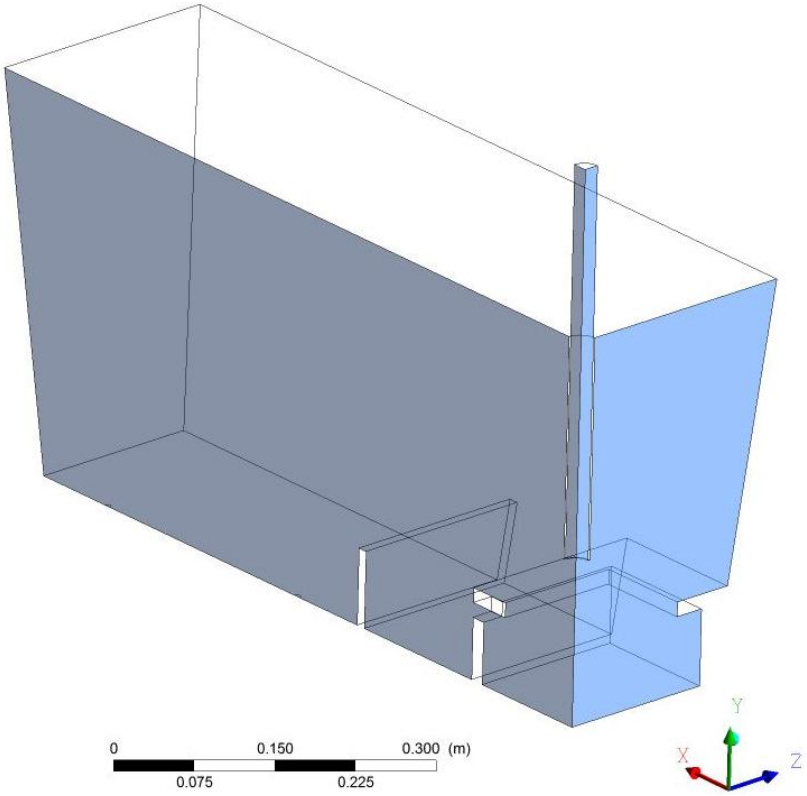

Figure 7.10 - Schematic representation of the volume of the tundish modelled with the symmetry planes shown in colour

7.5. Solution Procedure

Numerical simulations were performed using the ANSYS 14.5 software on a HPC server. Between 4 and 16 processing cores were used to perform each simulation.

7.5.1. Initial Conditions

Initially velocities and turbulent properties were specified as zero at the start of the process, simulating the tundish filled with stationary fluid. From there the flow patterns were allowed to develop in both steady and transient simulations.

7.5.2. Procedure

The simulations were started by solving the steady state flow and turbulence equations until a converged flow field was obtained. In some cases the mesh was then adapted using this initial solution and the steady state calculation was repeated until a new, more accurate, converged solution was reached. The mesh adaption is done using the gradient adaption tool in FLUENT, as described in Section 4.4. Once the final flow solutions have been found, the flow and turbulence equation were turned off in FLUENT and the species equation and transient solver were activated. At this stage the mass fraction of the tracer at the inlet boundary was changed to one. The first five seconds of the simulation was then solved with tracer being added at the inlet to simulate the procedure used in the physical experiment. After this period, the boundary condition was once again changed to a tracer mass fraction

Stellenbosch University http://scholar.sun.ac.za

of zero and the simulation was continued up to three times the mean residence time of the tundish.

7.5.3. Solution Controls

Nearly all previous tundish studies have used the SIMPLE (Semi Implicit Method for Pressure Linked Equation) scheme for pressure-velocity coupling. However, for this study, the PISO (Pressure-Implicit with Splitting of Operators) scheme, which is part of the SIMPLE family, has been chosen. The PISO scheme solves one of the biggest problems with the SIMPLE scheme, which is that the computed velocities often do not satisfy the momentum equation after the pressure equation has been solved. Two additional corrections, namely the neighbour correction and skewness correction, reduce the repetition of the calculation required to satisfy the momentum balance. This reduces the number of iterations required for a converged solution, especially where there is considerable skewness in the mesh. Because of the sometimes complex shapes to be meshed, some degree of skewness will exist in this study. However, throughout this study the minimum mesh orthogonal quality, a measure of the mesh quality, is maintained above 0.09 after gradient adaption. A higher orthogonal quality corresponds to less skewness and general guidelines suggest not using meshes with a minimum orthogonal quality of less than 0.05 (ANSYS, 2011); therefore sufficient mesh quality is maintained in this study. This will be increased when mesh adaptation is applied. The PISO scheme allowed larger under-relaxation factors to be used for the same mesh, allowing convergence to be achieved in fewer iterations. A comparison verified that the results were similar to those generated using the SIMPLE scheme.

The PRESTO! (Pressure Staggering Option) scheme, which is recommended for flow solutions involving swirl and strong streamline curvature, was used for pressure discretization. For gradient evaluation, the least squares cell-based method was used.

Few tundish studies mention the spatial discretization method used for momentum, turbulence and species. For this reason a 2^3 factorial experiment was performed with the three factors being the discretization method for momentum, turbulence (turbulence kinetic energy and turbulence dissipation rate) and species. The first-order upwind scheme was represented by the lower level, while the higher level represented the second order upwind scheme. The results, discussed in Appendix B, showed that all three factors are significant. Therefore, at least second-order discretization should be used for momentum, turbulence and species. This is expected, since first-order discretization is generally not suggested for tetrahedral meshes. When comparing the RTD curve for a case using second-order discretization for all factors with that of a case using the third-order MUSCL (Monotone Upstream-Centred Schemes for Conservation Laws) scheme for all factors, it was shown that third-order discretization has an insignificant effect on the results.

Stellenbosch University http://scholar.sun.ac.za

7.5.4. Convergence Criteria

The common convergence criterion in CFD studies is a value of less than 10^{-3} for the scaled residuals for all flow variables. However, in some cases, for example due to the initial estimate, this criterion may not be appropriate and it is suggested that relevant integrated quantities should be monitored (ANSYS, 2011). In this study problems were experienced with the continuity residual not reaching such a low value, despite convergence clearly being reached when looking at the average values of flow properties in the tundish. For this reason the convergence criteria was specified so that the average values of velocity, turbulence kinetic energy and turbulent dissipation rate should not vary with more than 1% in 2000 iterations. Figure 7.11 shows the convergence of volume-averaged velocity before and after adaptation of the mesh at 15 000 iterations.

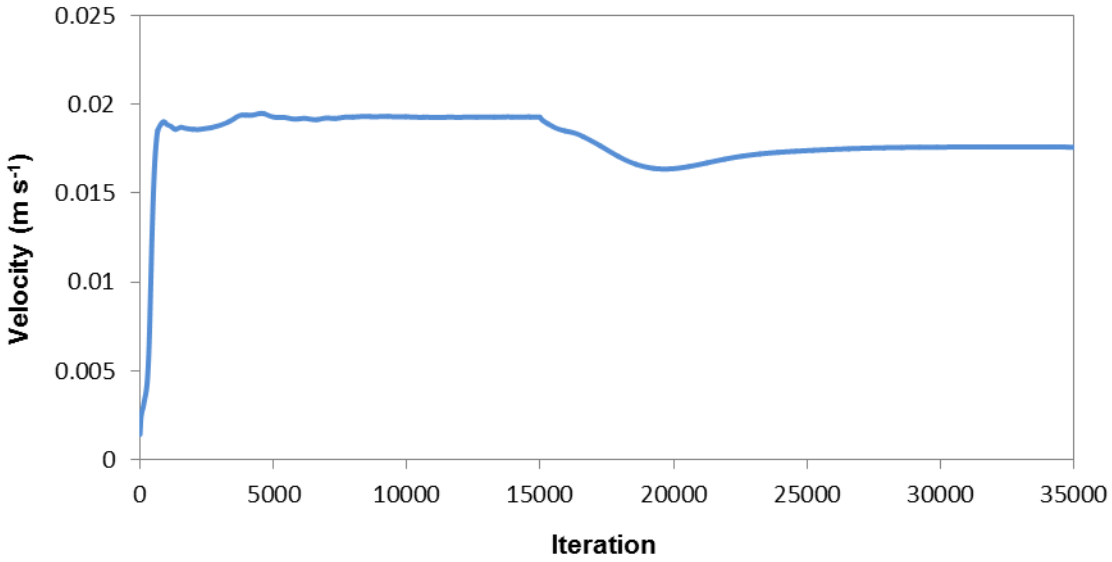

Figure 7.11 - Volume averaged velocity for the tundish plotted against the number of iterations, showing convergence of the values before and after refinement of the mesh at 15 000 iterations

Stellenbosch University http://scholar.sun.ac.za

Chapter 8: Mesh Study and Validation

The nature of the flow in a tundish that has been designed for inclusion removal is such that relatively high velocity turbulent flow occurs in the inlet and outlet regions, while the bulk of the volume has much more tranquil flow. This is good for producing clean steel, but does present some problems for the numerical modelling. The first difficulty is that the most generally used κ-ϵ turbulence models may not produce good results due to the fact that they are only valid for fully turbulent flows.

The second problem is with regards to the meshing of the system. The extensive range of flow velocities will cause large gradients to form in some regions of the tundish, with much smaller gradients in other regions. These different areas will require different sizes of cells for accurate solutions to be obtained. The simplest solution is to generate a uniformly sized mesh with all the cells the size of the smallest cells required. However, this will be a very inefficient approach and lack of computational power may force the use of coarser mesh than desired.

The alternative is to define different mesh sizes for parts of the flow volume. Several authors have applied this approach (Jha et al., 2008; Liu et al., 2008; Chattopadhyay et al., 2012; Raghavendra et al., 2013), with the finer mesh cells usually specified in the inlet region and the walls. The problem with this approach is that it is difficult to define precisely where the finer regions should start and end. Also, when several different designs are considered, the areas that required a finer mesh will be in different portions of the tundish. Therefore an individual investigation will be required for each setup to determine where the mesh should be refined.

This is where the gradient adaptation approach is very useful, since it allows a more automatic approach to determine the regions that will require a finer mesh. This is done by using an initial solution to mark the cells that will be refined. This chapter will describe the process followed to achieve good results using the gradient adaptation approach and will then compare these results with the experimental results to validate the numerical model.

8.1. Grid study

8.1.1. Initial Observations

The initial idea behind the gradient adaptation was to start with a very coarse mesh and then adapt the mesh successively over multiple levels. A factorial experimental design could then be followed to investigate factors such as the start size, number of adaptations and the gradient at which adaptation occurs to determine the most computationally economical mesh that yields a grid independent solution.

Stellenbosch University http://scholar.sun.ac.za

However, in the beginning this approach proved unsuccessful due to two reasons. The first was that the difference in mesh sizes required was smaller than expected. Therefore, starting with a very coarse mesh of 40mm cells had no benefit, since nearly all cells required refinement up to about 10mm. Several options were investigated to overcome this challenge, such as using turbulent kinetic energy, instead of velocity magnitude, as the adaptation property, changing the volume weighting and using the gradient approach, instead of the curvature approach, for adaptation. However, none of approaches were able to solve the problem.

The second complication was that successive adaptations up to a very small size made finding a converged solution more difficult due to decreasing mesh quality. This solution instability would require more iteration to be performed to obtain a steady solution, which would negate the benefit of using mesh adaptation.

These problems were solved by using only a single refinement from 10mm to 5mm cells. Initial results showed clearly that the numerical results using the gradient adapted meshes compared more favourably with the physical experiment results than those using a very fine uniform grid. This can be explained by comparing the meshes for a case with a uniform 5mm cell size and a case with a starting grid size of 10mm, with some cells refined once. In the gradient adapted case the 10mm cells should be refined to roughly the same size as for the 5mm case. However, from Figure 8.1 it can be seen that a finer mesh is generated in the inlet area, around the holes, at the top of the dam and near the outlets. This effect is caused by the meshing algorithm already having refined the cells in these areas to fit the geometry with an acceptable mesh quality. Conveniently, these are also the areas where the smallest mesh size would be required to accurately capture the flow gradients. This explains why the gradient adapted method is able to deliver results that compare better with experimental results than a uniform mesh. The additional benefit of the gradient adaptation approach is that not all cells need to be refined; therefore the gradient adapted mesh can generate a more accurate solution while using fewer cells.

Stellenbosch University http://scholar.sun.ac.za

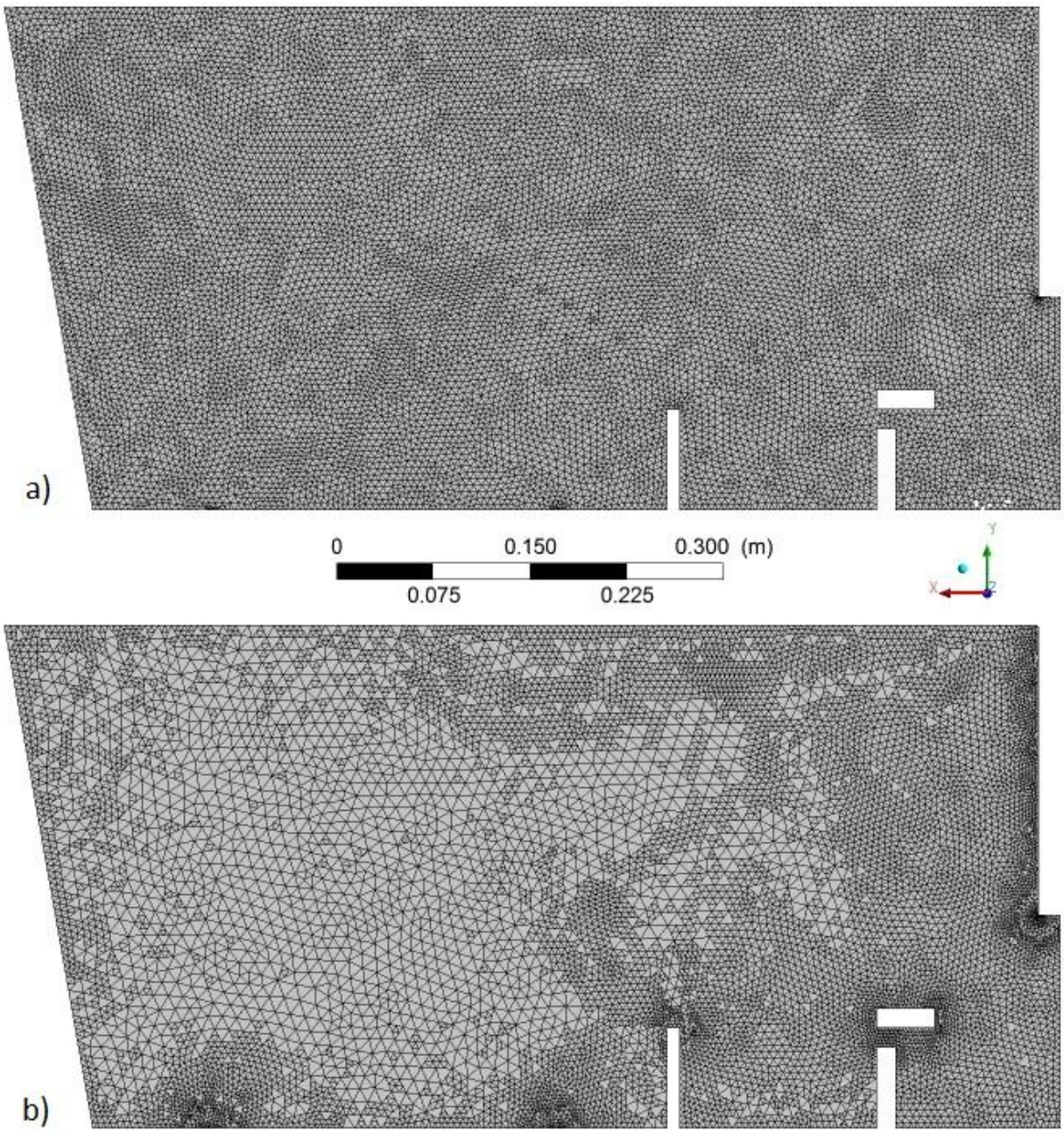

Figure 8.1 - Comparison of mesh sizes along the longitudinal symmetry plane for a) a uniformly sized 5mm mesh and b) a 10mm mesh refined once in certain areas by gradient adaptation

From the observations in this section the decision was made to use a step wise approach to obtain the mesh that would be used in further experiments. Firstly, a separate mesh size for the nozzle would be determined. Secondly, the tundish volume would be meshed with 10mm cells, applying one level of gradient adaptation to bring the maximum cell size down to 5mm. This assumption is based on the grid study done using the uniform meshes, shown in Figure 7.1, which showed grid independence to be reached at 5mm. It therefore appears that for the bulk of the tundish the required mesh size is 5mm. A second level of refinement will be performed at the walls in case the mesh is not already sufficiently refined near the surfaces. Finally, a minimum cell size will be applied for the cells to allow adaptation. This is

Stellenbosch University http://scholar.sun.ac.za

because the mesh is already very fine near the outlets and around the inlet nozzle in order to conform to the geometry. Allowing these cells to be further adapted would greatly increase the number of cells without significantly improving the solution accuracy.

8.1.2. Meshing the Nozzle

The study of the effect of the nozzle mesh was started by doing a simple simulation of a pipe with the nozzle inner diameter and a length that is sufficient for a fully developed profile to form. The mesh at the pipe wall was inflated for five cells. Figure 8.2 shows a plot of the velocity profile from the nozzle centre to the wall at the outlet for different grid sizes. It is therefore immediately clear that the velocity profile is far from flat, which explains why assuming the inlet boundary at the nozzle port significantly affects the results. However, it can also be seen that the profile obtained by the solution changes with the grid size, with changes becoming small below 2mm.

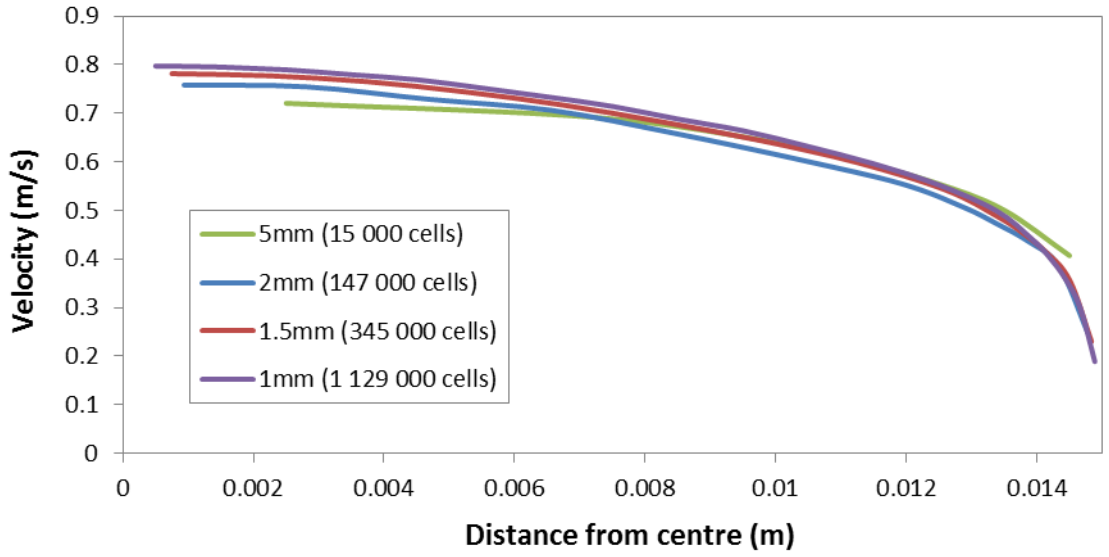

Figure 8.2 - Velocity profile at the nozzle outlet as for different mesh sizes

By looking at the development of the velocity profile from the inlet of the pipe, it was decided to simulate 400 mm of the nozzle as part of the tundish flow volume. However, it was observed that the profile was already nearly fully developed after 150mm. This corresponds to 300mm in the industrial tundish-ladle setup; therefore it is safe to assume that a fully developed velocity profile will develop from the ladle to the nozzle port in the tundish.

When comparing the RTD curves for the TID case using a mesh size of 10mm for the tundish and different mesh sizes for the nozzle, it can be seen in Figure 8.3 that changing the resolution of the grid in the nozzle has a negligible effect on the tracer response at the outlet. It can therefore be concluded that a uniform velocity profile should not be assumed at the nozzle port, but that highly accurate solutions of the profile are not necessary.

Stellenbosch University http://scholar.sun.ac.za

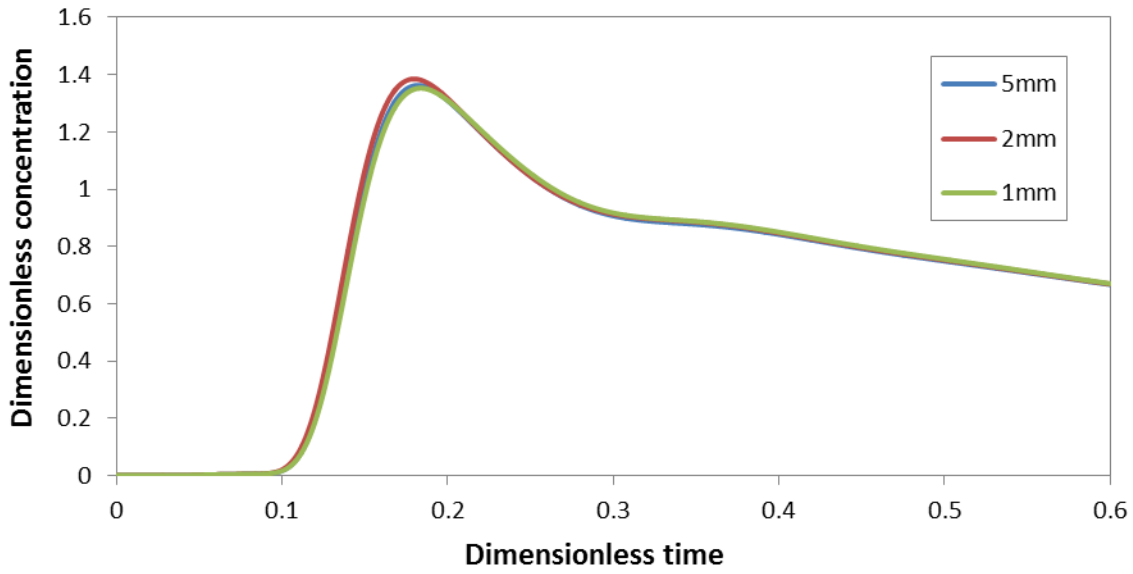

Figure 8.3 - Comparison of overall C-curves for the TID case for different mesh resolutions in the nozzle

Despite the similar overall c-curves, it was decided to use the 2mm mesh, instead of the 5mm mesh, in subsequent runs since the number of additional cells (approximately 70 000) is small compared to the overall number of cells used in the final adapted mesh. This will make the model more robust in case the effect of the difference in the port velocity profiles on the overall C-curves becomes significant for different configurations or for the gradient adapted mesh.

8.1.3. Gradient Adaptation

The next step in the grid study was to determine the value of the gradient function at which the cells should be adapted. Before the gradient adaptation, a boundary adaptation was done near the walls and the top surface. Through some experimentation a suitable criterion for boundary adaptation was determined: Cells within 1cm of the walls and with a gradient function larger than 1×10^{-5}.

After obtaining a solution with the boundary adaptation, the mesh was then refined using the curvature boundary adaptation approach. The value of the adaptation function was changed to increase the final mesh size in increments of 800 000 cells. In Figure 8.4 the C-curves of the simulations are compared to those of the physical experiment. It can be seen that with increased gradient adaptation the peak shifts later and lower. This moves the curve closer to that of the physical experiment and eventually past it. It must therefore be noted that a good comparison between the physical experiment and numerical C-curves does not necessarily assure accurate results, as a simulation using 3.6 million cells matches the physical model C-curve much more closely than that of the more accurate solution using 4.8 million cells. In this case likely causes for this occurrence are the numerical assumptions of symmetry and dynamically steady flow and the choice of turbulence model. As more cells

Stellenbosch University http://scholar.sun.ac.za

are adapted, the C-curve approaches a limit as grid independence is reached. Consequently, it was decided that the solution no longer changes appreciably after 4.4 million cells and the gradient adaptation function value of 3.85×10^{-7} was selected for the adaptation value for further simulations.

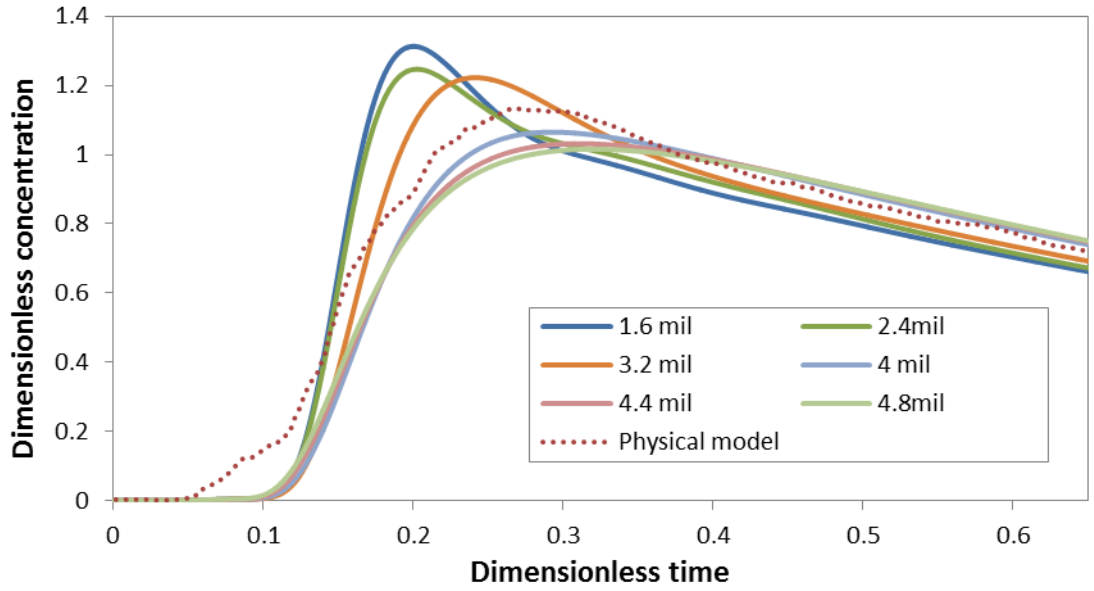

Figure 8.4 - Comparison of physical model and numerical simulation C-curves for different extentof gradient adaptation

Despite the peak of the numerical C-curve shifting slightly lower and later than that of the physical experiment, the slope of the tail data and the general shape is very similar. Another positive comparison comes from comparing the C-curves of the individual strands between the physical model and the numerical simulation using 4.4 million cells, as shown in Figure 8.5. It can be seen that the simulated C-curve for the outer strand is nearly identical when compared to the physical model result. Similar to the physical model, the peak for the inner strand is also predicted earlier and higher than for the outer strand and the two curves cross after the peek. Despite these differences between the inner and outer strands not being a large as for the physical results, the comparison is still very favourable and suggests that the numerical model is reasonably successful in predicting the real behaviour.

Stellenbosch University http://scholar.sun.ac.za

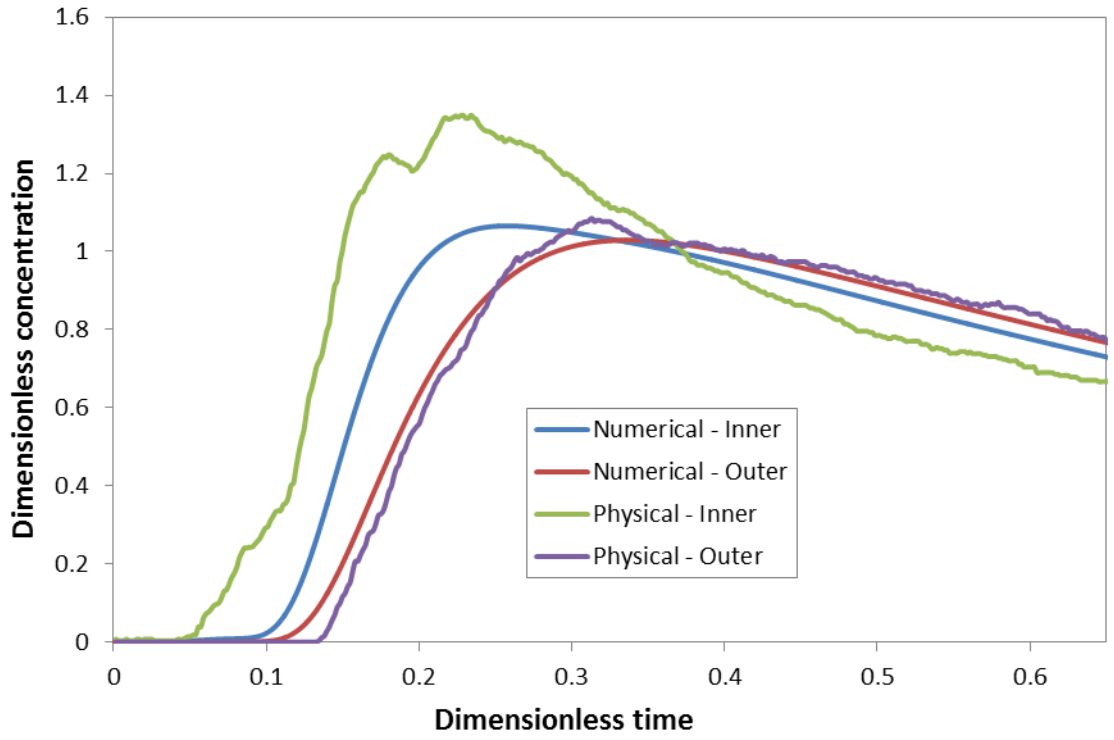

Figure 8.5 - Comparison of RTD curves for the individual strands of the physical experiment and numerical simulation

8.1.4. Boundary Adaptation

Subsequent to the gradient adaptation study, the gradient adapted solution using 4.4 million cells was compared to a case that did not apply the boundary adaptation. The change had a surprisingly small effect, with the only difference being a slightly lower peak (about 4%). This was deemed to be insignificant compared to the reduction in cells of about 30% that it allows. It therefore seems that the initial size of the cells in the important areas near walls was already small enough to fit the geometry that only one level of gradient adaptation was required to reach the desired size.

However, although the boundary adaptation may not be necessary for the TID case, it might not hold true for other configurations. Comparisons for the bare case showed an even smaller change when the boundary adaptation was neglected. This did not change when the distance of the adaptation area from the walls was increased to 3cm or when the adaptation value was lowered to 1×10^{-7}.

It was therefore concluded that unless visual inspection clearly showed that the gradients through certain regions were not resolved accurately, an additional boundary adaptation is not necessary.

8.1.5. Minimum Cell Volume

The final step in the grid study was to determine a minimum volume for cells after adaptation. Very fine cells occur at the outlets and around the nozzle to be able to fit the

Stellenbosch University http://scholar.sun.ac.za

geometry and maintain acceptable mesh quality. However, refining these cells will greatly increase the total number of cells, but would not necessarily affect the final solution significantly. It is therefore useful to assign a minimum size for the adapted cells to allow adaptation, to prevent unnecessary cells from forming.

A comparison of the C-curves for different minimum cell volumes applied to gradient adaptation is shown in Figure 8.6. It can be seen that a minimum of $1 \times 10^{-9}\, m^3$ is effectively identical to the case without a minimum cell volume, while the effect is significant for a minimum of $2.7 \times 10^{-8}\, m^3$. Using the C-curve comparison and by looking at where gradient adaptation is prevented in the mesh for each case, the $8 \times 10^{-9}\, m^3$ minimum was used for further work. It was also tested that limiting adaptation to this size also did not have a significant effect for the bare case.

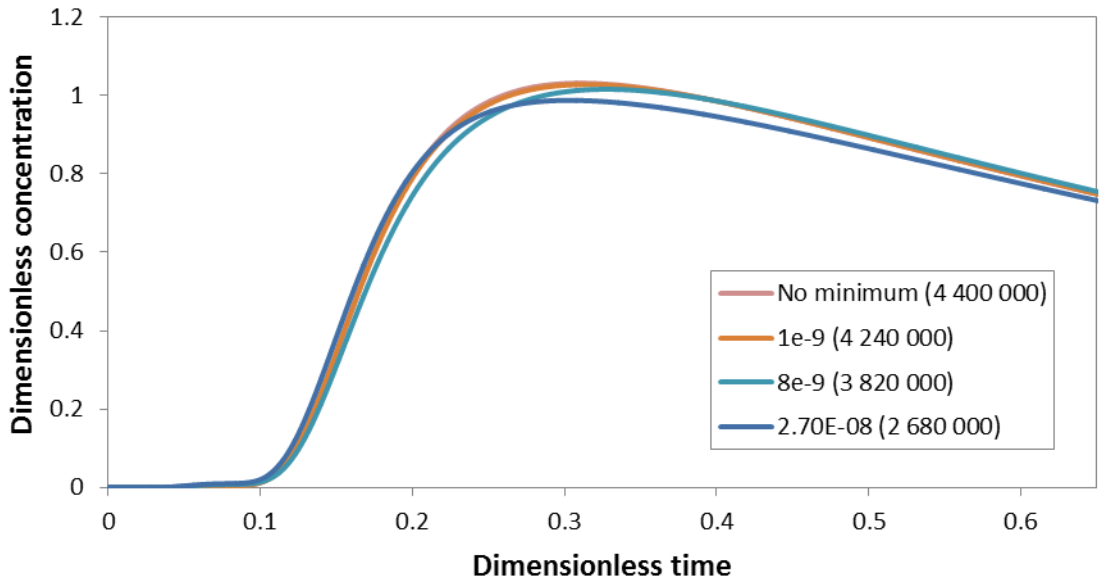

Figure 8.6 - Comparison of C-curves for different minimum cell volumes imposed during gradient adaptation

8.2. Time Step

The main reason for long computational times when using the dynamically steady and symmetry assumptions is the large residence time of the tundish. Therefore, using the largest time step that will yield accurate results for the transient part of the simulation can greatly reduce the required simulation time. To select a suitable time step, the first part of the RTD curve is compared for several time step sizes for the TID and bare case.

The results of the times step study for the bare tundish, shown in Figure 8.7, indicates that the solution in the first portion is very insensitive to the time step, with only very small changes in the solution over a very large range of time step sizes.

Stellenbosch University http://scholar.sun.ac.za

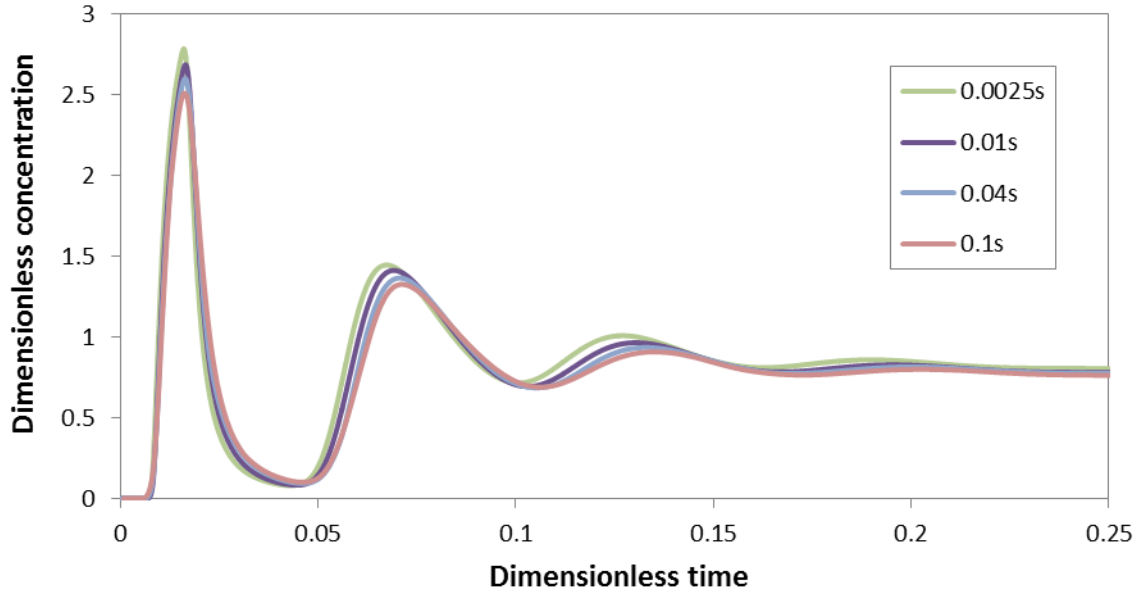

Figure 8.7 - Comparison of overall C-curves for the bare tundish for different time steps used

The TID case, however, is more sensitive to changes in the time step size. Despite this, the changes in the RTD curves are still not very large.

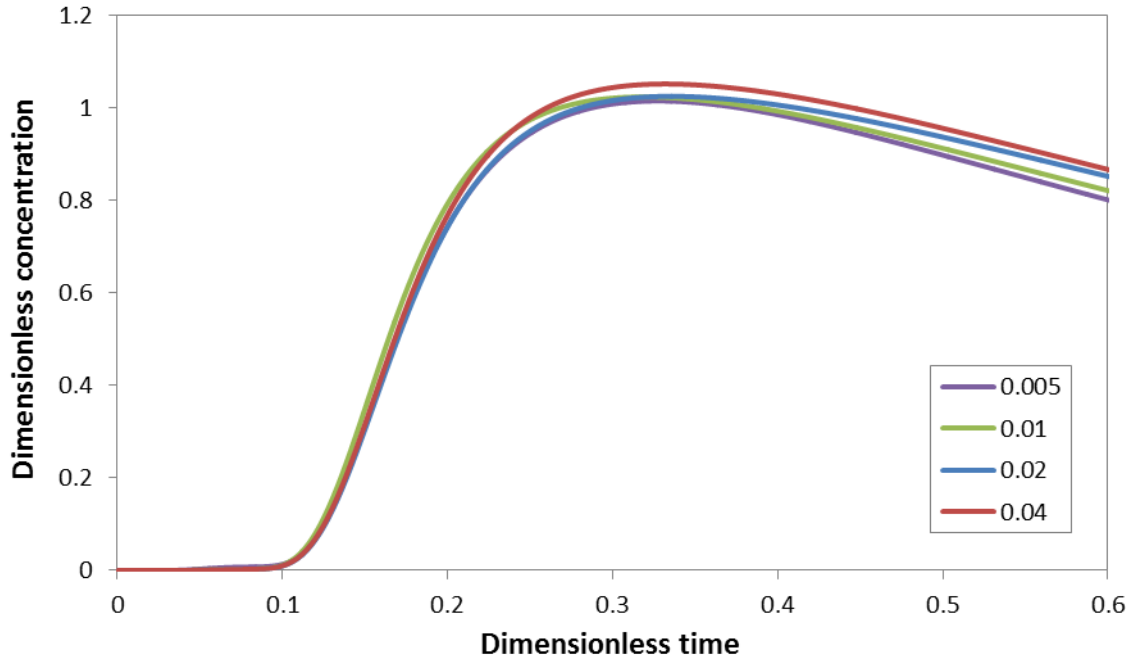

Figure 8.8 - Comparison of overall C-curves for the TID tundish for different time steps used

The residence time distribution therefore does not seem to be highly sensitive to time step. A large time step can therefore be used in early simulations to setup the numerical model and a smaller one can then be used for the final, more accurate runs. For this study a very conservative time step of 0.005 seconds was eventually chosen. The difference in the time step sensitivity of the TID case and the bare tundish determined this choice, since the

Stellenbosch University http://scholar.sun.ac.za

numerical model will be used on several other configurations. The selected time step should therefore be relatively accurate, regardless of the configuration used.

8.3. Validation of the Numerical Model

A good indication of how successful the numerical model is in modelling the physical system can be obtained by plotting the experimental and simulated C-curves of the individual strands on the same axes. It must be noted that the selection of the scale of the axes can have a significant impact on the interpretation. Previously, comparisons were made by focussing on the region surrounding the peak concentration, since these are the most affected by changes in the numerical model. For this section the comparison will be made over a larger portion of the residence time distribution to also compare the tail data.

For the tundish configuration with the turbulence inhibitor with holes, used in combination with low dams, such a comparison, shown in Figure 8.9, shows a nearly exact match between the results of the numerical and physical models for the outer strand. Unfortunately, that is not the case for the inner strand, where there is a significant difference between the two sets of results. Despite this difference, the numerical model is still able to predict several aspects of the inner strand C-curve. The minimum and maximum residence times predicted by the numerical model are nearly exactly the same as that obtained in physical experiments, although the peak is reached at a lower concentration. Additionally, the numerical model also predicts an extend of short-circuiting, although not as much as the physical modelling and a lower concentration for the inner outlet at later residence times, but with the difference being smaller than for the physical model.

Stellenbosch University http://scholar.sun.ac.za

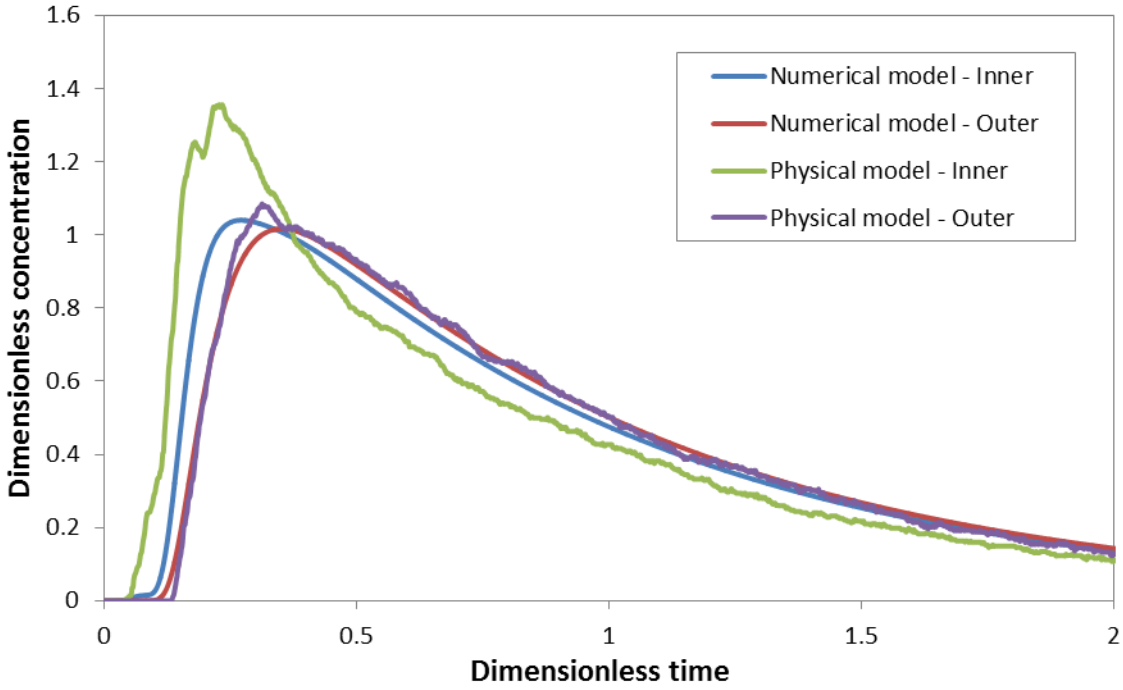

Figure 8.9 - Comparison of experimental and numerical C-curves for the individual strands of the tundish with turbulence inhibitor with holes in combination with low dams

For the bare tundish some variation in the peaks are expected. This is due to the delays in tracer injection and measurement being significant compared to the short time from injection to the peaks. Regardless of this, Figure 8.10 shows a reasonably good comparison, with the numerical model predicting multiple peaks for both strands at roughly comparable times and concentrations to that obtained in the physical model. The tail is established after a very short time and here the comparison is very good, with the concentration at the outer strand being slightly higher than that of the inner strand for both sets of data.

Stellenbosch University http://scholar.sun.ac.za

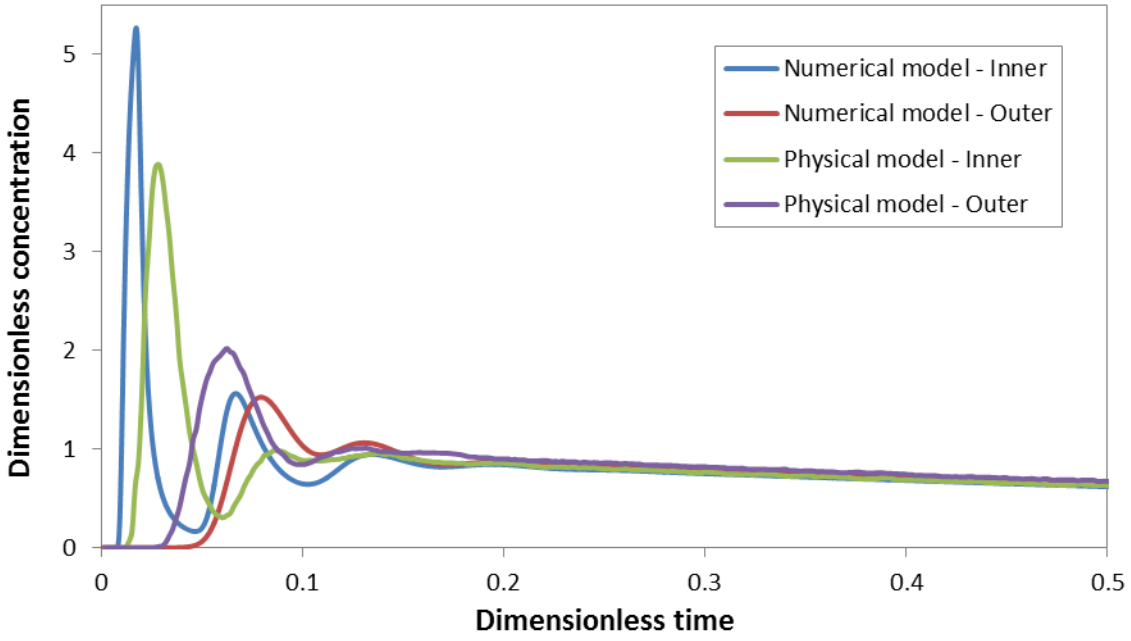

Figure 8.10 - Comparison of experimental and numerical C-curves for the individual strands of the bare tundish

Finally, for the case with the turbulence inhibitor, it can be seen that the peaks are once again predicted lower than for the experimental data. However, this time the peaks also occur slightly later than for the physical model results. The minimum times are still predicted very accurately and the relative positions of the peaks correspond roughly.

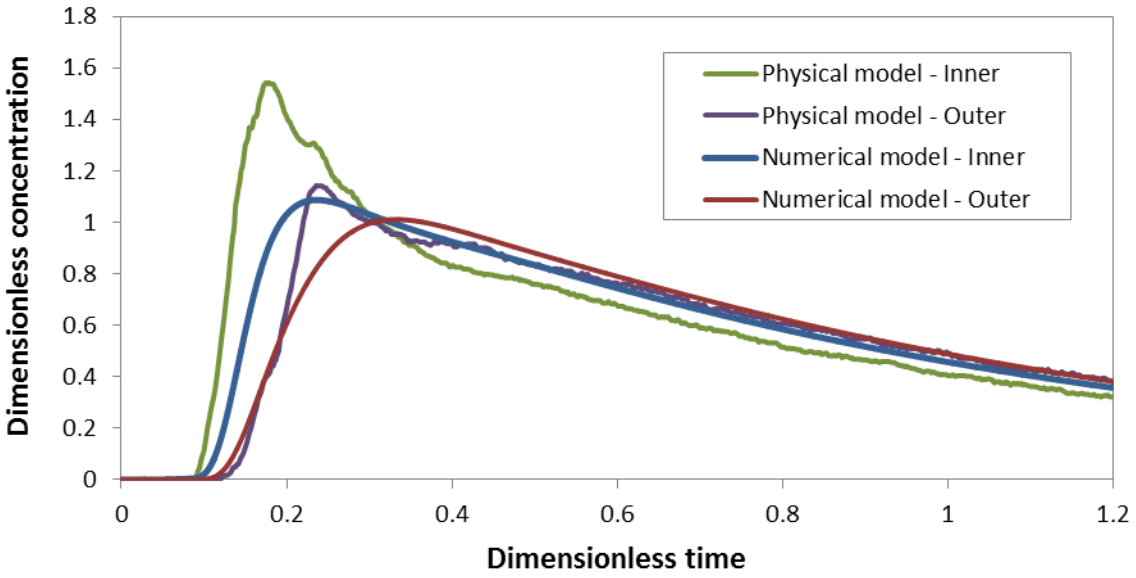

Figure 8.11 - Comparison of experimental and numerical C-curves for the individual strands of the TI case

Comparing the important dimensionless times and properties calculated from the modified combined model for the physical and numerical results for the three configurations an average difference of about 10% is calculated between the two sources of data. The largest

Stellenbosch University http://scholar.sun.ac.za

difference, recorded for the breakthrough time in the bare model, is easily explained by the delay in input and measurement in the physical model, which becomes highly significant for the very short minimum time. The other value where large differences are detected is for the peak time for the cases using a turbulence inhibitor. The numerical model predicts longer times for the peak concentration to be reached, which in turn translates into larger plug flow volumes and lower dead volumes.

Table 8.1 - Comparison of flow properties calculated from physical and numerical experiments for the three configurations studies

Setup	Data source	θ_{min}	θ_{peak}	θ_{mean}	V_p	V_d	V_m
Bare	Physical	0.0101	0.0670	0.687	0.039	0.370	0.591
	Numerical	0.0077	0.0732	0.705	0.040	0.375	0.585
	% Difference	27.5	8.84	2.64	4.76	1.19	1.08
TI	Physical	0.089	0.234	0.756	0.162	0.306	0.532
	Numerical	0.091	0.298	0.784	0.195	0.278	0.528
	% Difference	1.89	24.1	3.62	18.5	9.61	0.915
TID	Physical	0.035	0.291	0.747	0.163	0.299	0.538
	Numerical	0.043	0.326	0.790	0.184	0.259	0.557
	% Difference	18.7	11.3	5.61	12.2	14.4	3.46

What is important is that, despite these differences, general trends between the different configurations are the same for the physical and numerical model. The numerical model predicts the much lower breakthrough time due to short circuiting in the bare setup, as well as the small amount of short-circuiting for the case with the turbulence inhibitor with holes. Also, the bare tundish clearly has much lower plug flow and larger dead volumes than the configurations using turbulence inhibitors. The TID case has a significantly delayed peak, but the mean residence time and plug and dead volume fractions are more similar.

It can therefore be concluded that the numerical model is acceptable for predicting the flow properties of different tundish configurations. This is especially the case when considering the assumptions employed to reduce the computational time: symmetry, dynamically steady flow and a flat, frictionless surface. These assumptions make perfect prediction through numerical modelling unlikely. Unfortunately the one aspect that is not modelled accurately is the variation between individual strands. When calculating the fractional

Stellenbosch University http://scholar.sun.ac.za

variation between strands, as defined in Section 6.4, the values are much lower for the numerical solution and shows different trends.

It is also important to note the importance of the grid size. Although the strand variations predicted in the numerical model are far from perfect, nearly no variation was detected when using a uniform mesh. In this study special attention was given to developing an accurate mesh, using as few cells as possible and still approximately 2.8 million cells were determined to be necessary for grid independence. This is in contrast with most studies in literature that use grid sizes in the general range of 30 000 to 150 000 cells (Kumar et al., 2008; Jha et al., 2008; Mishra et al., 2012). Cell numbers in numerical studies by Raghavendra et al. (2013) and Zhong et al. (2007), using 1.5 and 0.8 million cells respectively, are the most comparable to those used in this study. It must, however, be taken into account that simple geometries can be meshed much more efficiently with hexagonal cells, whereas the complex geometries in this study require tetragonal meshes. Other factors, such as the tundish size and throughput rate, will also determine the number and size of cells. Nonetheless, it still seems unlikely from the results of this study that very accurate results would be obtained using meshes as coarse as those reported in literature.

In studies based on multi-strand tundish, most authors only compared overall RTD responses when validating the numerical model or when doing a grid independence study. However, experience in this study showed that individual C-curves can produce an overall C-curve very similar to experimental data, even though the individual curves are very different from those in the physical model. Although this will allow comparison of systems using the parameters of the combined model, conclusions drawn about other aspects, such as flow patterns, turbulence levels and strand similarity, from numerical modelling results may not necessarily be correct.

In the end it comes down to the fact that care must be taken that the numerical model and mesh are sufficiently accurate for the conclusions that are drawn from them. In the numerical model development, highlighted in the last two chapters, it is clear that there are several places where the computational time can be reduced with only a small change in the results. Time step size especially comes to mind. Therefore, for only a rough comparison of different tundish setups using the combined model parameters for the overall flow, a CFD model with low computational requirements will be sufficient. However, that does not mean that comparisons of different properties of the system and different systems using the same model will necessarily be valid.

Stellenbosch University http://scholar.sun.ac.za

Chapter 9: Flow Analysis from Numerical Results

One of the major advantages of the CFD approach is that it provides a solution of the flow for the entire flow domain. This information can then be used to visualize the flow and help explain the differences between the different configurations. Therefore, whereas the flow analysis of the physical model using the modified combined model is useful for evaluating the performance of the different configurations, flow analysis from CFD results can better explain why these differences occur. Furthermore, this knowledge can then be implemented to improve the design in order to create better performing tundish.

In this chapter the numerical model solution of the water model will be analysed and used to explain trends in the RTD results from the physical model for the three configurations discussed up to now.

9.1. General Flow Patterns

9.1.1. Bare Tundish

The flow in the bare tundish consists of two dominant flow patterns. The first portion of the fluid simply flows to the outlets after striking the bottom of the tundish. This behaviour can be observed in the vector plot along the longitudinal symmetry plane in Figure 9.1. This will explain the first peak in both the inner and outer strand C-curves.

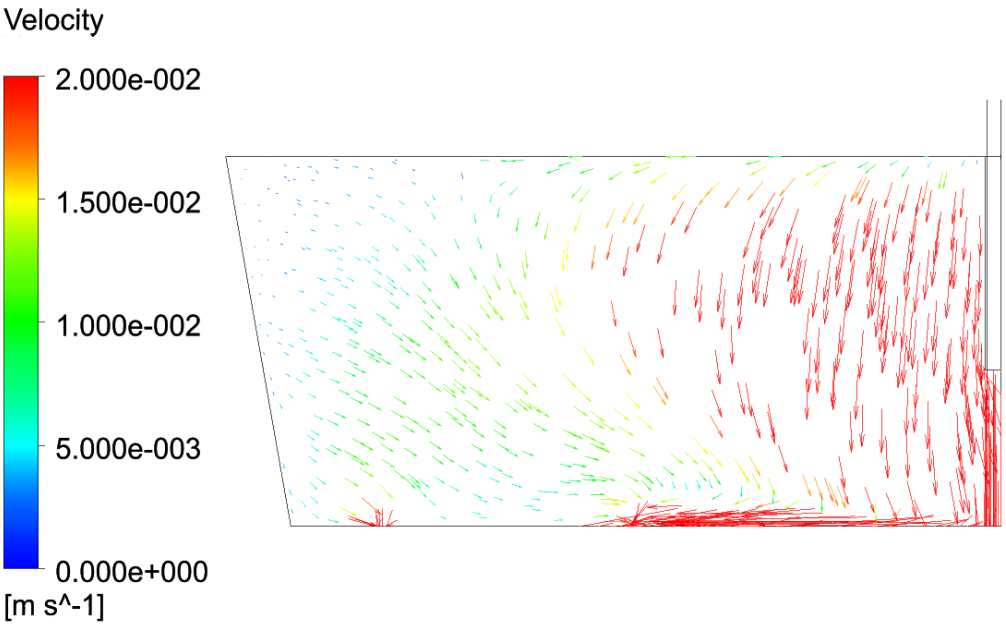

Figure 9.1 - Velocity vector plot along the longitudinal symmetry plane for the bare tundish

It should also be noted that, although vector plots are very useful to illustrate flow patterns, the large range of velocities in the tundish makes it difficult to view clearly. Therefore, some

Stellenbosch University http://scholar.sun.ac.za

of the very large vector arrows near the inlet and outlets have been cropped to enable clear presentation.

Evidence of the second flow pattern seen in Figure 9.1, with the dominant flow along the longitudinal symmetry plane being downward towards the outlets, can be better explained by viewing the vector plots along the transverse symmetrical plane, shown in Figure 9.2, and on planes near the bottom and side walls of the tundish, shown in Figure 9.3. Along the transverse symmetry plane a portion of the flow striking the bottom goes up the side walls and circulates down the longitudinal symmetry plane after being forced to turn at the surface.

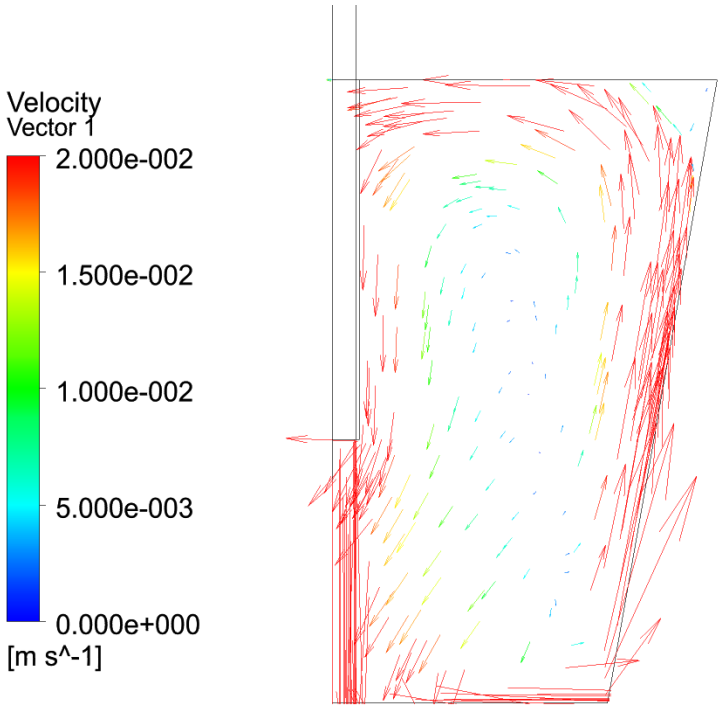

Figure 9.2 - Velocity vector plot along the transverse symmetry plane for the bare tundish

From Figure 9.3 it can be seen that a similar phenomenon exists through most of the tundish, with flow moving over the bottom being forced upwards by the side walls and then circulating back to the outlets. The first flow arriving from this circulation explains the presence of a second peak in both the inner and outer strand C-curves. Also to be noted is that short-circuiting to the outer strand occurs through a circulation pattern along the bottom plane. This flow pattern goes along the bottom of the side wall and circulates back to the outer strand along the bottom wall after striking the back wall. This explains the significantly later minimum residence time for the outer strand, compared to the inner strand.

Stellenbosch University http://scholar.sun.ac.za

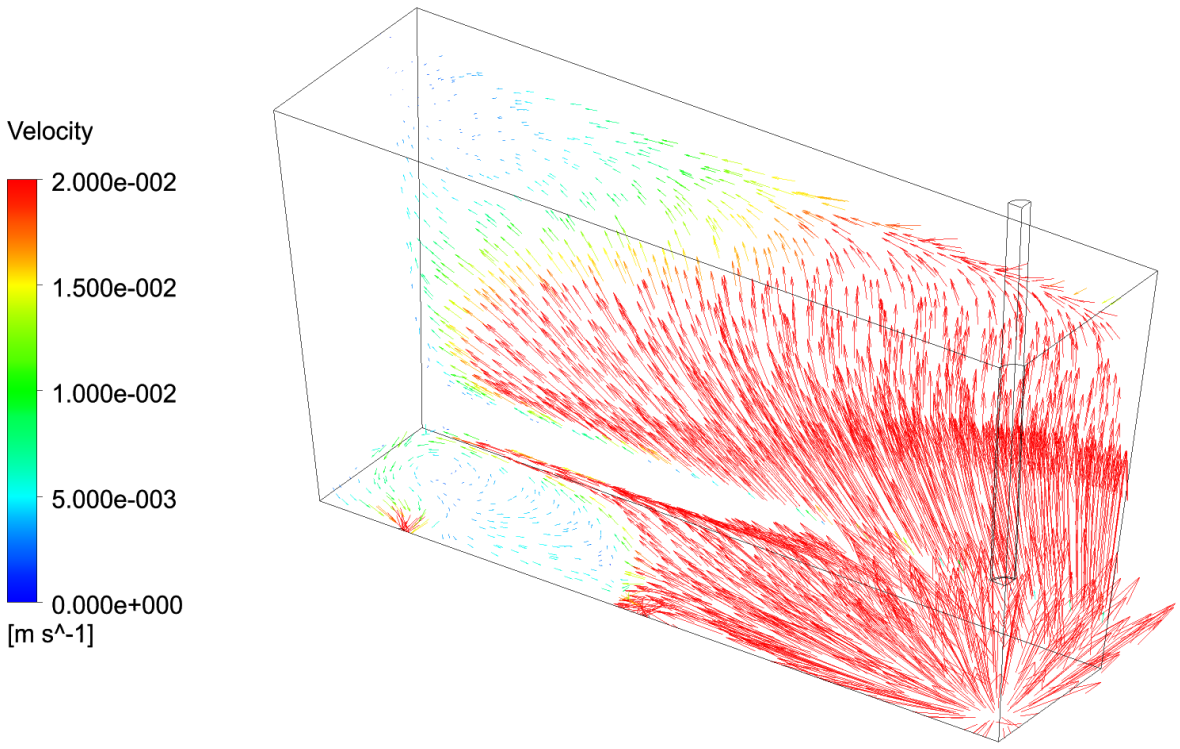

Figure 9.3 - Velocity vector on planes near the bottom and sidewalls of the bare tundish

9.1.2. Tundish with Turbulence Inhibitor

From the flow fields of the bare tundish, it is clear that there are two major factors that contribute to the very short minimum and peak residence times in the bare tundish. Firstly, the flow inlet position and tundish geometry cause a portion of the flow to short-circuit directly to the inlet. The easiest way to prevent this is by simply changing the geometry by inserting a flow control device that obstructs this flow. Three approaches can achieve this: a) a dam forces flow upwards and over the inner strand, b) a baffle only allows flow through certain passages, of which the angle and size can be designed to prevent short-circuiting, and c) a turbulence inhibitor redirects the inlet flow upwards.

The second problem is that even the flow that reaches the outlets through the circulation pattern along the side walls and down the longitudinal centre plane has a short residence time due to the high velocities of the flow. This is where the turbulence inhibitor comes in, as its purpose is to dampen the flow throughout the tundish and increase the residence time. This effect is immediately evident when considering that the addition of the turbulence inhibitor to the bare tundish reduces the volume average of the velocity from 0.0166 m/s to 0.00927 m/s (44%) and that of the turbulence kinetic energy from 1.31×10^{-4} m^2/s^2 to $0.951 \times 10^{-4} m^2/s^2$ (27%).

The operation of the turbulence inhibitor can be better understood by comparing the turbulence kinetic energy values in the bare tundish and the tundish with the turbulence inhibitor. Such a comparison is shown along the longitudinal symmetry plane in Figure 9.4. It can be seen that the turbulence inhibitor causes an area of high turbulence near the inlet,

Stellenbosch University http://scholar.sun.ac.za

but that the turbulence quickly dissipates to much lower values through the rest of the bath. In contrast, except for the high turbulence area along the bottom of the tundish, the turbulence is much more uniform in the bare tundish, but the areas of low turbulence are smaller.

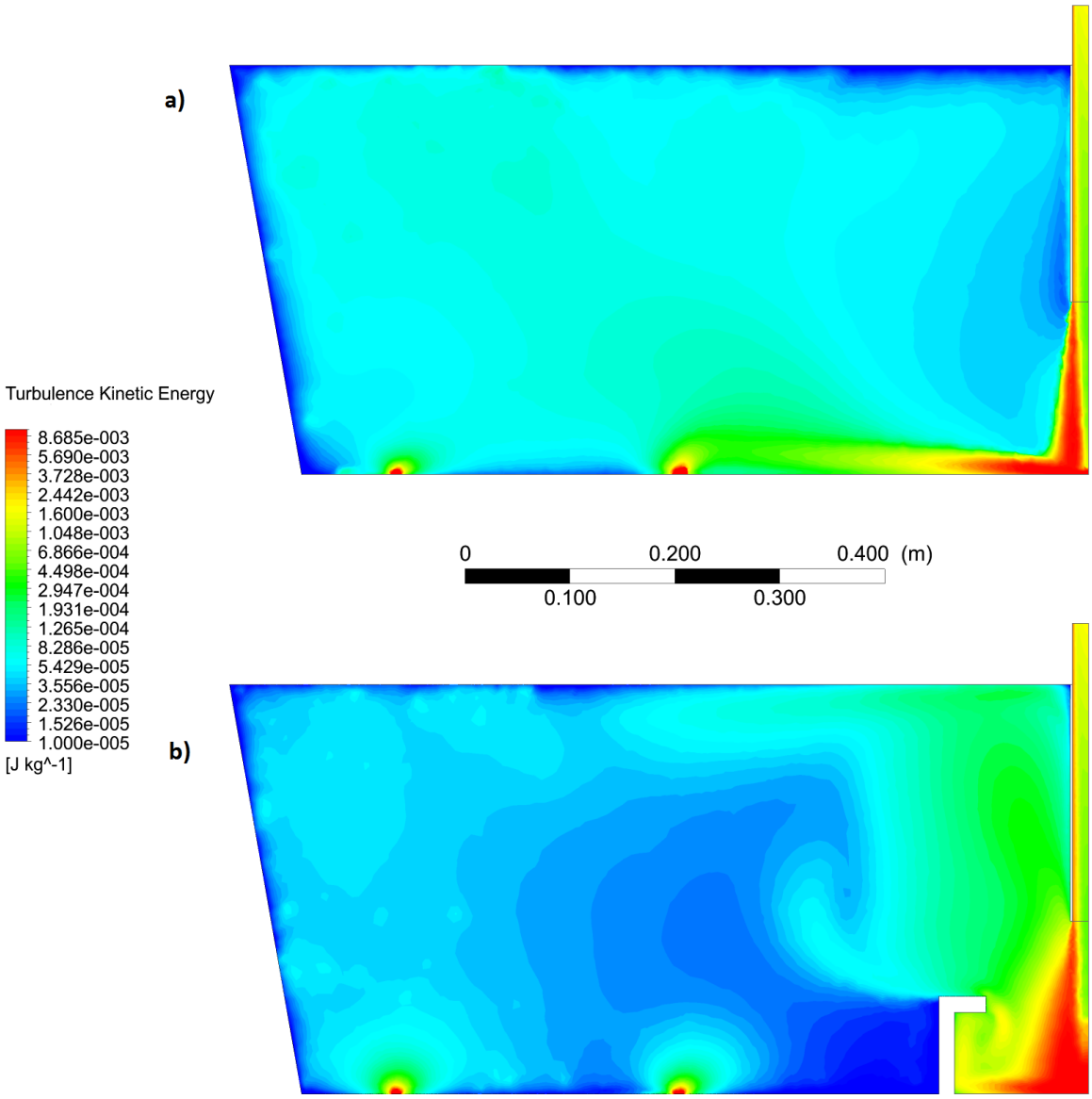

Figure 9.4 - Comparison of turbulence kinetic energy values along the longitudinal symmetry plan for a) the bare tundish and b) the tundish with a turbulence inhibitor

When looking at the velocity vector plot along the longitudinal symmetry plane for the tundish with turbulence inhibitor, the upward flow from the turbulence can easily be observed. The surface directed flow comes with the advantage of bringing the inclusions in contact with the slag layer for absorption. However, the relatively high velocity flow meeting the surface nearly perpendicularly is worrying, since this will cause turbulence at the surface, which may cause problems with slag entrainment. This aspect of the system will be discussed in the next section. Another observation is that a small circulation pattern

Stellenbosch University http://scholar.sun.ac.za

forms at the top of the tundish, above the inner strand. This circulation should help increase the mean residence time of the tundish.

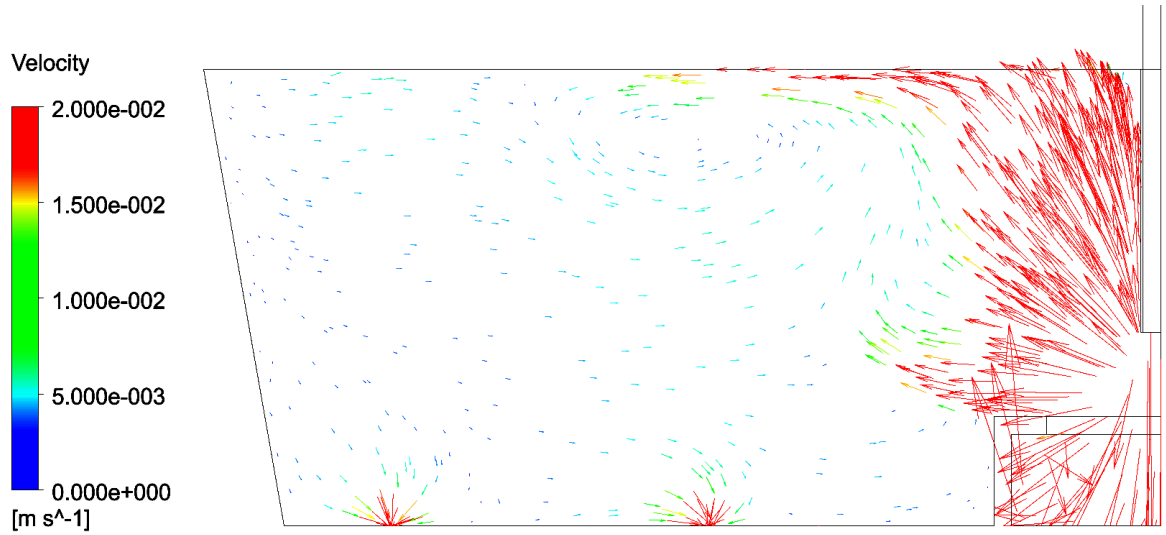

Figure 9.5 - Velocity vectors along the longitudinal plan for the TI case

Finally, it can be seen that there is a portion of horizontal flow that occurs just above the turbulence inhibitor wall. This might suggest that the opening area of the turbulence inhibitor is too small to allow the 180 degree direction change of the entire volume of fluid entering the tundish. A portion therefore circumvents this pattern, which may cause reductions in the residence time.

9.1.3. Tundish with Turbulence Inhibitor with Holes and Dams

The final configuration includes holes in the sides of the turbulence inhibitor and low walls between the turbulence inhibitor and the outlets. The purpose of the design, proposed by Kumar et al. (2008), is to accelerate surface directed flow further away from the inlet region, with the aim of reducing the dead zones and temperature distributions in the tundish. It seems likely that dead zones will form behind the turbulence inhibitor wall and that by diverting a portion of the flow to this area, the dead zones could be reduced.

Comparing the velocity contours along the longitudinal symmetry plane, plotted on a logarithmic scale to account for the large range of velocities, the effect of the addition of the hole and dam combination can be analysed. Figure 9.6 shows that the flow through holes does not eliminate the dead zone behind the turbulence inhibitor on the symmetry plane, although it might reduce it in areas behind the turbulence inhibitor closer to the side walls. Additional dead zones are in fact formed behind the dams. However, the RTD results from both the physical and numerical models show a small decrease (4.6% when using the average value of the two experimental methods) in dead volume when the holes and dams are added. Therefore, although the hole and dam combination may slightly reduce the dead volume, its effect is not highly significant.

Stellenbosch University http://scholar.sun.ac.za

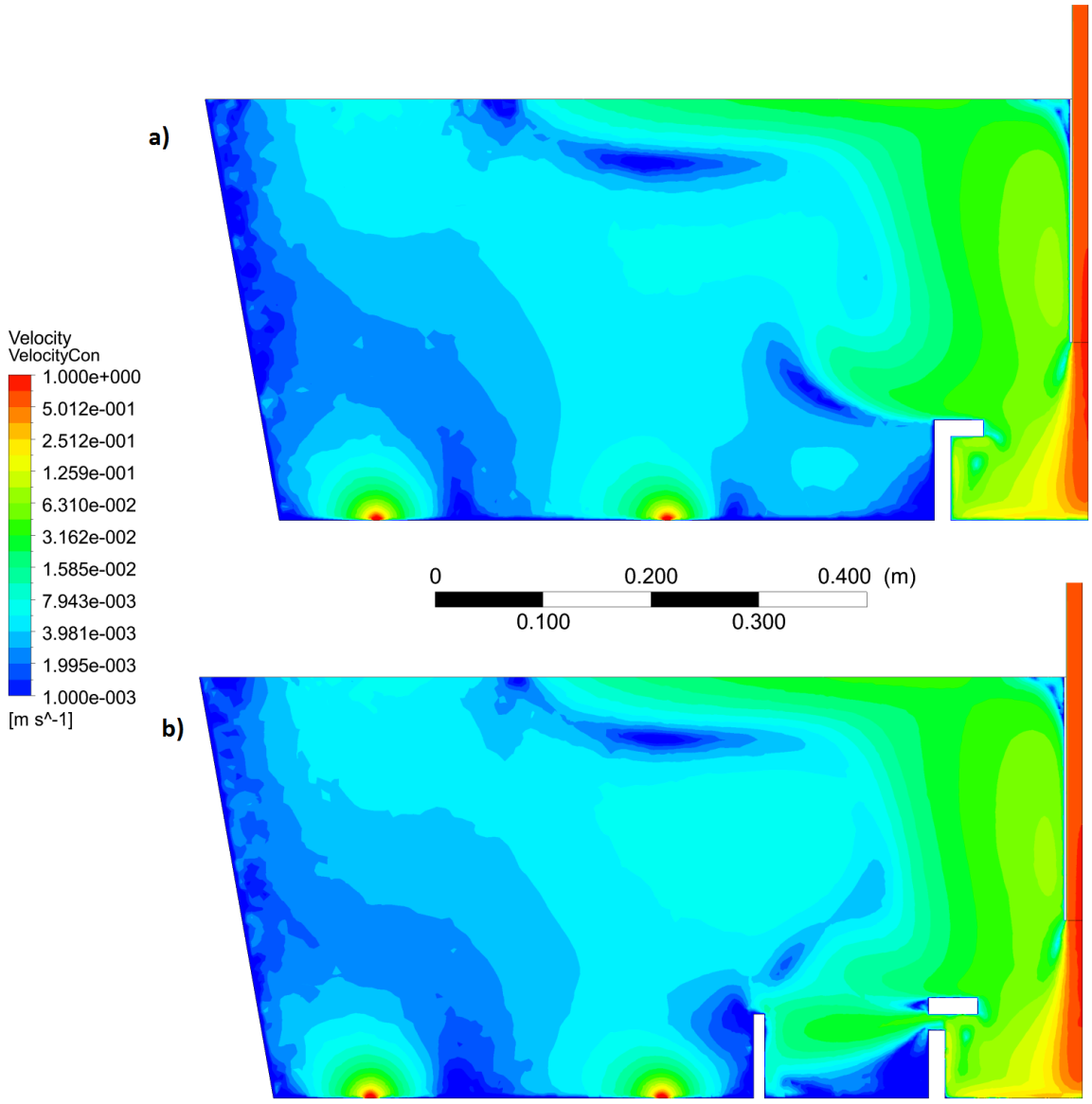

Figure 9.6 - Comparison of velocity contour plots along the longitudinal symmetry plane for a) the TI configuration and b) the TID configuration

The velocity contour plots show that apart from the flow through the holes and the flow above the dams, the velocity profiles remain very similar. The change in the flow above the dams can be observed in Figure 9.7. The dams deflect the flow coming through the holes upwards, where the flow joins the rising part of the circulation forming at the top of the tundish, increasing the strength and magnitude of the rising portion of the circulation. Therefore, the design does achieve its aim of increasing surface directed flow further away from the inlet region.

Stellenbosch University http://scholar.sun.ac.za

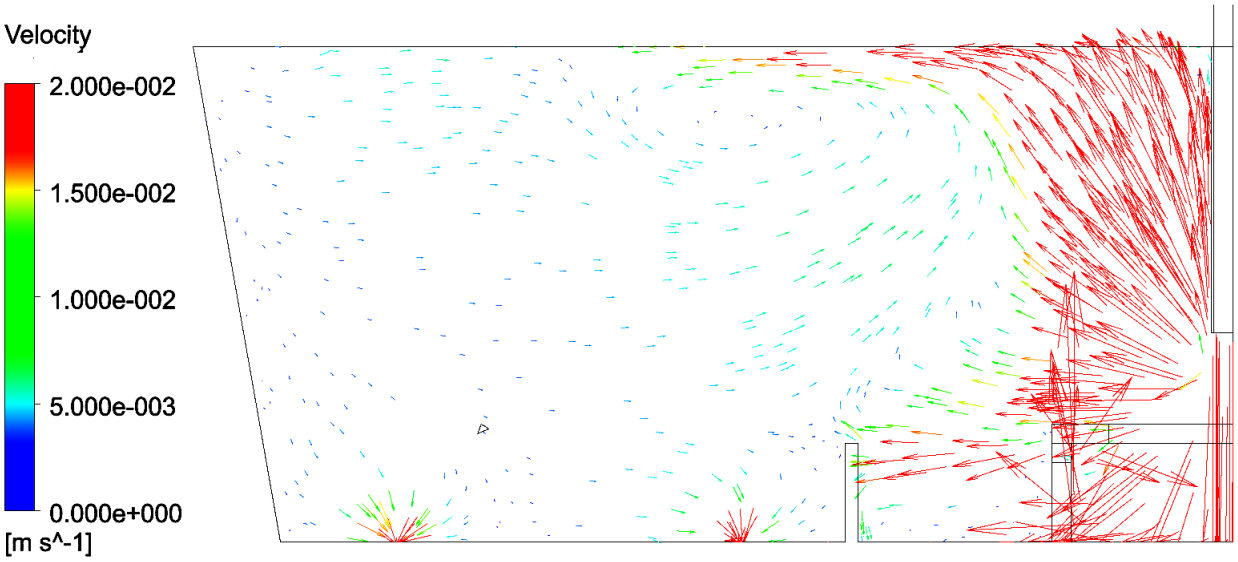

Figure 9.7 - Velocity vectors along the longitudinal plane for the TID case

9.2. Surface Turbulence

The magnitude of the turbulence near the tundish surface is very important due to the potential of slag entrainment. From previous discussions it is also obvious that the addition of the turbulence inhibitor influences the flow near the surface to a large extent. It is therefore necessary to evaluate the effect of the upward flow on surface turbulence, because entrainment due to increased turbulence may offset any benefits of longer residence times and increased plug flow gained by the addition of the turbulence inhibitor. It should be noted that without a separate study to determine the dependency of slag entrainment on turbulence conditions, the discussion regarding entrainment in this study will be qualitative in nature.

Comparing the turbulence kinetic energy values on a plane 2cm below the surface of the tundish in Figure 9.8, it can be seen that the turbulence inhibitor changes the nature of the surface turbulence significantly. Firstly it is noted that regions with slightly more turbulence form at the far end from the inlet in all three configurations due to a circulation formed at the surface after flow is turned back at the back wall. However, this discussion will focus on the area near the inlet, where more surface turbulence occurs. In the bare tundish a high turbulence region is formed near the side walls close to the inlet due to the flow rising along the walls. When the turbulence inhibitor is introduced, the high turbulence region is centred on the inlet due to the rising flow from the turbulence inhibitor. Important to note is that the maximum value of turbulence ($2.17 \times 10^{-4}\ m^2/s^2$) is significantly increased from the bare case ($9.67 \times 10^{-5}\ m^2/s^2$). It is therefore recommended that surface turbulence should be considered when changing the design of a tundish to include a turbulence inhibitor. It would be valuable to study whether the turbulence generated near the surface would be sufficient to entrain slag droplets, either by physical or numerical modelling.

Stellenbosch University http://scholar.sun.ac.za

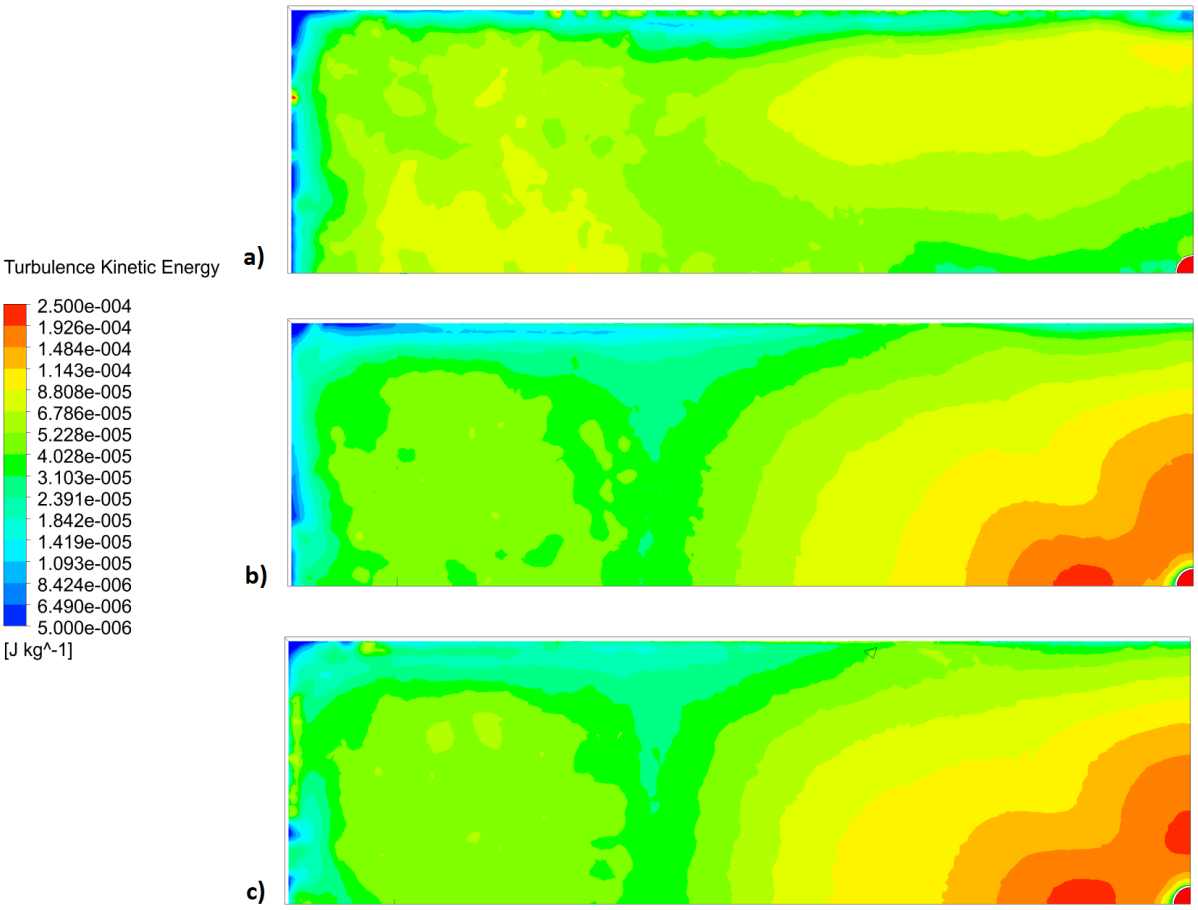

Figure 9.8 - Comparison of turbulence kinetic energy value near the surface of the tundish for a) the bare tundish, b) the TI configuration and c) the TID configuration

Visual comparison between the TI and TID cases in Figure 9.8 shows that the areas of higher turbulence expand very slightly due to the addition of the holes and dams. To gain a better understanding of this, the difference in turbulence kinetic energy between the TID and TI cases is plotted in Figure 9.9. An increase in turbulence at the surface is observed above the dam. The most likely explanation for this increase is that due to the increased strength of the circulation pattern at the top of the tundish for the TID case, more turbulence is generated when the flow rising from the inlet joins the flow from this circulation pattern.

Stellenbosch University http://scholar.sun.ac.za

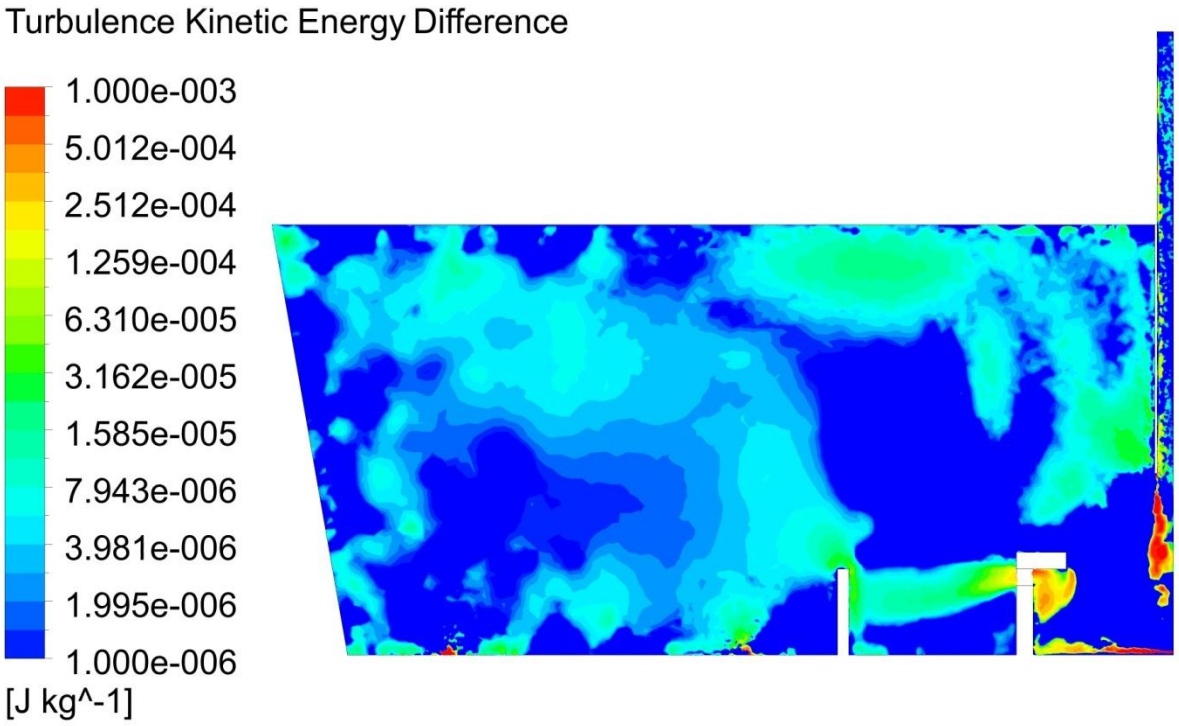

Figure 9.9 - Contour plot showing the areas of increased turbulence along the centre longitudinal plane when the holes and dams are added to the TI case.

The maximum and average values of turbulent kinetic energy at the plane 2cm from the surface are compared in Figure 9.10. It shows nearly equal increases in the average values from the bare to the TI to the TID cases. The very significant information that can be derived from the comparison is that the maximum turbulence kinetic energy closer to the surface doubles with the introduction of the turbulence inhibitor.

Stellenbosch University http://scholar.sun.ac.za

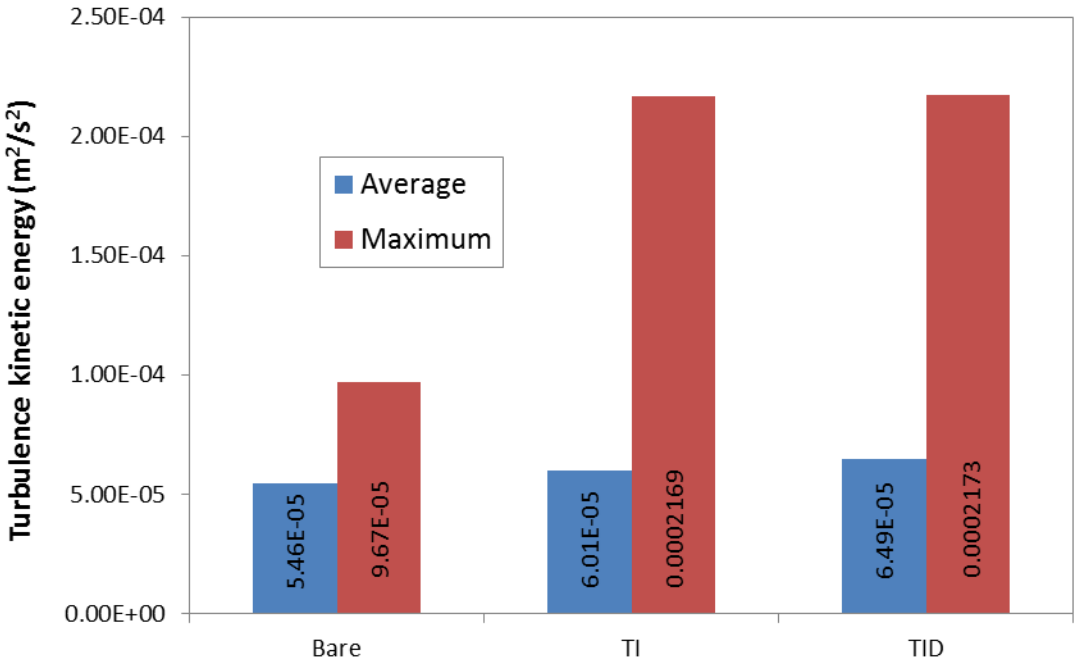

Figure 9.10 - Comparison of average and maximum turbulent kinetic energy values near the surfaces of the three tundish configurations

9.3. Dead Volume

The dead volume fraction calculated from the combined approach in the physical model gives an indication of how much dead volume is present in the tundish. It does not, however, give any information regarding where the dead volumes occur. Using the numerical results, an indication of where the dead volumes occur can be obtained by plotting iso-surfaces of a selected low velocity in the tundish. Knowledge of the slow moving flow regions can then be used to suggest improvements in the design.

Low velocity iso-surfaces are shown for the three configurations in Figure 9.11. The velocity of 0.002 m/s is sufficiently low to show slow moving areas. Clearly illustrating the results is difficult without showing the iso-surfaces for each case from multiple angles. However, angles were selected that show the main features.

Stellenbosch University http://scholar.sun.ac.za

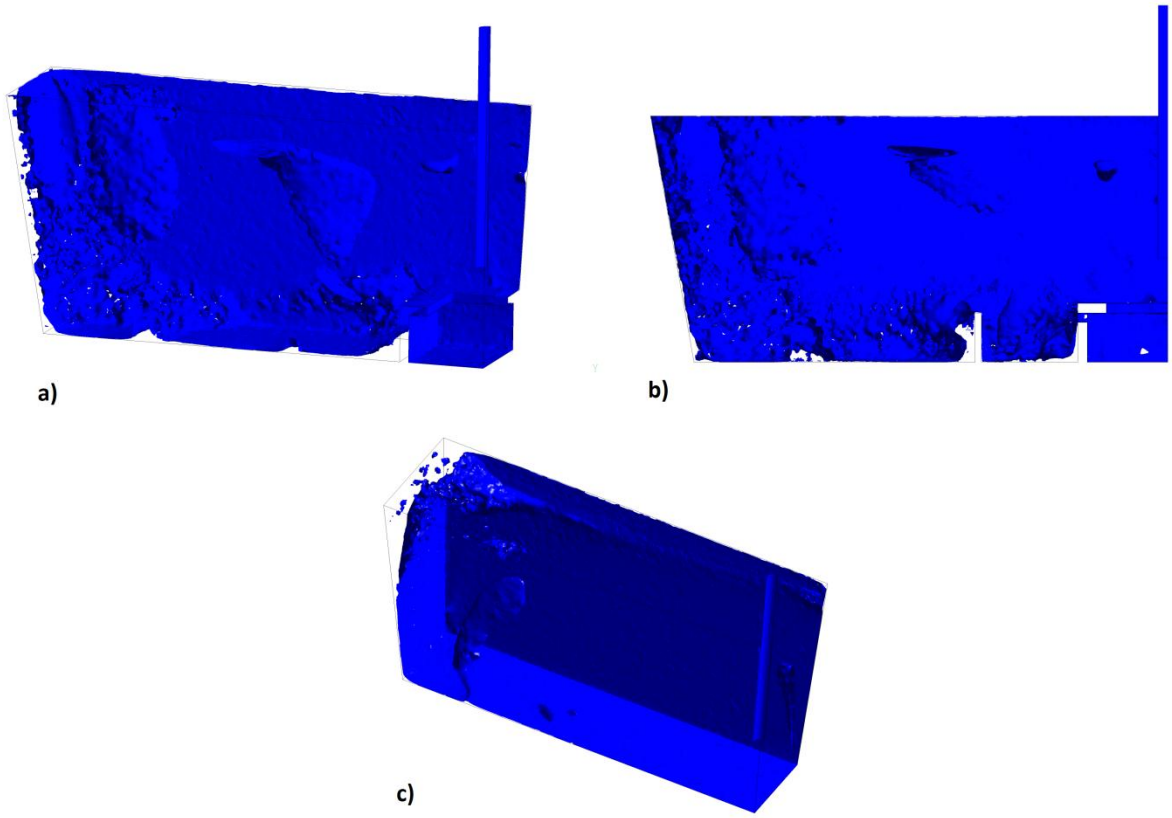

Figure 9.11 – Iso-surface at velocities of 0.002m/s for a) the TI case, b) the TID case and c) the bare tundish

It is immediately obvious that when specifying the same velocity for all three cases, the apparent dead zones are much smaller for the bare tundish. This is due to the dampening of the flow by the turbulence inhibitor, which significantly reduces the velocities throughout the tundish. This contradicts the values for dead volumes that are calculated from the RTD results for the three cases. Therefore, it appears that to appropriately show dead volumes using this method, the velocity of the iso-surfaces should be somehow selected relative to the velocities found in each configuration. Unfortunately, simply using the same ratio between the iso-surface velocity and the average velocity was unsuccessful. It therefore appears that a more complex scaling method is required for the volumes below a velocity iso-value to correspond with the dead volumes fractions, however, developing such a method is outside the scope of this study. For this reason the discussion will proceed using the plots in Figure 9.11.

For both cases using turbulence inhibitors dead volumes exist in the lower back corners of the tundish and behind the turbulence inhibitor wall. Two slow moving regions also form at the centres of circulation patterns: one close to the back corner of the tundish and the other at the top centre, roughly above the dam wall. What is interesting to note is that the dead zone above the dam decreases significantly in size with the introduction of the holes and dams. This is due to the increased strength of the circulation pattern due to the upwards flow from the dams in the TID case, as previously discussed. Another observation is that the

Stellenbosch University http://scholar.sun.ac.za

holes through the dams slightly decrease the dead zone behind the turbulence inhibitor, but that additional dead zones are formed behind the dam. For the bare tundish, slow moving regions are found in the corner between the back wall and the surface. Small dead zones also form at the back corner and in the centre of the transverse symmetry plane at the centre of circulation patterns.

Two conclusions can be drawn from the above discussion. Firstly, although some circulation patterns can be beneficial in increasing the residence time and eliminating dead zones, the circulation pattern will contain a slow moving volume in the centre. By increasing the circulation strength, the size of the slow moving region can be reduced. Secondly, the use of flow control devices to alter the path of the fluid will inevitably result in dead zones forming behind the obstructions. However, it is likely that by determining the optimal placement of flow control devices and outlets, flow patterns will form that will help reduce dead zones in these areas.

9.4. Strand Similarity

When comparing the physical and numerical model results, it was observed that the largest inaccuracy in the numerical model lies in the prediction of the separate strand C-curves. Some trends are seen in both models, such as earlier minimum and peak residence times for the inner strands, higher concentrations for the inner strand at later residence times and higher peak concentration for the inner strand. However, although these trends were observed, the differences were generally smaller than the physical model predicted. The source of this error is unknown, but likely causes are the symmetry and dynamically steady assumptions, or possibly the choice of turbulence model. Unfortunately, the trends in variation between the strands are not similar when comparing the different configurations. Therefore it appears that the numerical model fails in accurately predicting strand variations.

However, the numerical model can still help in understanding why the trends in the strands variations detected in the physical model exist. The most important trend observed was much greater strand similarity for the bare tundish than for the tundish configurations using a turbulence inhibitor. A possible explanation for this is that in the bare tundish there is strong circulation over the breadth of the tundish, while in the turbulence inhibitor cases the flow is mostly along the length. The circulation in the bare tundish causes the bulk of the flow to follow a more similar path to the individual outlets.

It might be worth mentioning that these differences in flow may also have an effect on the validity of the symmetry assumption, which was only tested for the TID case. Flow in the TI and TID cases are mostly along the longitudinal symmetry plane. However, in the bare tundish the dominant flow pattern causes flow perpendicular to the top of the longitudinal symmetry plane before it is turned down to the outlets. This perpendicular meeting of flows at the symmetry is therefore more likely to cause deviations from symmetrical flow. It might

Stellenbosch University http://scholar.sun.ac.za

therefore be worthwhile to investigate the effect of the symmetry assumption for different configurations in future work, as it might not have an equally small effect in all cases.

9.5. Adjusting the TID Model

When comparing the TI and TID cases, it was seen that one of the major disadvantages of the TID model was a small amount of short-circuiting taking place at the inner inlet. It was also suggested that it might be possible to eliminate this problem by increasing the height of the dams. A numerical simulation was performed for the case of a turbulence inhibitor with high dams (abbreviated as TIHD), where the height of the dams were increased by 50% over the TID case. Comparison of the flow characteristic properties in Figure 9.12 shows that the higher dam is in fact able to remove the short-circuiting in the system, since the value of the dimensionless minimum residence time increases from 0.043 to 0.084. Unfortunately, this improvement comes with a cost as the peak residence time is significantly reduced and the dead volume is increased slightly.

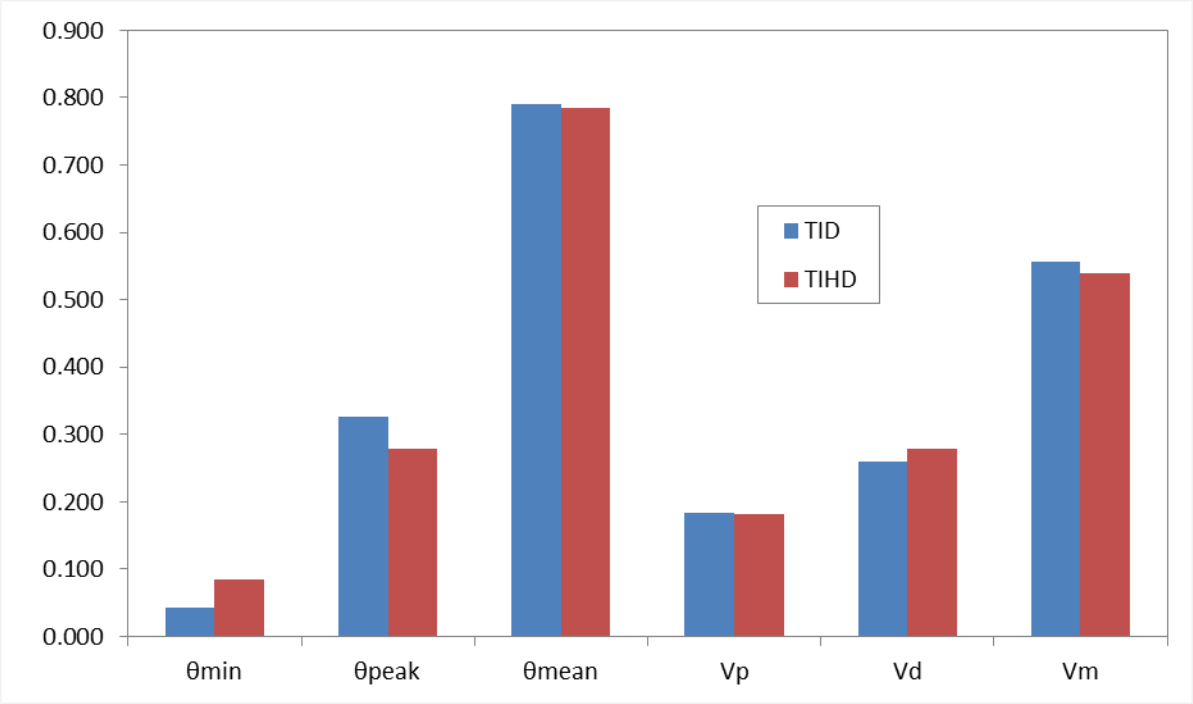

Figure 9.12 - Comparison of flow characteristic properties for the TID and TIHD configurations

The likely reason for this deterioration of the flow quality is that the higher dam causes larger dead volumes in the volume between the turbulence inhibitor and the dams, as well as behind the dams. Industrial trials would be required to determine whether the effect of large inclusion passing through by short-circuiting in the TID case is worth the reduction in peak residence time and increase in the dead volume.

Stellenbosch University http://scholar.sun.ac.za

Chapter 10: Investigation of Turbulence Inhibitor Design through Numerical Simulation of the Tundish Prototype

Results in the previous chapter indicated that a turbulence inhibitor can be beneficial to the flow in a tundish. Several different approaches to turbulence inhibitor designs are presented in literature and several studies have shown the improvements that the turbulence inhibitor provides over that of the bare case. However, there are few studies that compare the performance of different turbulence inhibitor designs to each other. For this reason, the numerical model developed previously will be used to simulate the flow in four tundish configurations, using different general shapes of turbulence inhibitors. The same flow rate, bath height, tundish geometry and outlet nozzle will be used as in previous experiments.

10.1. Numerical Modelling of the Tundish Prototype

So far the discussion regarding numerical modelling results was based on the numerical simulation of the water model. The numerical model was initially applied to the water model setup for validation. The results obtained in the validation runs for the numerical model were then also used to compare the different configurations applied in the water model. Assuming that the physical model is an accurate representation of the real industrial system, this discussion of the flow based on the numerical water model should be valid.

However, for further numerical investigations it would be preferred if the numerical simulations were performed on the high temperature steel process to eliminate any errors produced in the physical modelling. This also offers an interesting opportunity to test how well the physical model, based on Froude number similarity, is able to predict the industrial process. Previous studies in the available literature have either based the numerical model on the water system or the high temperature steel system, with no comparison being made between the two.

10.1.1. Scaling the Numerical Model

To apply the numerical model to the tundish prototype several changes are required. Firstly, the geometry needs to be scaled back to its original size; therefore every dimension in the numerical water model is multiplied by two. Next, the fluid properties and boundary conditions have to be changed to that of the high temperature steel system. The property values are summarised in Table 10.1.

Stellenbosch University http://scholar.sun.ac.za

Table 10.1 - Comparison of fluid properties and inlet boundary conditions for the numerical models based on the water model and the prototype at temperature

Property	Water model	Prototype
$\rho\ (kg/m^3)$	998	7100
$\mu\ (kg/m.s)$	0.001002	0.006482
$v_{inlet}\ (m/s)$	0.604	0.855
$Q\ (l/s)$	0.427	2.42
$\kappa\ (m^2/s^2)$	0.00365	0.00730
$\epsilon\ (m^2/s^3)$	0.0208	0.0147

Since the geometry is scaled, the mesh sizes used will also have to change. This is a very important step, since it must be ensured that the numerical accuracies of the two numerical models are the same, otherwise changes in the results might be attributed to differences in the meshing accuracy or the time step size, and not to differences between the water model and the industrial system.

However, there was some uncertainty with regards to how this scaling should be done, with two possible arguments. The first is that the shape of flow patterns remains the same between the two setups; therefore the same number of cells should be used and the size of the cells should be scaled by the same factor as the rest of the geometry. The second argument is that since the lengths are scaled by a factor of 2, but the velocities only by a factor $\sqrt{2}$, the gradient becomes smaller in the prototype. Comparison by numerical simulations showed a very good correlation when using a mesh with the same number of cells as the numerical water model, while using a mesh with the cells size increased by a factor of $\sqrt{2}$ caused significantly earlier peak residence times to be predicted. Therefore, it was decided to use a mesh with the same number of cells for the numerical simulation of the prototype, as was used for the water model.

In order to generate an identical mesh, apart from the size being increased by a factor of two, the correct value of the gradient adaptation function had to be determined for the numerical simulation of the prototype. To produce the same final amount of cells as for the final mesh of the numerical water models, values of $1.02 \times 10^{-6}$and 1.1×10^{-6} were required for the bare and TI cases. An average value of 1.06×10^{-6} was therefore used for further simulations of the prototype tundish.

Finally, the time step had to be adjusted. Based on equation 5.17, the new time step was calculated by multiplying the time step used in the numerical simulation of the water model by a factor of $\sqrt{2}$.

10.1.2. Comparison of Numerical Models

A comparison was made for the numerical models of the water and steel systems for the TI case. A very good correlation is seen in Figure 10.1 between the RTD curves for the water model and the prototype. A small difference is observed in the predicted peak values, with

Stellenbosch University http://scholar.sun.ac.za

the difference between the peaks increasing when the numerical model is based on the high temperature steel system.

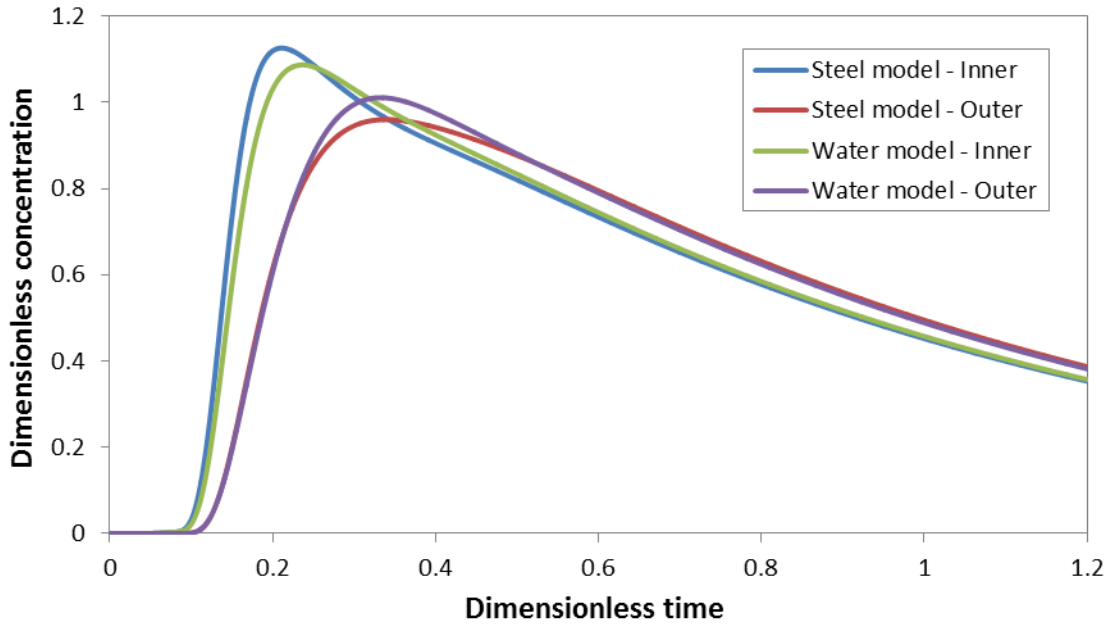

Figure 10.1 - Comparison of the C-curves for numerical models based on the water model and on the high temperature steel system

In Figure 10.2 the velocity contours are compared for the two numerical models. The contour values are multiplied by a factor of $\sqrt{2}$, therefore the same colour in each plot will represent the same relative velocity. A few minor differences can be seen, especially behind the turbulence inhibitor wall, but in general the velocities correspond very well between the two cases.

Stellenbosch University http://scholar.sun.ac.za

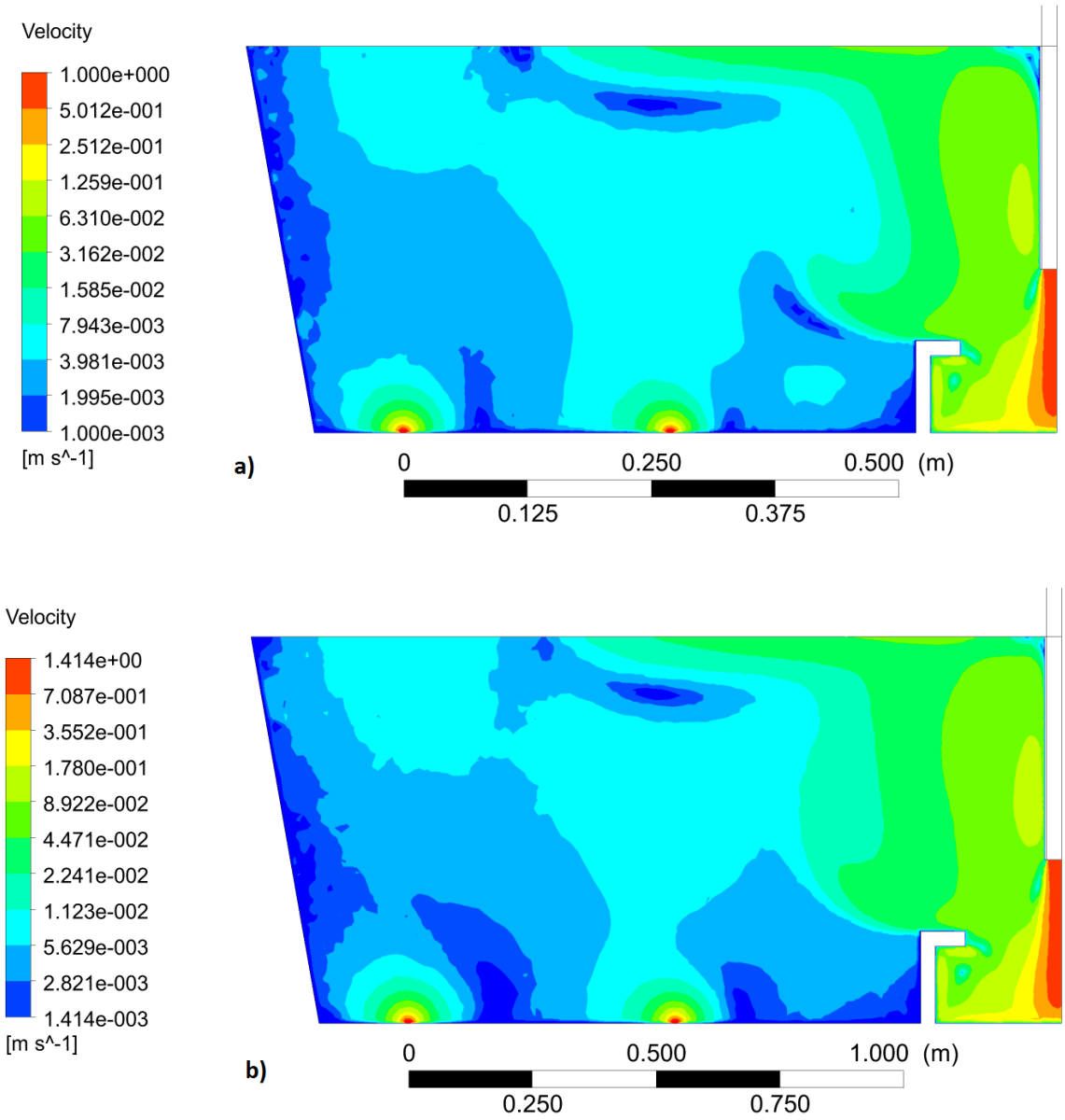

Figure 10.2 - Comparison of velocity contours on the longitudinal symmetry plane for the numerical simulations based on a) the water model and b) the high temperature steel process

In conclusion it can be stated that there is a very good correlation between the numerical model results obtained by simulating the water model and those obtained from the steel numerical model. Care was taken to eliminate any effect of the meshing and numerical setup on the comparisons. Therefore, this comparison indicates that the water model based on Froude number similarity delivers an accurate representation of the flow taking place in the industrial process.

10.2. Turbulence Inhibitor Designs for the Prototype Tundish

In the previous chapter it was shown that the use of a turbulence inhibitor can be very beneficial to the flow behaviour in the tundish. However, it was also observed that the

Stellenbosch University http://scholar.sun.ac.za

turbulence inhibitor can increase turbulence near the slag layer, which has potential to cause slag entrainment and harm the product quality. Several different turbulence inhibitor designs have been the subject of studies in literature. Each of these designs should have a different impact on the flow behaviour. The primary aim of this chapter is therefore to compare the flow characteristics of the tundish for different generalized turbulence inhibitor designs.

Four different approaches to turbulence inhibitor designs were analysed in this study. The first was the rectangular turbulence inhibitor with flanges at the top that was used in the water modelling study. The dimensions of the turbulence inhibitor used in the water model were given in Figure 5.2. For the numerical model of the high temperature steel process, each dimension is multiplied by 2.

In the other three designs, the ultimate care was taken to maintain the same opening area at the top of the turbulence inhibitor as was used in the case of the first design. Therefore, any changes in the flow should be mainly as a result of the different turbulence inhibitor shapes and not be influenced by the opening area and the turbulence inhibitor height.

The first design, abbreviated as TI-S, is based on the Advanced Pour Box used by Jha et al. (2001) and was derived by simply removing the flanges from the original design. However, the distances from the centre to the inner walls were reduced to result in the same opening area as for the original TI design. The distances to the outer sides were left unchanged. This would result in a thicker turbulence inhibitor, but would allow filling the same volume in the tundish. Therefore any possible effects of having a smaller turbulence inhibitor, influencing secondary flows reaching the outer walls differently, were eliminated. The dimensions are shown in Figure 10.3.

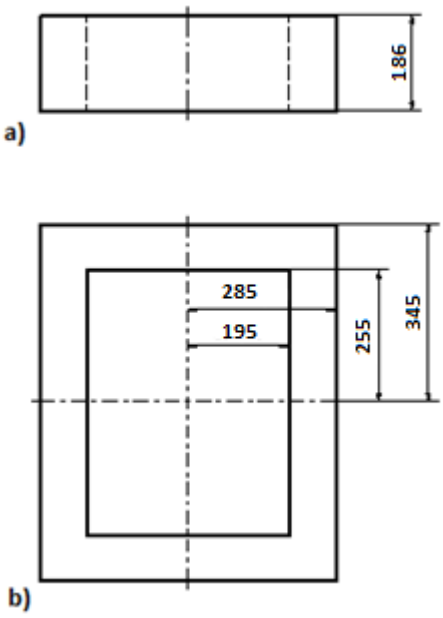

Figure 10.3 - Dimensions (in mm) of the TI-S design from a) the front view and b) the top view

Stellenbosch University http://scholar.sun.ac.za

The second design (TI-R) simply replaces the rectangular shape of the original turbulence inhibitor with a round one. The diameters of the geometry were calculated in order to maintain the volume inside the turbulence inhibitor and the opening area as for the original geometry. The dimensions of this design are shown in Figure 10.4.

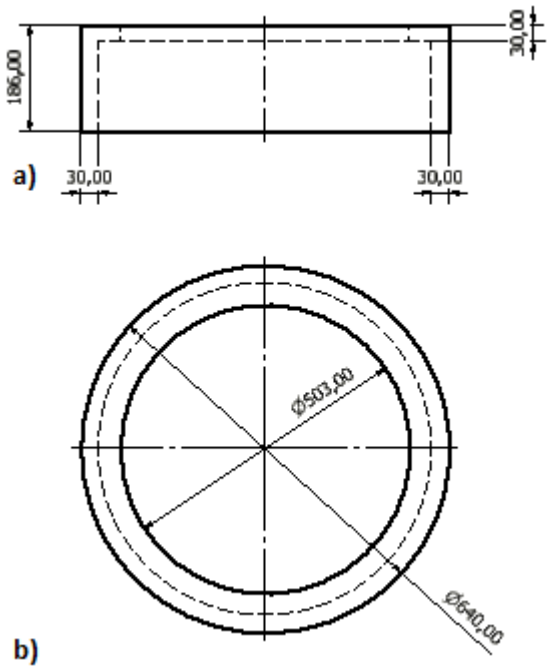

Figure 10.4 - Dimensions (in mm) of the round turbulence inhibitor design shown from a) the front and b) the top.

In the final design (TI-C) the sharp corners in the original design was removed by adding 45° chamfers at the bottom and top of the four walls forming the turbulence inhibitor. The dimensions of one wall are shown in Figure 10.5. The distance from the centre of the turbulence inhibitor to the outside of the walls remained the same as in the original design.

Stellenbosch University http://scholar.sun.ac.za

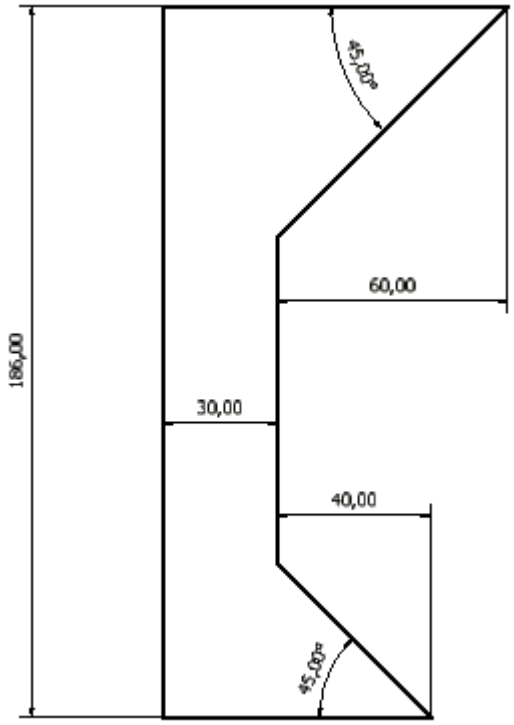

Figure 10.5 - Dimensions of the turbulence inhibitor wall (in mm) for the TI-C design

10.3. Flow Characteristics

The first impression when comparing the RTD responses for the four different turbulence inhibitor designs, shown in Figure 10.6, is that even relatively small changes in the turbulence inhibitor geometry can have a drastic effect on the flow in the tundish. Each of the C-curves has a very different shape, with peak times and concentrations changing significantly with changes in the turbulence inhibitor design. Additionally, the straight (TI-S) and the round (TI-R) designs show multiple peaks being formed. The second observation is that the original design significantly outperforms the other designs, with much longer residence times being predicted.

Stellenbosch University http://scholar.sun.ac.za

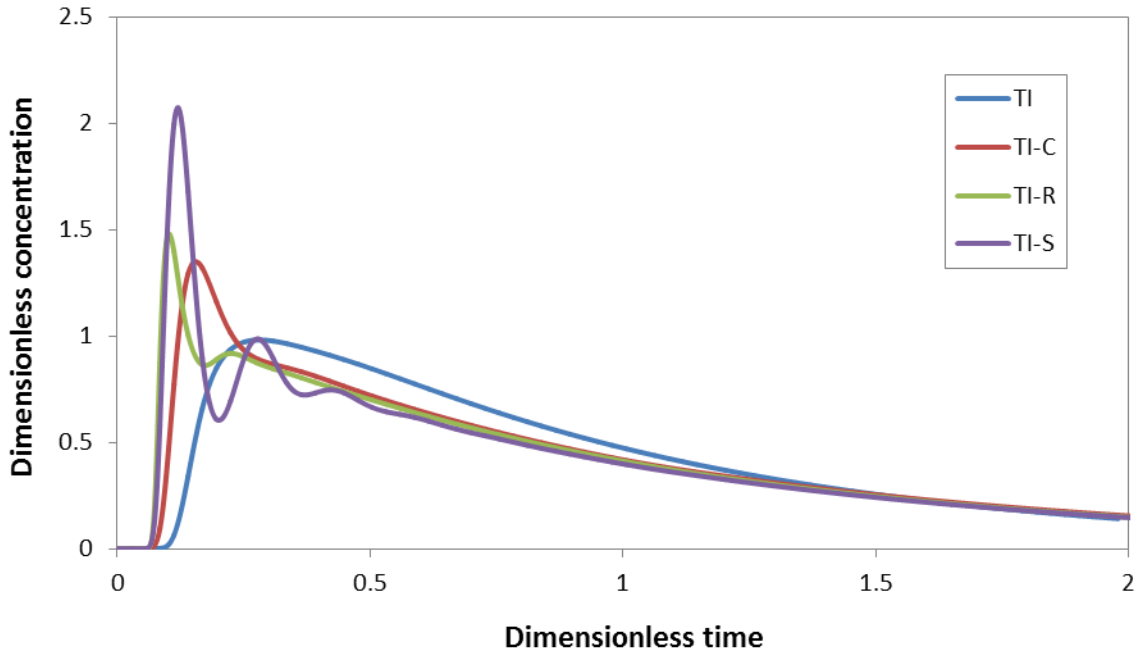

Figure 10.6 - Comparison of overall C- Curves for the four turbulence inhibitor designs

Comparison of the flow characteristics properties in Figure 10.7 clearly confirms this. All residence times and the plug flow volume are larger than for any of the other designs, while the dead volume fraction is also significantly reduced. For the other three designs the performance is similar, with the chamfered design (TI-C) performing slightly better than the other two. The values for the flow characteristics are shown in Table 10.2.

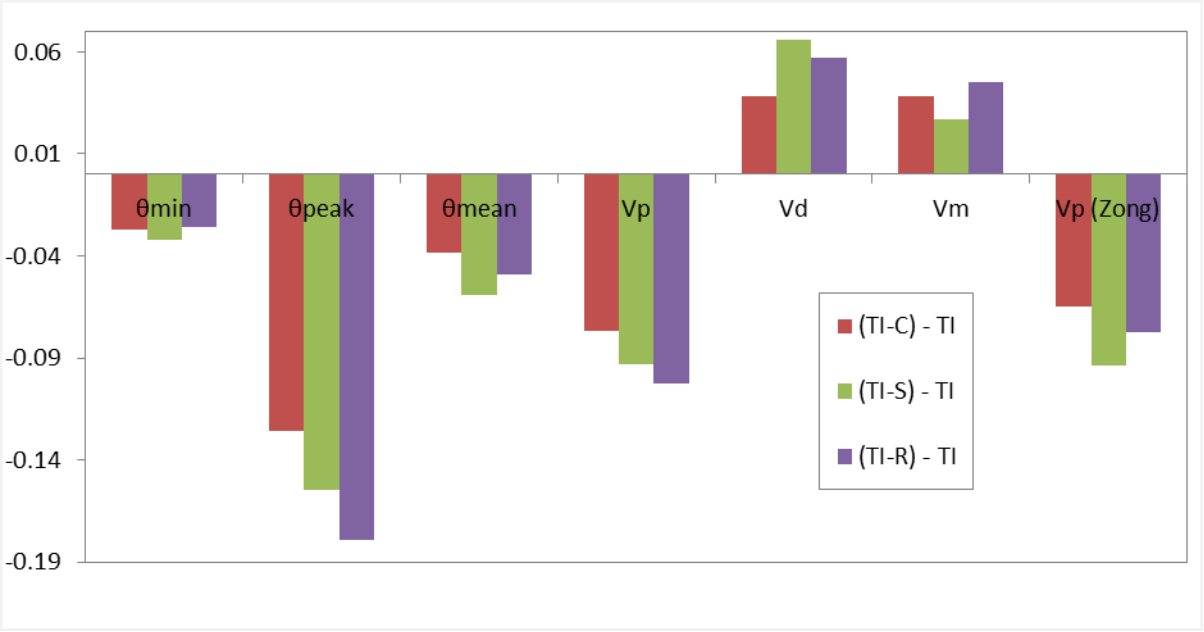

Figure 10.7 - Plots of the difference between the flow properties calculated for the TI-S, TI-C and TI-R cases from that calculated for the TI design

Stellenbosch University http://scholar.sun.ac.za

Also interesting to note is the comparison in trends of the dispersed plug flow and the plug flow proposed by Zong et al. (1999). For the TI, Ti-C and TI-S designs the trends are very similar. However, for the round design, the method by Zong et al. (1999) predicted more plug flow relative to the other designs. A possible explanation is that for the round design there was a very large difference between the two strands, which will be discussed later, with the performance of the outer strand being much better than that of the inner strand. Therefore it is likely that the effect of the inner strand is being exaggerated by calculating the plug flow volume from only the peak and minimum residence times.

Table 10.2- Flow characteristic properties for the four turbulence inhibitor designs investigated

Design	θ_{min}	θ_{peak}	θ_{mean}	V_p	V_d	V_m	Vp [Zong et al. (1999)]
TI	0.0881	0.281	0.783	0.185	0.279	0.537	0.244
TI-C	0.0608	0.155	0.745	0.108	0.317	0.575	0.180
TI-S	0.0562	0.126	0.724	0.091	0.345	0.564	0.150
TI-R	0.0623	0.102	0.734	0.082	0.336	0.582	0.167

10.4. General Flow Patterns

The easiest way to develop an understanding of the large differences in the flow properties for the different designs is to compare the velocity contours along the longitudinal plane, as shown in Figure 10.8. It immediately becomes apparent that the differences are mainly caused by the amounts of suppression delivered by each turbulence inhibitor design. The flow in each alternative design will now be discussed to better understand what is happening. However, it must be noted that this general comparison of turbulence inhibitors does not account for the optimal dimensions of each design. This means that the alternative designs may possibly perform better if they are optimised for the tundish being used. This comparison therefore only serves as a general discussion of possible advantages and disadvantages of each design strategy.

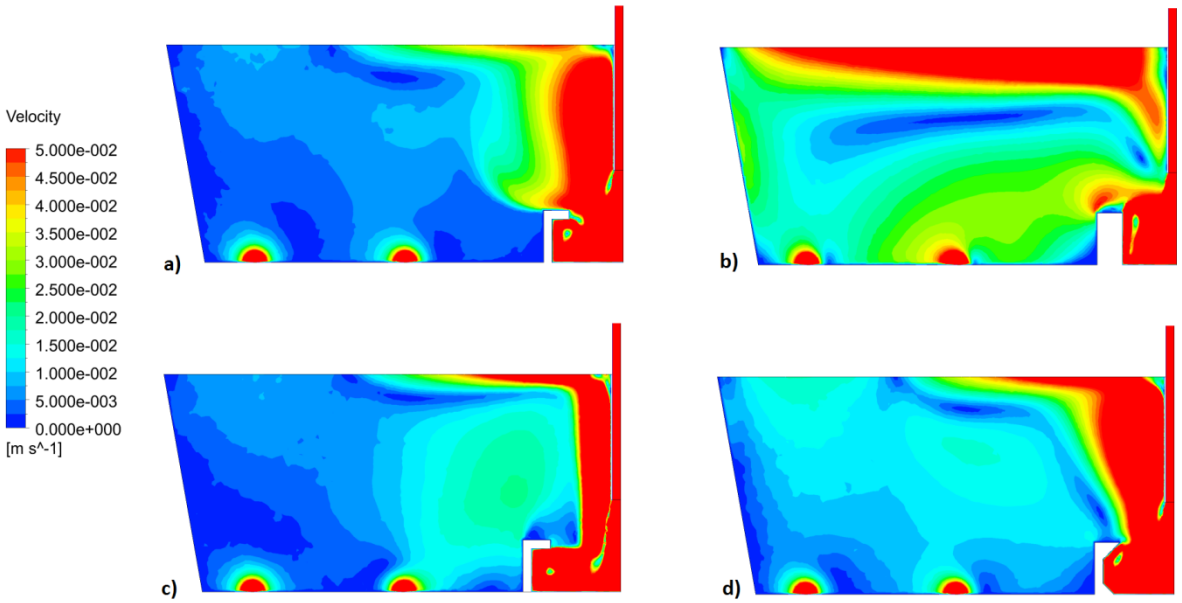

Figure 10.8 - Comparison of velocity contours along the longitudinal centre plane for the four turbulence inhibitor designs: a) TI, b) TI-S, c) TI-R and d) TI-C

10.4.1. TI-S

In the case of the turbulence inhibitor without flanges, the turbulence inhibitor effectively became a low dam placed very close to the inlet. The result is that nearly no turbulence suppression took place and that a very strong circulation pattern developed in the tundish, as shown in Figure 10.9. This explains the multiple peaks and the short residence times. Although the residence times were relatively short, the TI-S did prevent short-circuiting from taking place and delivered surface directed flow.

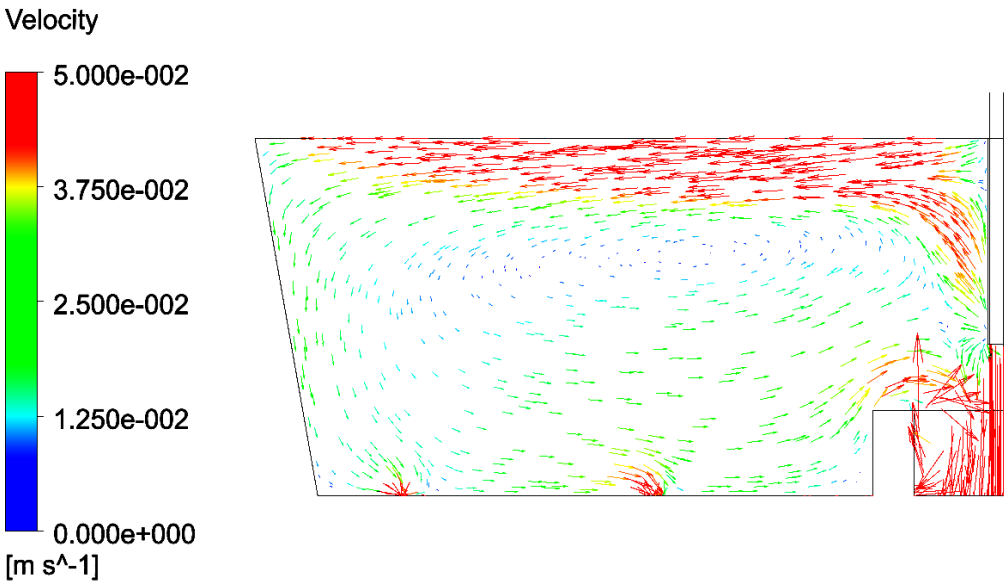

Figure 10.9- Vector plot along the longitudinal symmetry plane for the TI-S design

Stellenbosch University http://scholar.sun.ac.za

10.4.2. TI-C

With the addition of the chamfers in the turbulence inhibitor, the flow path of the melt is smoothened. Therefore, suppression will take place, but will be reduced from that of the TI case. The vector plot along the longitudinal symmetry plane, shown in Figure 10.10, shows that the flow is indeed similar to that of the original turbulence inhibitor, as a similar circulation pattern develops above the inner strand. This similarity can also be seen in the C-curves, where the TI-C and TI cases are the only ones with only one peak forming. However, the reduced suppression leads to faster circulation in the tundish, resulting in much shorter residence times. It is possible that the angle of the chamfer could be used to control the suppression and achieve an optimum effect.

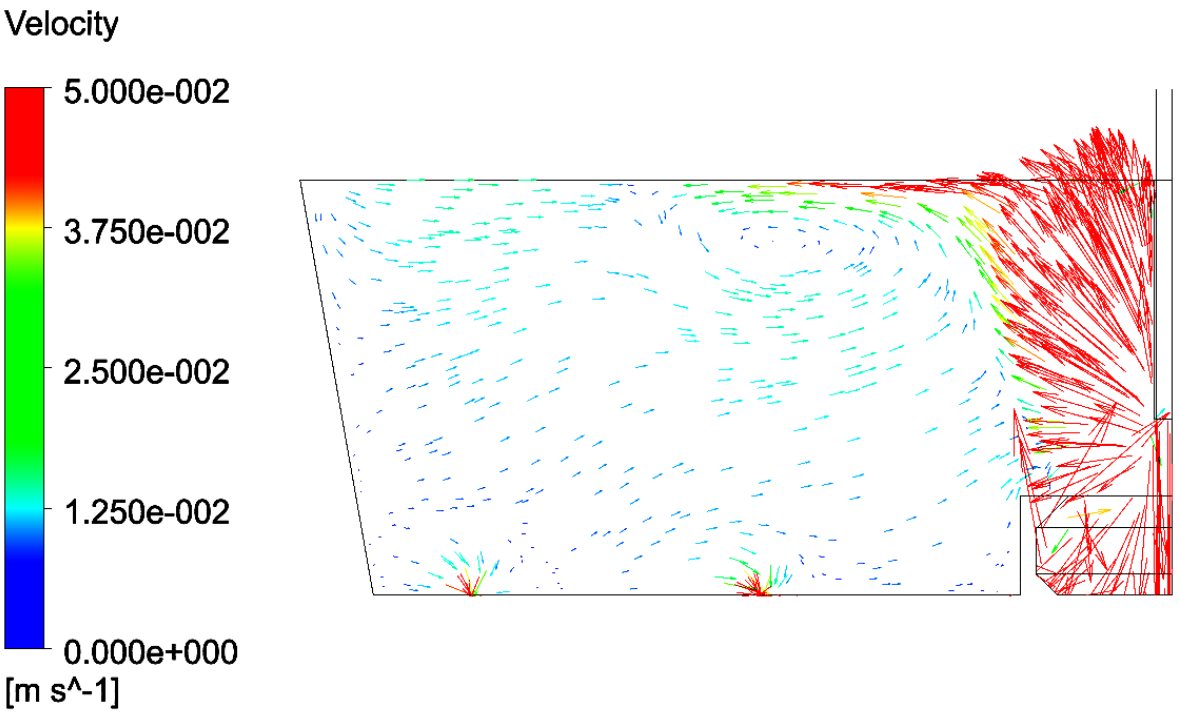

Figure 10.10- Vector plot along the longitudinal symmetry plane for the TI-C design

10.4.3. TI-R

The most surprising of the results were obtained for the round design, since similar results to the original TI design were expected. However, very poor performance is predicted, compared to the original turbulence inhibitor design. The velocity contours in Figure 10.8 show that a very large amount of suppression occurs due to the circular shape forcing the melt to converge on the inlet stream. This results in a dramatic change in the flow pattern, with clockwise circulation forming on the transverse planes, as shown in Figure 10.11. As a result the flow in the direction of the back of the tundish is reduced significantly.

Stellenbosch University http://scholar.sun.ac.za

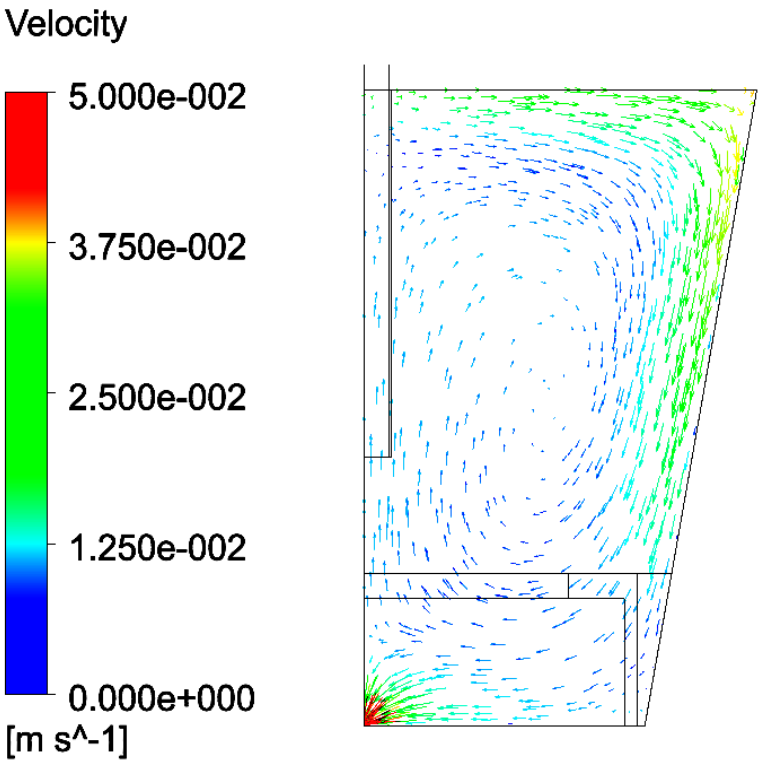

Figure 10.11 - Vector plot on the transverse plane through the inner strand of the TI-R case

The effect of this is evident when comparing the C-curves of the separate strands in Figure 10.12. Due to the slow movement of flow in the direction of the back of the tundish, tracer reaches the inner outlet long before it arrives at the outer outlet. This leads to major differences between the individual strands, with the performance of the inner strand being highly inferior to that of the outer strand.

Stellenbosch University http://scholar.sun.ac.za

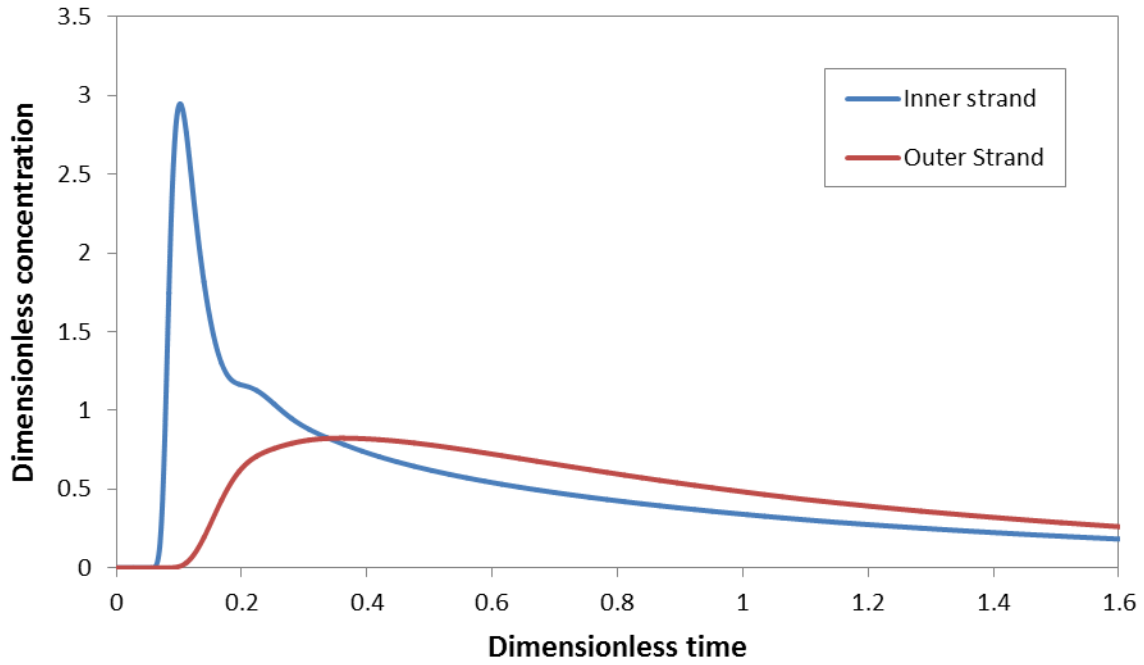

Figure 10.12 - C-curves for the individual strands for a tundish using the round turbulence inhibitor design

10.5. Surface Turbulence

From the comparison of tundish flow patterns for the four turbulence inhibitor designs discussed it is evident that the design of the inhibitor has a very strong effect on the resulting flow. Therefore, surface turbulence should also change with the different designs. A comparison of turbulence kinetic energy levels on a horizontal plane 4cm from the tundish surface, shown in Figure 10.13, displays these changes. The case with the straight turbulence inhibitor shows very different contours from the other three cases. The very high turbulence values near the inlet region are caused by the lack of suppression causing high velocity upward flow reaching the surface. Additionally, the strong circulation at the surface causes significant turbulence levels across most of the surface.

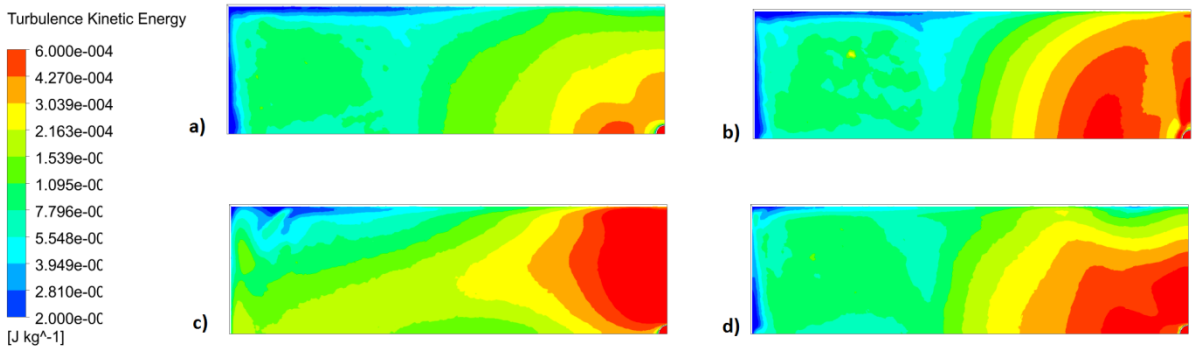

Figure 10.13 - Comparison of turbulence kinetic values near the surface for the four turbulence inhibitor designs: a) TI, b) TI-R, c) TI - S, d) TI-C

Stellenbosch University http://scholar.sun.ac.za

The TI-C and TI-R cases show roughly similar turbulence patterns to the original turbulence inhibitor design, with high turbulence centred on the inlet and low turbulence towards the back ends. However, both designs lead to increased turbulence near the surface. For the case of the chamfered turbulence inhibitor this is caused by insufficient suppression, which allows high velocity upward flow to reach the surface. In the tundish with the round turbulence inhibitor the explanation is less obvious, with the most likely explanation being increased turbulence generated by the convergence of flow around the inlet stream.

Figure 10.14 depicts the relative turbulence values near the surface for the four different designs of turbulence inhibitors. Previously it was found that the upwards flow formed by turbulence inhibitors will increase the surface turbulence. These results indicate that the design of the turbulence inhibitor will have an important effect on the amount of turbulence generated near the surface, with the maximum turbulence being nearly four times more for the TI-S case than for the original turbulence inhibitor design.

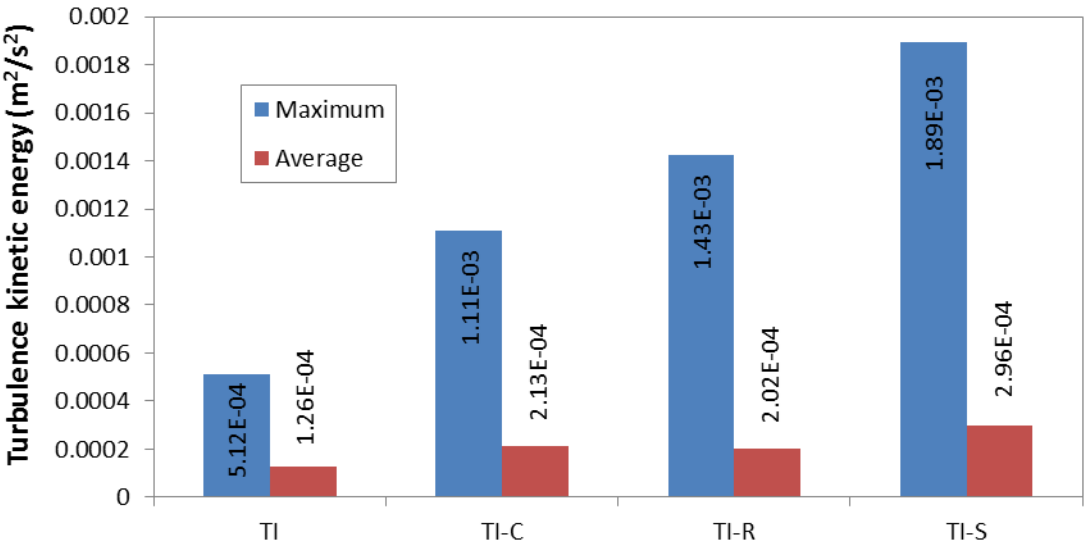

Figure 10.14 - Comparison of maximum and average turbulence kinetic energy levels for the four different designs of turbulence inhibitors on a horizontal plane near the melt surface

However, it should be noted again that to give full meaning to these results, a study of the turbulence levels associated with slag entrainment is required.

10.6. Strand Similarity

Although the comparison of the numerical and physical model results indicated that the numerical model does not predict the strand variation as accurately as it predicts overall properties, an interesting conclusion regarding strand similarity can be reached from the comparison of the different turbulence inhibitors. This is best observed by comparing a plot of the individual C-curves of the TI-S case, shown in Figure 10.15, with that of the TI-R case, shown previously in Figure 10.12. Clearly the TI-S configuration has much greater strand similarity than the TI-R case. Also, returning to physical modelling results; it was shown that

Stellenbosch University http://scholar.sun.ac.za

the bare case had more similar C-curves for the individual strand than for the cases using turbulence inhibitors.

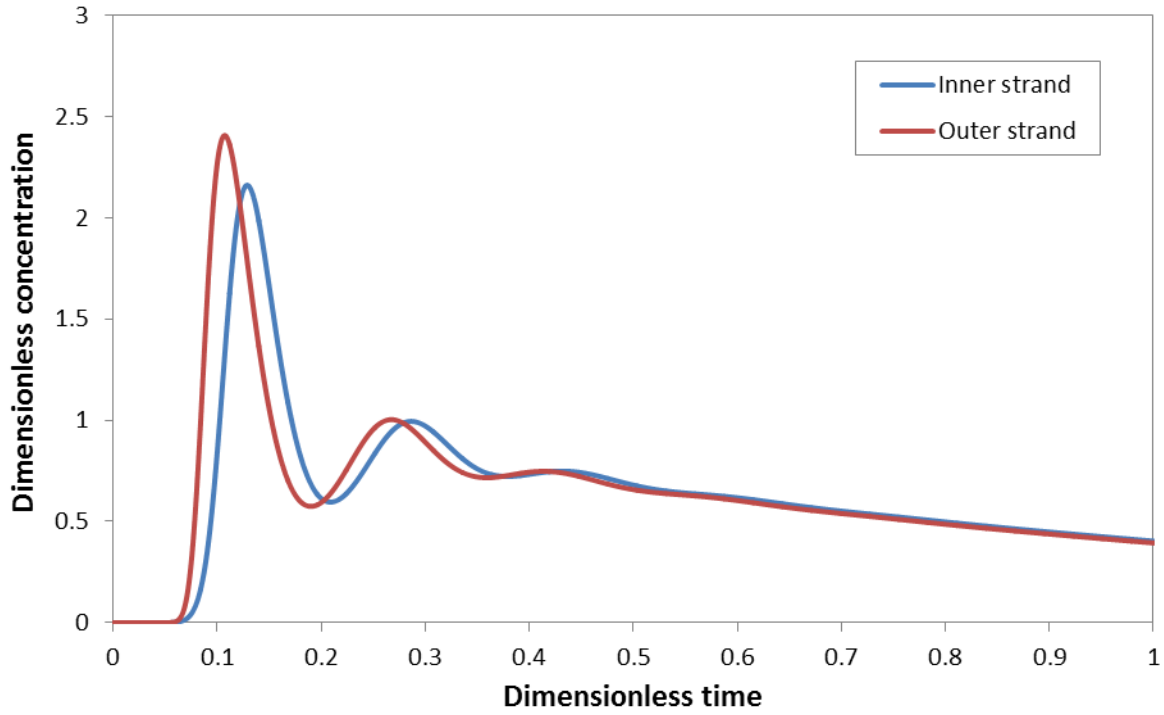

Figure 10.15 - Individual strand C-curves for the TI-S tundish configuration

It is therefore hypothesised that in setups with no or little turbulence suppression, strong circulation patterns will form that dominate the flow in the tundish. Therefore, fluid follows very similar pathways to the inner and outer strands, causing higher strand similarity. For example, in the TI-S case the largest portion of the flow follows a path upwards from the turbulence inhibitor, along the surface, down the back wall and across the bottom towards the inlets. A portion of the flow leaves at the outlets and the rest joins the circulation again. The tracer reaching the inner outlet therefore follows a similar pattern to that of the one reaching the outer strand, except for an additional short time that it takes to cross the distance between the two strands.

In the case of turbulence suppression, the aim was to eliminate these strong circulations in order to reduce turbulence and to increase residence time. However, this caused higher numbers of smaller circulations to form, which resulted in different pathways for the tracer to the individual outlets.

The conclusion is that turbulence suppression could lower strand similarity in the tundish, if not implemented properly. The TI-R case perfectly illustrates that one strand can have exceptional properties, while melt reaching the other will probably contain large inclusions. Such large differences in product quality will complicate tundish practice. Therefore, turbulence inhibitor designs for multi-strand tundish must aim at producing similar steel from all the outlets.

Stellenbosch University http://scholar.sun.ac.za

10.7. Conclusions on Turbulence Inhibitor Design

The results of this chapter indicate that the flanged turbulence inhibitor, first used in the water model studies, offers superior performance when it comes to providing flow for inclusion removal and limiting surface turbulence. However, optimal design of the other inhibitor designs would likely lead to improved performance, which might in some cases rival that of the rectangular, flanged design. For example, the chamfer angle could be increased to increase suppression in the TI-C case, while the opening area could be increased in the round turbulence inhibitor to compensate for the increased suppression that occurs when the flow converges to a central point.

This chapter therefore mainly served the purpose of showing the large effect that turbulence inhibitor shape can have on the nature of the flow, with significantly different flow patterns forming in each case. Results also highlighted the importance of finding an optimum amount of turbulence suppression to balance increased residence time with strand similarity and other important factors. This emphasizes the optimal design of a turbulence inhibitor dimensions for a specific tundish, as the use of the incorrect turbulence inhibitor can in fact decrease the quality of the melt flow.

Stellenbosch University http://scholar.sun.ac.za

Chapter 11: Conclusions

Numerous important results were obtained during this study with regards to the design and operation of a four-strand steelmaking tundish. The first portion of the study investigated the process of setting up the numerical model for the tundish and looked at numerical assumptions, methods and grid sizes. The rest of the study dealt with the effect of various configurations of flow control devices, with emphasis being placed on the use of turbulence inhibitors on the flow behaviour of the tundish.

11.1. Numerical Setup

The effect of two numerical assumptions commonly employed in tundish studies, dynamically steady flow and symmetry, was analysed. It was found that the effect of the dynamically steady assumption was very small, while the effect of assuming two symmetry planes was more significant, predicting a 17% higher peak RTD response. However, it was concluded that the effect of the symmetry assumption is small relative to that of the grid size and that its use will be justifiable if necessary to obtain a grid independent mesh while maintaining acceptable computational times.

The grid independence study performed as part of this thesis highlighted the importance of using a finer mesh size near the inlet, outlets and certain surfaces. This is necessary, since uniformly sized meshes containing up to 8.5 million cells were shown to be unable to accurately predict physical model results, especially where the variation between strands was considered. Starting with a 10mm mesh size and refining cells in high velocity gradient regions to 5 mm, a much better correlation with experimental results was obtained. The final grid contained roughly 2.8 million cells, which is significantly more than in most studies found in literature.

11.2. Validation

Comparison of the numerical model results with those obtained from a ½ scale water model, based on the Froude number similarity criterion, showed the numerical model was successful in predicting characteristic flow properties for three different tundish configurations. Both modelling methods showed the same trends in residence times and parameters of the modified combined model, with the average difference in the values calculated from experimental and numerical results being approximately 10%. However, the numerical model was less successful in predicting variation between the inner and outer strands of the tundish.

Stellenbosch University http://scholar.sun.ac.za

11.3. Turbulence Inhibitor

A combination of physical and numerical model results were used to compare three tundish configurations: a bare tundish, a tundish with a turbulence inhibitor and a tundish with a turbulence inhibitor with holes and dams. It was shown that the bare tundish was prone to significant short-circuiting, which would allow large inclusions to pass through to the mold and reduce the product quality.

By including a turbulence inhibitor below the inlet this short-circuiting was eliminated, significantly increasing the residence time and plug flow volume fraction, as well as decreasing the dead volume. The surface-directed flow caused by the turbulence inhibitor will aid inclusion removal by bringing the inclusions into contact with the slag layer for absorption. However, a possible concern is a rise of approximately 125% in the maximum turbulence kinetic energy near the surface. This increased turbulence near the surface due to the surface-directed flow may cause the slag to be entrained, forming large inclusions. It is therefore concluded that surface turbulence should be considered during turbulence inhibitor design.

Comparison of the tundish with a turbulence inhibitor and the tundish with a turbulence inhibitor with holes and dams showed that the addition of the holes and dams did not provide significant improvements in flow quality. However, short-circuiting, leading to a 53% shorter minimum residence time, and an 8% higher average turbulence kinetic energy value near the surface are causes for concern. By increasing the height of the dams the minimum residence time was restored to within 8% of the value when using the turbulence without holes. However, this comes at the cost of a decreased peak residence time and increased dead volumes. These examples illustrate that changes to the turbulence inhibitor design should be done with careful consideration of the impact on the flow quality, as unintentional deterioration of tundish performance is possible.

11.4. Scaling the Numerical Model from Water to Steel

The numerical model, initially based on the water system for validation through physical model results, was scaled to predict the flow behaviour in the high temperature steel process. Necessary changes to the numerical setup included scaling the geometry by a factor of two, changing the velocity and turbulence inlet boundary values according to Froude similarity and scaling the time step by a factor of $\sqrt{2}$. Initial grid cells were sized and the adaptation function value for gradient adaptation was chosen at suitable values in order to generate a mesh with the same final number of cells used for the numerical approach for the water model. The numerical simulations based on the steel process yielded C-curves that are very similar to that of the numerical model based on the water model. This serves as additional proof that the water model based on Froude number similarity is able to accurately simulate the flow behaviour in the real industrial process.

Stellenbosch University http://scholar.sun.ac.za

11.5. Turbulence Inhibitor Shape

Using the numerical model of the industrial tundish, four different shapes of turbulence inhibitors were investigated:

- A rectangular turbulence inhibitor with a flange at the top
- A round turbulence inhibitor with a flange at the top
- A rectangular turbulence inhibitor without the flange at the top
- A rectangular turbulence inhibitor with chamfered flanges

From the results it was evident that the shape of the turbulence inhibitor has a highly significant effect on the overall flow behaviour, as substantially different values of RTD parameters, surface turbulence and variation between strands were predicted for the different turbulence inhibitors. For the dimensions used in this study, the design with a rectangular shape and flanges at the top produced the largest mean residence time, the largest plug volume fraction and the smallest dead volume. Additionally, the surface turbulence was the least. Only in strand variation did the other two rectangular turbulence inhibitors outperform the rectangular turbulence inhibitor with the flanges at the top.

It was concluded that for the same height and opening area, the shape of the turbulence inhibitor will determine the amount of turbulent suppression provided. If insufficient suppression occurs, the flow patterns will be fast and the residence time will be low, not providing sufficient time for inclusion flotation. However, if the amount of suppression is very large the melt will follow very different routes to the different outlets and strand similarity will become problematic. This study emphasises the importance of designing the turbulence inhibitor, considering both size and shape, to achieve the best possible flow behaviour to produce clean steel.

Stellenbosch University http://scholar.sun.ac.za

Chapter 12: Recommendations and Future Work

Results from this study indicated several interesting points that would be worthwhile to explore in more detail. Further work can also benefit from the information regarding the numerical modelling procedure used in this study and knowledge regarding the effects of various assumptions.

The first recommendation would be to investigate possible causes for the challenges by accurately predicting the differences between the individual strands, since the results of this study indicate that grid size is not the root of the problem. The main suspects are the symmetry and dynamically steady assumptions, as well as the choice of turbulence model. In initial work the first two assumptions were analysed, but the work was done using a coarse 14mm grid size, resulting in approximately 220 000 cells. It would therefore be useful to quantify their effect when using the final, grid independent mesh obtained in Section 8.1. However, the numerical procedure using the final meshing method required 2 to 3 days using 12 cores of a HPC, only to obtain the first part of the residence time distribution in order to compare the different cases. Neglecting the assumptions of symmetry and dynamically steady flow the computational time required for the transient part of the simulation is expected to increase by approximately 32 times. Therefore, investigation of the symmetry and dynamically steady assumptions using the grid independent mesh will require large investments of computational time. Investigation of the RSM turbulence model using the grid independent mesh would also be worthwhile, since the results of the few studies (Kumar et al., 2004; Solorio-Diaz et al., 2004) that have investigated its use, seem to indicate that it predicts results that compare better with those of physical modelling studies. These three factors should be able to improve the accuracy of the current numerical model, but their implementation might be hindered by time and computational power limits.

Expansion of the current numerical model to more accurately simulate the real industrial process would be the second recommendation. The first step would be to eliminate the isothermal assumption employed in the current study by including heat losses from the tundish and thereby also the buoyancy driven flows present in the industrial tundish. The second step would be to include the movement of inclusion particles through the tundish in the numerical model. This would serve as a more direct method of quantifying the inclusion removal performance of the tundish than by simply inferring it from quantities calculated from the RTD response. However, ideally, both of these improvements would also require validation from the physical model, which would require complex improvements to the physical model as well.

One of the aspects of the tundish with different flow control device configuration that was frequently looked at was the magnitude of surface turbulence. It was found that the surface directed flow used to eliminate short-circuiting and increase the residence time of the

Stellenbosch University http://scholar.sun.ac.za

tundish would also increase the turbulence near the slag layer. This has the potential of entraining the slag into the melt, causing large inclusions to form that will be very harmful for the process. However, it is impossible to quantify this problem without a detailed study of the slag entrainment in these studies. This could be done by either physical modelling, using kerosene to simulate the slag layer, or by numerical modelling. The problem with numerical modelling is that the accurate simulation of the entrainment of slag droplets with dimensions in the micron range would require a very fine mesh, which would lead to large computational times. In the physical model, the detection and measurement of slag entrainment presents the difficulty. Therefore both methods would include its own challenges, but the results should be very relevant for future research on tundish.

Finally, it was observed that methods used to increase residence time and plug flow volume fraction for improved inclusion removal has the potential to increase dissimilarity in strand composition and temperature. This variation in properties would decrease the value of the product and make control of the process more difficult. Although this study has looked briefly at the problem, further work is suggested to investigate the correct use of flow control devices and outlet position to limit this variation. This would be especially important for larger six strand tundish, where previous authors have reported very large variations between strands. For maximum relevance, such a study should be performed using a numerical model that has been shown to be accurate in predicting strand variations in a variety of systems.

Stellenbosch University http://scholar.sun.ac.za

References

Ahuja, R. & Sahai, Y., 1986. Fluid Flow and Mixing of Melt in Steelmaking Tundishes. *Ironmaking & Steelmaking*, 13, pp.241–247.

ANSYS, 2011. *ANSYS FLUENT Theory Guide* Version 14., Southpointe: ANSYS.

Bessemer, H., 1865. Improvement in the Manufacture of Iron and Steel. , pp.1–3.

Bolger, D. & Saylor, K., 1994. Development of a Turbulence Inhibiting Pouring pad/Flow control device for the Tundish. In *Steelmaking Conference Proceedings*. ISS-AIME, pp. 225–234.

Cameron, S.R., 1992. The Reduction of Tundish Nozzle Clogging During Continuous Casting at Dofasco. In *75th Steelmaking Conference Proceedings*. Warrendale: Iron and Steel Society, p. 327.

Chattopadhyay, K., Isac, M. & Guthrie, R.I.L., 2012. Modelling of Non-isothermal Melt Flows in a Four Strand Delta Shaped Billet Caster Tundish Validated by Water Model Experiments. *ISIJ International*, 52(11), pp.2026–2035.

Chattopadhyay, K., Isac, M. & Guthrie, R.I.L., 2010. Physical and Mathematical Modelling of Steelmaking Tundish Operations: A Review of the Last Decade (1999–2009). *ISIJ International*, 50(3), pp.331–348.

Emi, T., 1999. Process Integration for Making Clean Steels for Stringent Applications. In K. C. Liddel & D. J. Chaiko, eds. *Metal Separation Technologies Beyond 2000*. TMS, pp. 207–218.

Hou, Q. & Zou, Z., 2005. Comparison Between Standard and Renormalization Group k-e Models in Numerical Simulation of Swirling Flow Tundish. *ISIJ International*, 45(3), pp.325–330.

Ilegbusi, O.J. & Szekely, J., 1989. Effect of Magnetic Field on Flow, Temperature and Inclusion Removal in Shallow Tundishes. *ISIJ International*, 29(12), pp.1031–1039.

International Iron and Steel Institute, 1978. *A Handbook of World Steel Statistics*, Brussels. Available at: http://www.worldsteel.org/dms/internetDocumentList/statistics-

Stellenbosch University http://scholar.sun.ac.za

archive/yearbook-archive/A-handbook-of-world-steel-statistics-1978/document/A handbook of world steel statistics 1978.pdf.

Irving, W.R., 1993. *Continuous Casting of Steel*, London: The Institute of Materials.

Jha, P.K., Dash, S.K. & Kumar, S., 2001. Fluid Flow and Mixing in a Six Strand Billet Caster Tundish: A Parametric Study. *ISIJ International*, 41(12), pp.1437–1446.

Jha, P.K., Ranjan, R., Mondal, S.S. & Dash, S.K., 2003. Mixing in a Tundish and a Choice of Turbulence Model for its Prediction. *International Journal of Numerical Methods for Heat & Fluid Flow*, 13(8), pp.964–996.

Jha, P.K., Rao, P.S. & Dewan, A., 2008. Effect of Height and Position of Dams on Inclusion Removal in a Six Strand Tundish. *ISIJ International*, 48(2), pp.154–160.

Kemeny, F., Harris, D.J., McLean, A., Meadowcroft, T.R. & Young, J.D., 1981. Fluid Flow Studies in the Tundish of a Slab Caster. In *Proceeding of the 2nd Process Technology Conference*. Chicago: TMS, p. 232.

Kumar, A., Koria, S.C. & Mazumdar, D., 2004. An Assessment of Fluid Flow Modelling and Residence Time Distribution Phenomena in Steelmaking Tundish Systems. *ISIJ International*, 44(8), pp.1334–1341.

Kumar, A., Koria, S.C. & Mazumdar, D., 2007. Basis for Systematic Hydrodynamic Analysis of a Multi-strand tundish. *ISIJ International*, 47(11), pp.1618–1624.

Kumar, A., Mazumdar, D. & Koria, S.C., 2008. Modeling of Fluid Flow and Residence Time Distribution in a Four-strand Tundish for Enhancing Inclusion Removal. *ISIJ International*, 48(1), pp.38–47.

Lange, K.W., 1988. Thermodynamic and Kinetic Aspects of Secondary Steelmaking Processes. *International Materials Reviews*, 33(2), pp.53–89.

Launder, B.E. & Spalding, D.B., 1974. The Numerical Computation of Turbulent Flows. *Computer Methods in Applied Mechanics and Engineering*, 3, pp.269–289.

Stellenbosch University http://scholar.sun.ac.za

Levenspiel, O., 1972. *Chemical Reaction Engineering* 2nd ed., John Wiley & Sons, Inc.

Li, C., Liu, B. & Zhu, S., 2012. Numerical Simulation on the Flow State of Dross Layer in Tundish. *AASRI Procedia*, 3, pp.313–318.

Liu, S., Yang, X., Du, L., Li, L. & Liu, C., 2008. Hydrodynamic and Mathematical Simulations of Flow Field and Temperature Profile in an Asymmetrical T-type Single-strand Continuous Casting Tundish. *ISIJ International*, 48(12), pp.1712–1721.

Loth, E., 2006. *Overview of Multiphase modelling* C. T. Crowe, ed., CRC Press.

Mazumdar, D. & Guthrie, R.I.L., 1999. The Physical and Mathematical Modelling of Continuous Casting Tundish Systems. *ISIJ International*, 39(6), pp.524–547.

McPherson, N.A., 1985. Continuous Cast Clean Steel. In *68th Steelmaking Conference Proceedings*. Warrendale: ISS, pp. 13–25.

Merder, T. & Warzecha, M., 2012. Optimization of a Six-Strand Continuous Casting Tundish: Industrial Measurements and Numerical Investigation of the Tundish Modifications. *Metallurgical and Materials Transactions B*, 43B, pp.856–868.

Miki, Y. & Thomas, B.G., 1999. Modeling of Inclusion Removal in a Tundish. *Metallurgical and Materials Transactions B*, 30, pp.639–654.

Mishra, S.K., Jha, P.K., Sharma, S.C. & Ajmani, S.K., 2012. Effect of Blockage of Outlet Nozzle on Fluid Flow and Heat Transfer in Continuously Cast Multistrand Billet Caster Tundish. *Canadian Metallurgical Quarterly*, 51(2), pp.170–183.

Ohno, T., Ohashi, T., Matsunaga, H., Hiromoto, T. & Kumai, K., 1974. Study of Large Nonmetallic Inclusions in Continous Cast Al-Si Killed Steel. *Transactions of the Iron and Steel Institute of Japan*, 15, pp.407–416.

Pehlke, R.D., 2012. Steel Manufacture. *AccessScience*. Available at: http://www.accessscience.com.ez.sun.ac.za.

Stellenbosch University http://scholar.sun.ac.za

Qu, T., Liu, C. & Jiang, M., 2012. Numerical Simulation for Effect of Inlet Cooling Rate on Fluid Flow and Temperature Distribution in Tundish. *Journal of Iron and Steel Research International*, 19(7), pp.12–19.

Raghavendra, K., Sarkar, S., Ajmani, S.K., Denys, M.B. & Singh, M.K., 2013. Mathematical Modelling of Single and Multi-strand Tundish for Inclusion Analysis. *Applied Mathematical Modelling*, 37(9), pp.6284–6300.

Sahai, Y. & Burval, M.D., 1992. Validity of Reynolds and Froude Similarity Criteria for Water Modeling of Melt Flow in Tundishes. In *Electric Furnace Conference Proceedings*. I.S.S. Publication, pp. 469–474.

Sahai, Y. & Emi, T., 1996a. Criteria for Water Modeling of Melt Flow and Inclusion Removal in Continuous Casting Tundishes. *ISIJ International*, 36(9), pp.1166–1173.

Sahai, Y. & Emi, T., 1996b. Melt Flow Characterization in Continuous Casting Tundishes. *ISIJ International*, 36(6), pp.667–672.

Sahai, Y. & Emi, T., 2008. *Tundish Technology for Clean Steel Production*, World Scientific Publishing Co.

Schwarze, R., Obermeier, F., Hantusch, J., Franke, A. & Janke, D., 2001. Mathematical Modelling of Flows and Discrete Phase Behaviour in a V-shaped Tundish. *Steel Research*, 72, p.215.

Shih, T., Liou, W.W., Shabbir, A., Yang, Z. & Zhu, J., 1995. A New k-e Eddy Viscosity Model for High Reynolds Number Turbulent Flows. *Computers and Fluids*, 24(3), pp.227–238.

Singh, S. & Koria, S.C., 1996. Tundish Melt Dynamics With and Without Flow Modifiers Through Physical Modelling. *Ironmaking & Steelmaking*, 23(3), pp.255–263.

Solorio-Diaz, G., Morales, R.D., Palafax-Ramos, J., Garcia-Demedices, L. & Ramos-Banderas, A., 2004. Analysis of Fluid Flow Turbulence in Tundishes Fed by a Swirling Ladle Shroud. *ISIJ International*, 44(6), pp.1024–1032.

Thomas, B.G., 2004. Continuous Casting (metallurgy). *AccessScience*. Available at: http://www.accessscience.com.ez.sun.ac.za.

Stellenbosch University http://scholar.sun.ac.za

Tripathi, A., 2011. Mathematical Modelling of Flow Control in a Tundish Using Electro-magnetic Forces. *Applied Mathematical Modelling*, 35, pp.5075–5090.

Tripathi, A. & Ajmani, S.K., 2011. Effect of Shape and Flow Control Devices on the Fluid Flow Characteristics in Three Different Industrial Six Strand Billet Caster Tundish. *ISIJ International*, 51(10), pp.1647–1656.

Tripathi, A. & Ajmani, S.K., 2005. Numerical Investigation of Fluid Flow Phenomenon in a Curved Shape Tundish of Billet Caster. *ISIJ International*, 45(11), pp.1616–1625.

World Steel Association, 2009. *Steel Statistical Yearbook*, Brussels. Available at: http://www.worldsteel.org/dms/internetDocumentList/statistics-archive/yearbook-archive/Steel-statistical-yearbook-2009/document/Steel statistical yearbook 2009.pdf.

Zhang, L. & Cai, K., 1997. *Project Report: Cleanliness Investigation of Low Carbon Al-Killed Steel in Bao Steel*,

Zhang, M.J., Gu, H.Z., Huang, A., Zhu, H.X. & Deng, C.J., 2011. Physical and Mathematical Modeling of Inclusion Removal with Gas Bottom-Blowing in Continuous Casting Tundish. *Journal of Mining and Metallurgy Section B: Metallurgy*, 47(1), pp.37–44.

Zhong, L., Li, B., Zhu, Y., Wang, R., Wang, W. & Zhang, X., 2007. Fluid Flow in A Four-strand Bloom Continuous Casting Tundish with Different Flow Modifiers. *ISIJ International*, 47(1), pp.88–94.

Zhong, L.C., Li, L.Y., Wang, B., Zhang, L., Zhu, L.X. & Zhang, Q.F., 2008. Fluid Flow Behaviour in Slab Continuous Casting Tundish with Different Configurations of Gas Bubbling Curtain. *Ironmaking & Steelmaking*, 35(6), pp.436–440.

Zong, J., Yi, K. & Yoon, J., 1999. Residence Time Distribution Analysis by the Modified Combined Model for the Design of Continuous Refining Vessel. *ISIJ International*, 39(2), pp.139–148.

Stellenbosch University http://scholar.sun.ac.za

Appendix A: Nomenclature

A.1. Symbols

This section lists the symbols used in equations in this thesis. Symbols with an over-bar ($\bar{\theta}$) represent an averaged value, while an arrow over-bar ($\vec{F}$) represents a vector quantity. Various subscripts, used in combination with symbols, are also explained.

θ	Dimensionless time	[ ]
$\bar{\theta}$	Dimensionles mean residence time	[ ]
κ	Turbulent kinetic energy	[m^2/s^2]
λ	Scale factor	[ ]
μ	Dynamic viscosity	[kg/s.m]
ρ	Density	[kg/m^3]
σ^2	Dimensionless variance of RTD	[ ]
σ_t^2	Variance of RTD	[s^2]
$\bar{\bar{\tau}}$	Stress tensor	[$kg/s^2.m$]
ϵ	Turbulent dissipation rate	[m^2/s^3]
c	Concentration	[kg/m^3]
C	Dimensionless concentration	[ ]
D	Diameter	[m]
F	Force	[$kg.m/s^2$]
Fr	Froude number	[ ]
g	Gravitational acceleration	[m/s^2]
I	Unit stress tensor	[ ]
J_i	Diffusive flux of species i	[$kg/m^2.s$]
L	Length	[m]

Stellenbosch University http://scholar.sun.ac.za

m	Mass	[kg]
$\dot{m}$	Mass flow rate	[kg/s]
Q	Volumetric flow rate	[m^3/s]
Q_a	Volumetric flow rate through active region	[m^3/s]
Re	Reynolds number	[ ]
R_i	Net production rate by reaction	[kg/m^3.s]
S_m	Mass source	[kg/s.m^3]
t	Time	[s]
t_{ave}	Theoretical average residence time	[s]
$\bar{t}$	Mean residence time	[s]
T	Temperature	[K]
u	Velocity magnitude	[m/s]
v	Velocity	[m/s]
V	Volume	[m^3]
V_d	Dead volume	[m^3]
V_{dp}	Dispersed plug flow volume	[m^3]
V_m	Well mixed volume	[m^3]
V_p	Plug flow volume	[m^3]
Y_i	Mass fraction of species i	[ ]

A.2. Acronyms

BOF	Basic Oxygen Furnace
CAD	Computer Aided Design
CFD	Computational Fluid Dynamics
DI	Deep drawing & Ironing
DN	Dispersion Number
EAF	Electric Arc Furnace

Stellenbosch University http://scholar.sun.ac.za

HPC	High Performance Computing
MUSCL	Monotone Upstream-Centred Schemes for Conservation Laws
PISO	Pressure-Implicit with Splitting of Operators
PIV	Particle Image Velocimetry
PRESTO!	Pressure Staggering Option
RANS	Reynolds-averaged Navier-Stokes
RNG	Renormalized group
RSM	Reynolds Stress Model
RTD	Residence Time Distribution
SIMPLE	Semi Implicit Method for Pressure Linked Equation
TI	Turbulence Inhibitor
TID	Turbulence Inhibitor and Dams

Stellenbosch University http://scholar.sun.ac.za

Appendix B: Discretization Scheme

This section will discuss the results that were obtained when investigating the effect of the order of discretization on the numerical solution. A 2^3 factorial experiment was performed with the three factors being the discretization method for momentum, turbulence (turbulence kinetic energy and turbulence dissipation rate) and species. The first-order upwind scheme was represented by the lower level, while the higher level represented the second-order upwind scheme. The experimental design is shown in Table B.1. The average values calculated for the velocity and turbulence kinetic energy, as well as the peak concentration in the RTD response, is also shown. Figure B.1 shows the RTD responses that were obtained.

Table B.1 - Experimental design and results obtained while investigating the effect of the discretization scheme on the numerical results

Case	Momentum	Turbulence	Species	Velocity (m/s)	Turbulent kinetic energy (m^2/s^2)	Peak concentration
A	1	1	1	0.000647	5.09E-06	1.20
B	1	0	0	0.000653	4.01E-06	1.08
C	0	1	0	0.000547	4.22E-06	1.08
D	0	0	1	0.000593	3.53E-06	1.26
E	1	1	0	0.000647	5.09E-06	1.11
F	0	1	1	0.000547	4.22E-06	1.13
G	1	0	1	0.000653	4.22E-06	1.20
H	0	0	0	0.000593	4.01E-06	1.16

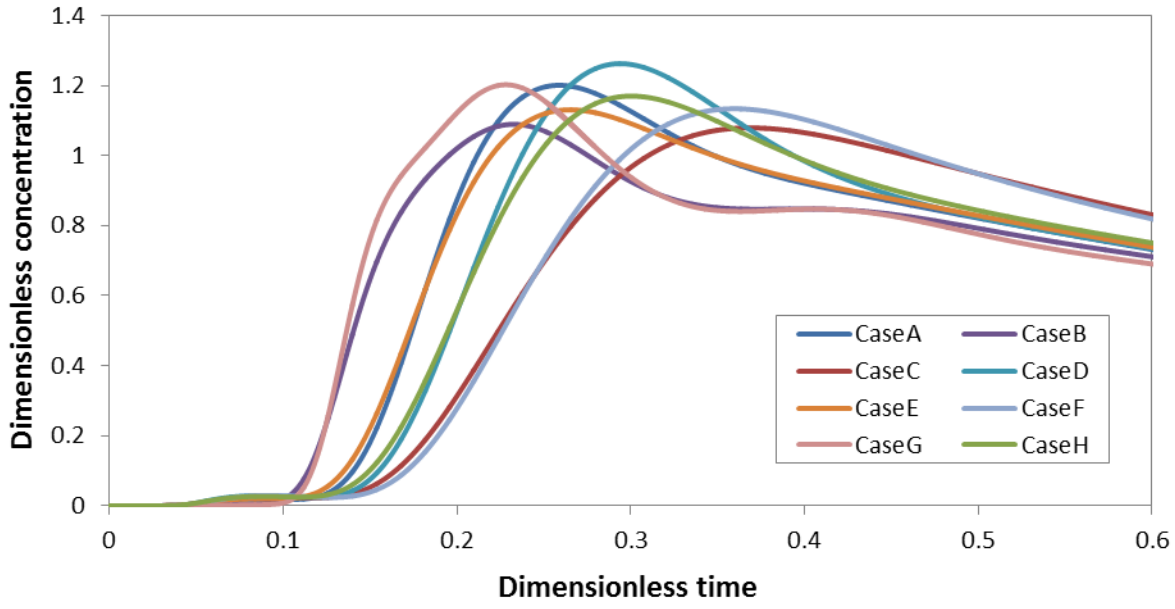

Figure B.1 - RTD curves obtained while investigating the effect of the discretization scheme

Stellenbosch University http://scholar.sun.ac.za

It is evident that the discretization method has a significant effect on the solution that is obtained. Further investigation reveals that the RTD shapes are of greater similarity for the cases with the same discretization schemes for momentum and turbulence. In all cases the use of second-order discretization for species resulted in a slightly higher peak concentration being predicted. Using these results multiple regressions involving the order of discretization for momentum, velocity and species as dependent variables were performed to investigate the significance of these factors on the predicted average velocity, average turbulence kinetic energy, peak concentration and peak time. The results are summarised in Table B.2. It is found that momentum discretization has a highly significant ($P < 0.01$) effect on the predicted average velocity and peak residence time and a significant effect ($P < 0.05$) on the average turbulence kinetic energy. Turbulence discretization significantly ($P < 0.05$) influenced the average turbulence kinetic energy and the peak residence time, while the effect on the average velocity approached significance ($P = 0.06$). The effect of the species discretization was only significant to some extent ($P = 0.051$) when considering the peak concentration value. It was concluded that it is essential to use second-order discretization for momentum and turbulence, while second-order discretization for species had a smaller, but still significant, effect.

Table B.2 - Results of the multiple regression performed to analyse the effect of the discretization scheme on the numerical solution

Effect	R Square	P-Value: Momentum	P-Value: Turbulence	P-Value: Species
Velocity	0.946	0.00132	0.0600	1
Turbulence kinetic energy	0.869	0.0291	0.0174	0.730
Peak concentration	0.706	0.774	0.240	0.0508
Peak time	0.979	0.000267	0.00376	0.124

Next, the solution using second-order discretization for momentum, turbulence and species was compared to the solution when using third-order discretization in all three cases, as shown in Figure B.2. From these results it was concluded that extension to third-order discretization offers no significant improvement over second-order discretization. For this reason further numerical simulation in this study was performed using second-order discretization for momentum, turbulence and species.

Stellenbosch University http://scholar.sun.ac.za

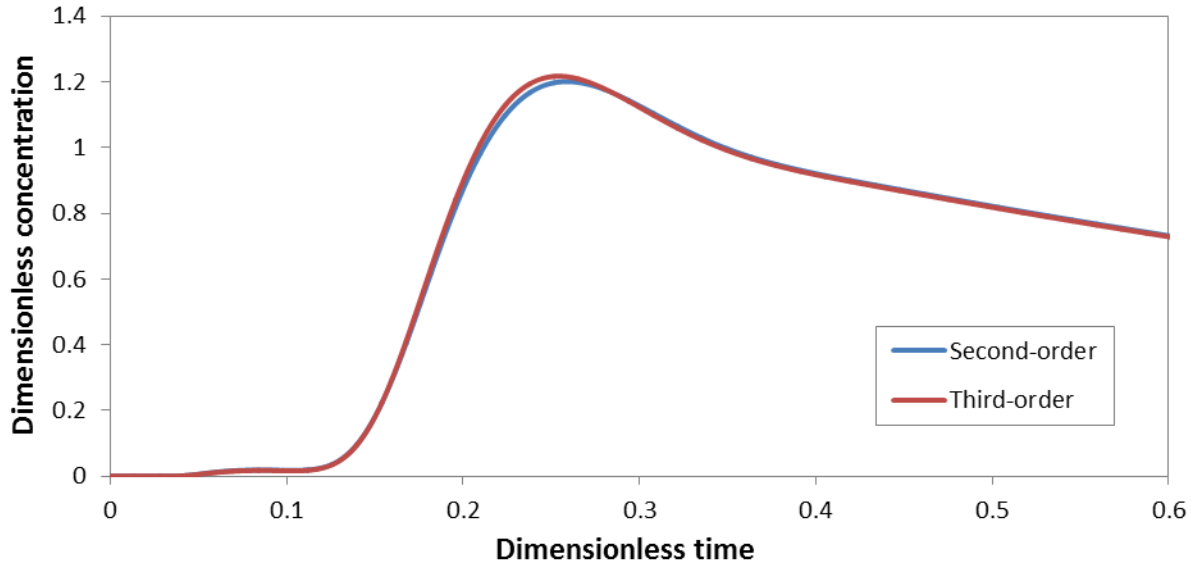

Figure B.2 - Comparison of RTD curves when using second- and third-order discretization